Computational Studies in the Planar Symmetric Six-body Problem

Neelum Bashir

School of Mathematical and Computational Sciences
Massey University

This dissertation is submitted for the degree of
Doctor of Philosophy

November 2023

I would like to dedicate this thesis to my beloved mother and my beloved kids Hamza and Izzah

Abstract

This thesis presents the study of the gravitational six-body problem which describes the motion of a group of six stars interacting with each other gravitationally. The bodies undergo collisions due to the attractive nature of interactions, which are singular. The singularity is one of the difficulties in exploring the problem. It is necessary to use regularization techniques to avoid singularity when there is a possibility of collisions between the stars.

This study involves finding solutions to the six-body problem, especially periodic ones. One important solution to this problem is the Schubart orbit. Schubart orbits were previously discovered for the three-body [52] and four-body [63] problems. We find the Schubart orbit in a setup of six bodies, where the six bodies are positioned at the vertices of two aligned equilateral triangles. The existence proof of the Schubart orbit is also presented.

Later, we extend our study of the six-body system to the case, where the bodies are placed on the vertices of two non-aligned equilateral triangles. In this case, we generate families of periodic orbits when the bodies have equal masses. One of the featured results of this problem is the Schubart family of periodic orbits. This family starts from the Schubart orbit and when we move along the family the orbits become more complex and unstable.

Another equal-mass family of periodic orbits is generated from the

hexagonal orbit. These families of periodic orbits are parametrized by angular momentum. In general, the masses are chosen equal to unity, and the total energy of the system is fixed as $E = -1$.

We perform a non-linear stability check of the discovered solutions under the symmetric perturbations. An algorithm for the search of periodic orbits is presented.

Acknowledgements

I praise and thank Almighty Allah for his blessings and strength that helped me to complete this study.

I would like to express my sincere gratitude to my supervisor, Associate Professor Winston Sweatman for providing me with the opportunity to work on this project. I appreciate his invaluable guidance, continued support, and outstanding feedback during this research. He taught me the techniques and strategies to conduct the research and to present my research as clearly as possible. Without his guidance, this research work would not have been achievable.

An immense thank you to my co-supervisors Associate Professor Alona Ben-Tal and Associate Professor Shaun Cooper for their academic support, great feedback, and valuable discussion. I am extremely thankful to Alona for her thoughtful remarks, encouragement, and providing advice regarding investigation and formulation during the meetings. Thanks are also due to Shaun for his constructive comments and scientific approach that helped me in writing this thesis.

I am extremely thankful to the School of Mathematical and Computational Sciences and Massey University for providing me with a doctoral scholarship and access to facilities to complete this research work.

I would like to extend my thanks to my mother and siblings for their prayers, love, and support since my childhood.

Lastly, but most importantly, I would like to thank my husband Rizwan Ahmad for his patience and for providing me with the time and space to complete this research. Thank you Rizwan for helping and encouraging me through the difficult times during my research work.

Contents

Notations

Capital letters

A	Angular momentum
B	Perturbation matrix for differential corrections
D	Centre of mass
E	Total energy of the system
F	Generating function
G	Gravitational constant
H	Hamiltonian
I	Identity matrix
K	Kinetic energy
L	Lagrangian
M	Total mass of the system
N	Number of bodies of the system
P, Q	Regularized momenta and position coordinates
R	Sum of distances
S	Maximum distance of outer body in the Schubart orbit
T	Period of an orbit
U	Potential energy

Greek letters

Δ Step size

δ Perturbation

Γ Regularized Hamiltonian

τ Regularized time

θ Angle of rotation of the system

ξ Relative error

Small letters

$\ddot{x}$ Acceleration

$\dot{x}$ Velocity components in real coordinate system

ω Momenta components in real coordinate system

b_i i^{th} body

g Transformation of time

m Mass of a body

p, q Interbody momenta and distance coordinates in real coordinate system

r_{ij} Distance between the bodies i and j

t Time

x Position components in real coordinate system

Subscript

δ Perturbation

i, j, k Index of i^{th}, j^{th} and k^{th} body

ij Index of a relative quantity between bodies i and j

0 Related to time $t = 0$

Chapter 1

Introduction

The N-body problem is the age-old challenge of predicting the individual motions of a group of celestial objects that interact with each other under the laws of gravity. Investigation of the solution to this problem has been motivated by the desire to understand the dynamics of few-body systems. For example, to explore the motion of various bodies in the solar system and many other stars in the stellar systems that range from binary star systems to globular star clusters and galaxies [24].

Unfortunately, there exists no complete and general solution to the N-body problem. The two-body problem is the gravitational problem in dynamics for which we have an analytical solution. Newton was the first who stated and proposed a solution for the two-body problem. The two-body problem can be stated as follows: "Given at any time the positions and velocities of two massive particles moving under their mutual gravitational force, the masses also being known, calculate their position and velocities for any other time"[51].

The two-body problem is important in the sense that a wide variety of practical orbital motion problems can be treated as approximate two-body problems [51], for example, the motion of a planet around the sun and the motion of an artificial satellite or moon around the earth.

The three-body system is a problem with non-analytical solutions except for some special cases, for example, the Lagrangian case where three bodies are located on the vertices of an equilateral triangle, and Euler's three-body problem, where a test mass moves unrestricted in the gravitational field of two fixed point masses. Poincaré explained in his paper [48] that the dynamics become extremely complicated when the gravitational influence of a third body is added, no matter what is the size of the third one.

After the Poincaré formulation, the general and restricted three-body problem was studied in detail. Some interesting solutions have been found in the case of the general and restricted three-body problems, for example, the Schubart orbit [52], planar Standish orbit [57], figure-eight choreography orbit [42], and Euler and Lagrange found the five stationary solutions of the planar circular restricted three-body problem [11].

The numerical study of the four-body problem started in the last century. Initially, this problem was studied as the perturbed three-body problem with an added fourth body having negligible mass [18]. Mikkola numerically explored the gravitational encounter of two equal-mass binary stars [33]. The simple one-dimensional four-body Schubart orbit was discovered by Sweatman [63]. Later, taking this four-body Schubart orbit as an initial point Chopovda and Sweatman found an equal-mass family of periodic orbits [15]. They also considered some five-body systems [16].

The six-body system can physically occur as a result of the interaction of three binary stars, a trinary with three planets, or a binary with accompanying planets. An example of the six-body system in outer space is the system of the dwarf planet Pluto with its five moons − Charon, Hydra, Kerberos, Nix, and Styx. Pluto and its biggest moon Charon is considered a binary planet with four small bodies Hydra, Kerberos,

Nix, and Styx orbiting this binary planet. The smallest moon Styx lies fairly close to the stable orbit of the central binary. The remaining three moons Hydra, Kerberos, and Nix are packed as tightly as possible [29].

Another example of the six-body system is the sextuply-eclipsing star system TYC 7037-89-1. This was discovered with the help of the Transiting Exoplanet Survey Satellite (TESS). The system comprises three gravitationally-bound eclipsing binaries in a hierarchical structure of an inner quadruple system with an outer binary subsystem [49].

In the present research, we examine a planar symmetric six-body system and find the periodic families of the six-body orbits. Such kinds of families are also explored in three body cases by Hénon [25, 26], Mikkola and Hietarinta [38, 39], and in four and five body cases by Sweatman [63, 64], and Chopovda and Sweatman [15, 16]. The goal of the present research is to extend the results to the case of six bodies. The six-body system can be considered a stepping stone between the three and four-body systems and N-body systems with a larger number of bodies.

We start our search by considering an equal-mass planar symmetric six-body problem with aligned triangles, where the six bodies are arranged on the vertices of two concentric equilateral triangles, and find the Schubart orbit and some typical orbits for the six-body system. Later, we extend our search to the case of non-aligned triangles and explore two families of periodic orbits: the Schubart family and the hexagon family of the periodic orbits.

The desire to study a symmetric gravitational system is because of its greater simplicity than a general N-body problem. Such problems can still provide ideas and insight to understand the more general N-body problems [66].

1.1 Thesis outline

We present a sketch of our thesis in this section. In the next section, we survey the literature on past research in three-, four-, five-, and six-body problems. Some particular studies of three- and four-body problems presented by Hietarinta and Mikkola [38–40], Hénon [25, 26], Sweatman [63, 64], and Chopovda and Sweatman [15, 16] proved to be very helpful to overcome the difficulties that appear when studying the symmetric six-body problem.

We examine the symmetric six-body problem with two different cases.

- Six-body system with aligned triangles.
- Six-body system with non-aligned triangles.

Chapter 2 introduces the six-body problem with aligned triangles. The assumptions used to model this problem are described. The Hamiltonian and equations of motion for six bodies in the case of aligned triangles are derived. This problem is useful as it is helpful for exploring the family of periodic orbits for the planar symmetric six-body problem with non-aligned triangles. An equal mass six-body Schubart orbit and some more general orbits are studied in this case.

In Chapter 3 we provide analytical proof to show the existence of the Schubart orbit for the six-body system. For this proof, we follow a similar technique as done previously for the three- and four-body Schubart orbits [47, 73].

In Chapter 4 we introduce the symmetric six-body problem with non-aligned triangles. This planar symmetric six-body problem provides the kinds of periodic orbits we are looking for. The Hamiltonian and equations of motion for the six bodies arranged on the vertices of two

non-aligned triangles with Levi-Civita regularization are derived in this chapter.

In the last section of this chapter, we outline the approach used to search for the planar six-body periodic orbits. A detailed description of the algorithms used to produce our results with equal masses is provided.

All the algorithms are implemented in MATLAB, including the integrators for the symmetric six-body system with aligned triangles from Chapter 2 and the planar symmetric six-body problem from Chapter 4.

Chapter 5 describes a family of periodic orbits generated from the six-body Schubart orbit that was found in Chapter 2. We describe the results obtained for six equal masses and discuss their properties. A detailed description of the behavior of parameters of the six-body system along the family is given in this chapter. A non-linear stability check for the Schubart family of periodic orbits is performed and results are presented in the last section of Chapter 5.

We found another family of periodic solutions with equal masses that starts from the hexagonal orbit and is presented in Appendix B. A few more orbits that do not belong to either of the two families of periodic solutions are presented in Appendix C.

1.2 Literature review

This section reviews the literature related to extensive research on three-, four-, and six-body problems. There exists a considerable body of literature covering the few-body problem and explaining the methods used to study a gravitational system. We particularly focus on studies related to the Schubart orbit and the families of periodic orbits.

Another part of the review is dedicated to the theory of regularisation used to transform singular equations into regular ones. These singularities arise in the equations of motion during the numerical simulations of the N-body problem. So, it is important to discuss the methods to avoid such singularities. This part of the review presents the different types of regularization for the equations of motions during the numerical integration of few-body problems.

The last part of this literature review explains the Poincaré map which is a discrete dynamical system with a one-dimensional lower state space than the original continuous dynamical system. This map is an effective tool to examine the orbits in the state space of a continuous dynamical system.

There are many books about stellar dynamics and the theory of celestial mechanics that present a good picture of the few-body problems and explain the methods that are used to study gravitational systems. Goldstein [19] explains the basic theory of classical mechanics. He discussed in detail the closed-form solution of the two-body problem, which involves the motion in elliptic, parabolic, and hyperbolic orbits depending upon the eccentricity of one body around the other. He also provides some examples of what happens when a third body is added to the two-body problem. One of the chapters is dedicated to the canonical transformation that is helpful in replacing the singular equation with a regular one.

Szebehely [68] explains the analytical and numerical simulations in the restricted three-body problem. He provides a detailed summary of the results of the circular restricted three-body problem and the modification of this problem to Hill's problem and the elliptic problem is also given.

Stiefel and Scheifele [60] have written an interesting book that explains the geometry of Kustaanheimo-Stiefel regularization, also known as K-S regularization and the theory of Kepler motion. They provide numerical methods that deal with various problems of stellar dynamics.

Aarseth's [1] book "Gravitational N-body simulations" provides a detailed study of regularisation containing algorithms that are used with few- and N-body problems. This provides a complete description of the formulation of the chain algorithm proposed by Mikkola and Aarseth [36]. This book also presents practical features of the general N-body problem, such as planetary systems, star clusters, and galaxies.

Roy [51] provides a detailed description of the evolution of the solar system, particularly the Saturn-Jupiter systems with satellites and the system of the earth and moon. He also discusses some artificial orbits and practical aspects of orbital motion by studying the dynamics of artificial satellites and rockets. One of the parts of this book is dedicated to explaining the different types of motion in stellar systems from the two-body problem to many-body problems. It also introduces the Caledonian symmetric $2N$-body problem for $N = 1, 2, 3$.

"The gravitational million-body problem" by Heggie and Hut [22] discusses the dynamics of stellar systems. This book discusses the importance of studying the million-body problem by considering it from the point of view of different disciplines, for example, mathematics, physics, and computer science. It provides an examination of the few-body problem with a system of two-stars, gravitational scattering, and triple-star systems with the relevant numerical methods. This book also investigates the evolution of the million-body systems including a discussion of the total mass and energy of star clusters and a measure of cluster radius.

1.2.1 Study of the few-body problem

Pioneering work to find the solution to the few-body problem was done by Schubart [52] in 1956 by computing a periodic orbit numerically for the three-body system known as the Schubart periodic orbit. This periodic orbit is a rectilinear orbit with two types of interactions, a first interaction occurs between body 1 and body 2, and a second interaction between bodies 2 and 3. Body 2 acts as an intermediary between the other two bodies: at time $t = 0$ body 2 closely interacts with body 1 and at a later time $t = T$, there is a close interaction of bodies 2 and 3. Then the motion is repeated. Thus, body 2 kicks away the other two bodies in turn and prevents them from approaching the centre. A topological existence proof of the periodic orbit found by Schubart for the three-body system was presented by Mockel [41].

Hadjidemetriou [20, 21] explored the families of periodic solutions in the general three-body system starting from the periodic orbit of the circular restricted three-body problem, where one body has a negligible mass and the motion of the other two massive bodies is restricted to a circle, by choosing the mass of the third body m_3 as a parameter [20]. He pointed out that the periodic orbits of the general three-body problem can be used as a bridge to make a link between the periodic orbits of the circular restricted problem and the elliptic three-body problem. Later, he [21] extended this family of periodic orbits in the case of equal masses.

Hénon showed in his papers [25, 26] that the periodic orbits of the planar three-body problem with given masses form one-parameter families both in general and restricted cases. He numerically [25] found the segments of two families that start from some known orbits computed by Szebehely [67] and Standish [57]. Hénon explained that we can trivially obtain an infinite number of periodic solutions by changing the origin of time and

by the rotation of the initial setting of the system around the centre of mass. Thus to avoid trivial solutions, the initial rotation and the origin of time of the system were fixed. He fixed the origin of the time by choosing it to coincide with the minimum distance between the central body with another body. To fix the rotation angle the starting point of the three-body system was considered on the x-axis with a velocity vector perpendicular to this line. The families of periodic orbits were obtained by taking angular momentum as the parameter of the system.

The next part of Hénon's study [26] was to explore the complete parametric family of periodic orbits for the planar three-body system rather than just a segment. The family starts from the well-known equal mass Schubart orbit and ends in a hierarchy of two binaries that rotate in different directions. The entire family was generated by varying the angular momentum A of the system. It was observed that the angular momentum increases along the family and reaches a local maximum and then it starts decreasing until a local minimum is achieved. After this, it continues to increase towards infinity.

Broucke [7] described a family of collision orbits for the case of the planar elliptic restricted three-body system. To compute close encounters during the integration of a restricted elliptic three-body problem a regularization scheme with Birkhoff coordinates (a set of coordinates that regularize the two-body collision and are related to original coordinates by a conformal mapping) and an energy differential equation is used. It is shown that some periodic orbits of the elliptic family are related to the collision orbits of the circular restricted family.

Broucke [8] also numerically explored two families of relative periodic orbits in the general three-body problem. He applied different strategies of the differential correction method to obtain the periodic orbits in the

heliocentric and barycentric coordinate systems.

Broucke and Boggs [9] discussed in detail the symmetric properties possessed by the orbits of many examples of three-body problems such as circular restricted, elliptic, and general planar three-body problems. They also presented two types of periodic orbits in the general three-body problem known as absolute and relative periodic orbits. For the absolute periodic orbits, the periodicity is because of the inertial frame of reference and the coordinates and velocity of all three bodies are periodic functions of time with the same period. While in relative periodic orbits, the position and speed of the system are relative to each period T during which the system rotates by a fixed angle θ. So, the positions of the bodies are rotated by a fixed angle, θ at the end of the period. Thus, in relative periodic orbits, periodicity is with respect to the rotating frame of reference moving with angular velocity $\omega = \theta/T$. They explained that relative periodic orbits would be absolute if the angle of rotation is a rational fraction of 2π. Some of the applications of three-body problems to natural satellites of the solar system are also presented in the article [9].

Martinez [30] proved the existence of double symmetric Schubart-like orbits with two collisions in one period by providing sufficient initial conditions. The results were applied to different sub-problems of the gravitational N-body problem, where singularities occur due to collision. For example, the collinear and the isosceles three-body problems. In the former, three bodies move on a line. In the latter, the bodies are placed at the vertices of an isosceles triangle, such that the distance between the first and third body is equal to the distance between the second and third body.

Martinez also studied the existence of families of double symmetric

Schubart-like periodic orbits having many singularities. She used the blow-up technique which has the effect of replacing the total collision with the collision manifold so that the system can be examined in the neighboured of collision [31].

Moore [42] proposed a topological approach known as the theory of braids to study the motion of N bodies in the plane and found an orbit that is now known as a criss-cross orbit [44]. This orbit was numerically found by Nauenberg [43] for different masses. Later, Nauenberg and Moore [44] extended it to three-dimensional orbits.

Mikkola and Hietarinta in a set of four articles from 1988 to 1993 studied the one-dimensional Newtonian three-body problem[27, 38–40]. They numerically investigated the problem to characterize different types of orbits in the one-dimensional three-body problem with equal masses for both the negative and positive energy of the system [38, 39]. It was explained that the system either has more potential or kinetic energy depending upon the sign of the total energy of the system. If total energy is negative then the system possesses more potential energy and in the case of positive energy of the system, it has more kinetic energy.

For the case of negative energy, the final outcome of the system is either it remains bounded for all time or the system breaks up into a single body and a binary [38]. With positive energy, at least one of the bodies always escapes but the most interesting orbit which is not possible with negative energy is full ionization, where all bodies move independently [39].

Hietarinta and Mikkola [27] classified the types of motion possible in the collinear three-body problem to distinguish the systems that break up and those that remain bounded forever. They explained the bounded

system includes periodic orbits and quasiperiodic orbits. The latter are close to periodic orbits but are not quite periodic. They consider the Schubart region which consists of a set of quasiperiodic regions that surrounds the Schubart orbit. Only for negative energies the existence of such orbits is possible because, as explained earlier, for positive energy one particle always escapes.

The breakup system is characterized by the dwell time or the time during which all three bodies stay close together. If the dwell time is close to zero the system is fast scattering, otherwise, it is chaotic or long interplay. The regions of all types were discovered using a Poincaré section. From the results of Hietarinta and Mikkola's study, it was found that the Schubart orbit and its stability play a vital role in the study of other orbits [27]. If the Schubart orbit is unstable we cannot observe quasiperiodic regions.

Tanikawa and Mikkola [69, 70] explored the structure of the Poincaré section in the one-dimensional three-body problem using symbolic sequences. During this study, a set of symbol sequences is considered instead of the orbit itself for all the possible types of collision in the three-body problem. For example, a triple collision, two binary collisions: first between the bodies m_1 and m_2, and another binary collision between the body m_3 and m_2.

They subdivided the surface of the Poincaré section into five regions using symbolic sequences and constructed a graph for the transition among various regions in the Poincaré section. This graph was used to show the number of periodic orbits in the Schubart region is infinite.

Ouyang and Yan [47] analytically proved the existence of the Schubart-like periodic orbit in the symmetric collinear four-body problem. By

analyzing the regularised Hamiltonian, they used the implicit function theorem and continuity argument on the differential equations of the system to show the existence of this type of periodic orbit. Later, Yan [73] showed analytically the existence of a three-body Schubart orbit. He used the same turning point approach as done previously for the four-body case to avoid the extra collision in the Schubart orbit.

Steves and Roy [59, 58] examined a Caledonian symmetric four-body equal mass problem, Caledonian symmetric few-body systems are characterised by rotational symmetry about the centre of mass (The name originates from the Glasgow Caledonian University, where this four-body problem was modelled). They found analytical solutions in the form of a straight line, a triangle, and a square. It was shown that many of these solutions correspond to Lagrange points of the restricted circular three-body problem by taking two of the masses in the four-body problem equal to zero. They [58] discussed possible types of motions in the Caledonian symmetric N-body problem with $N = 2, 4, 6$.

Steves and Roy [51, 59] also proposed studying the Caledonian symmetric problems for an odd number of bodies by adding one further mass at the centre of the mass of the system of even bodies.

Sweatman [63] investigated the collinear symmetric Newtonian four-body problem with equal masses, where the motion of bodies is restricted to a line and collision between the bodies is perfectly elastic. The system was symmetrically distributed about the centre of mass. To make sure that one pair of bodies will always remain bound the total energy of the system was taken to be negative.

Sweatman found a four-body Schubart orbit by refining the grid of coordinates at the centre of the Poincaré section. It was explained that

the discovered orbits in the collinear four-body problem can be divided into three groups which form distinct regions on the Poincaré section: a quasiperiodic region centered upon a periodic Schubart-like orbit, fast scattering encounters, and a chaotic region between the other regions. He also discussed in detail the stability of the Schubart periodic orbit.

The orbits found in the three regions of the collinear Newtonian four-body problem are similar to those discovered by Mikkola and Hietarinta [38–40] for the three-body problem. For most of the orbits of the four-body problem, the system starts and ends as distinct subsystems of single particles or binaries [63].

Sweatman [64] further extended his study of the collinear symmetric four-body problem in the case of unequal masses and generated a family of periodic orbits. This family starts with a collinear four-body Schubart orbit as discussed above. The family is parametrized by the ratio of the inner and outer masses of a symmetrical system. It was found that three ranges of the mass ratio have stable orbits and three ranges are found to have unstable orbits in unconstrained three-dimensional motion.

Sekiguchi and Tanikawa [53] also examined the one-dimensional Newtonian four-body problem using the symbolic sequences, Poincaré section, and McGehee coordinates [32]. They conducted similar research to that of Tanikawa and Mikkola [69]. The results explored by Sekiguchi and Tanikawa are in agreement with the results of Sweatman [63, 64] and Mikkola and Hietarinta [38–40].

Chenciner and Montgomery [14] proved the existence of the figure eight orbit for the planar three-body problem with equal masses using the variational approach. The special feature of this orbit is that the three bodies move on the same eight-shaped curve. The hip-hop orbit in the

case of a four-body system [13] was explored using the same principle.

Chen [12] proved the existence of a special star-shaped periodic orbit for the planar symmetric four-body problem that consists of two simple identical closed curves. This star-shaped orbit is known as a double choreography orbit, where each pair of bodies share the same path. Initially, the two curves intersect at the vertices of a square, and the configuration of masses periodically changes from a square to collinear but remains a parallelogram at all times.

Ouyang and Xie [46] used the variational method to show the existence of periodic and quasi-periodic orbits for the planar four-body system. They found many stable choreographic solutions for equal and unequal masses, the most interesting one was the stable star pentagon choreographic solution.

Sweatman [65] derived a planar periodic orbit from the equal mass collinear four-body Schubart orbit. It was also suggested that a family of related periodic solutions can be generated using this planar periodic orbit with similar properties to the three-body family explored by Hénon [26].

Chopovda and Sweatman [15] generated a family of planar equal-mass four-body periodic orbits from the Schubart orbit found by Sweatman [63]. The initial orbit for this family was the planar periodic orbit that was numerically discovered by Sweatman [65]. This family starts and ends with the equal mass four-body Schubart orbit. A double choreography orbit is found in the middle of the family and further continuation of orbits after this choreography orbit returns back to the Schubart orbit. This family has a close resemblance with the three-body planar family found by Hénon [26].

Later, Chopovda and Sweatman [16] extended their study of the Caledonian symmetric four-body problem to the Caledonian symmetric few-body problem with unequal masses. The family of periodic orbits was presented for the four-body problem with different mass ratios which exhibits the same properties as in the case of equal masses [15]. The starting orbit of this family is the Schubart orbit with large masses on the outside and it finishes as the Schubart orbit with smaller masses on the outside.

The Caledonian symmetric five-body problem was created by adding another mass m_0 at the centre of mass of the Caledonian symmetric four-body problem. The additional mass remains at rest at all times. Five-body Schubart orbits and double choreography orbits for different mass ratios are presented in this article. It was found that similar families occur for the five-body problem as in the four-body problem [16].

The three- and four-body problems have been studied extensively but there is not much research available to study the six-body problem. The study of the restricted six-body problem started this century. We present here a few articles that investigate the six-body problem in some special cases.

The work of Andreev, Goryainov, and Krasilnikov [5] on finding the best numerical method to study the six-body problem is of particular interest. The numerical algorithms to study the six-body problem are presented in this paper. They considered the implicit Euler method, the explicit second-order Runge-Kutta method, and a pair of semi-implicit methods, the Verlet and D-methods. They investigated the full energy dynamics of the system using these numerical methods. It was observed the explicit and implicit numerical methods change the total energy of the system in the long-run simulations which causes numerical instability. However,

the semi-implicit methods, being symplectic, conserve the total energy of the system and therefore are preferable.

Alsaedi et al. published a paper [4] on the topic of new periodic solutions to the six-body problem. An equal mass six-body system was explored using a variational method and computational algorithm. Two different kinds of periodic solutions were characterised in this study known as weaving periodic solutions and chasing periodic solutions. In weaving style solutions bodies move towards each other in pairs. The chasing style solutions are characterized by the bodies pairwise chasing each other. These solutions possess axial symmetry and are collision-free of bodies.

Idrisi and Ullah [28] recently explored the restricted six-body problem, in which four bodies with equal mass move on a circle about the centre of mass. One pair of bodies always lays on the x-axis and the other on the y-axis. The fifth body is at rest at the centre of mass and a sixth infinitesimal particle move under the gravitational effect of the first five bodies. It was shown that twelve liberation points or Lagrange points exist in the central body square configuration of the restricted six-body problem. They found that the eight Lagrange points lay on the axes while the remaining four are off the axes.

Siddique et al. [54] studied the rhomboidal restricted six-body problem with four bodies at the vertices of a rhombus and a fifth body located at the intersection of diagonals. The sixth body with infinitesimal mass does not influence the motion of other bodies. They investigated the different liberation points in the rhomboidal configuration by varying the mass parameter [55].

1.2.2 Regularization theory

The classical equations of motion for the N-body problem are

$$m_i \frac{d^2\mathbf{r}_i}{dt^2} = \sum_{j \neq i} -\frac{m_i m_j (\mathbf{r}_i - \mathbf{r}_j)}{|\mathbf{r}_i - \mathbf{r}_j|^3}, \quad i = 1, 2, ..., N, \tag{1.1}$$

where $\mathbf{r_i}$ and m_i are, respectively, the position vector and mass of the *i-th* body coordinates. The left-hand side of an equation (1.1) is just mass times acceleration ma and the right-hand side is F_{net} which is given by Newton's inverse square law of gravitational force and the extra power in the denominator balances the length of the vector $\mathbf{r}_i - \mathbf{r}_j$ in the numerator which specifies the direction of the force. The units are chosen such that the gravitation constant is fixed as $G = 1$.

It can be seen from the equation (1.1) that the distance $\mathbf{r}_i - \mathbf{r}_j$ becomes zero and the acceleration, as well as the gravitational attraction, become infinite whenever a collision occurs between two bodies, which correspond to a singularity of equations of motion. Similarly, if the bodies pass by each other very closely, a near collision event happens and the velocities of such bodies become very large. Both collision and near-collision events present a problem with numerical techniques used to study the motions of such bodies.

The regularization theory was developed in order to transform singular differential equations into regular ones and to provide an efficient mathematical technique to study the motion of bodies near collisions.

1.2.3 Types of regularization

In celestial mechanics, regularization is performed by transforming the variables that appear in the differential equations of motion. Poincaré was

the first who gave the idea to transform the independent variable in the Hamiltonian system. The time t is transformed to a new independent variable τ by defining the relation $t = g(p, q)\tau$, where p and q are, momentum and position coordinates of the system and g is a function to be chosen.

The Hamiltonian $H(p, q)$ of the system is extended to a new Hamiltonian Γ by adding the time and energy to $H(p, q)$. The basic idea behind this was to separate the time as a coordinate and as an evolution parameter in order to make all the desired coordinate changes and to describe the evolution no matter the coordinates.

The extended Hamiltonian $\Gamma(p, q, t, E)$, takes the form [35]

$$\Gamma = g(p, q)(H(p, q, t) - E), \tag{1.2}$$

where the energy E is the constant numerical value of the Hamiltonian. The equations of motion of the extended Hamiltonian [1, 35] Γ are

$$\begin{aligned} \frac{dt}{d\tau} &= -\frac{\partial \Gamma}{\partial E} = g, \\ \frac{dp}{d\tau} &= -\frac{\partial \Gamma}{\partial q}, \\ \frac{dE}{d\tau} &= \frac{\partial \Gamma}{\partial t}, \\ \frac{dq}{d\tau} &= \frac{\partial \Gamma}{\partial p}. \end{aligned} \tag{1.3}$$

These equations give us the same equations as in the original Hamiltonian by applying the chain rule. From relation (1.3) we see the equations of position and momentum are similar to those of time and energy only with a difference in sign. The energy $-E$ acts as a component of momentum and the vector $(p, -E)$ will change as a covector under the coordinate transformation. This can be noticed by rewriting equations (1.3) as

follows

$$\begin{aligned} \frac{dt}{d\tau} &= \frac{\partial \Gamma}{\partial(-E)} = g, \\ \frac{dp}{d\tau} &= -\frac{\partial \Gamma}{\partial q}, \\ \frac{dq}{d\tau} &= \frac{\partial \Gamma}{\partial p}, \\ \frac{d(-E)}{d\tau} &= -\frac{\partial \Gamma}{\partial t}. \end{aligned} \tag{1.4}$$

Bettis and Szebehely [6] explained that the original regularization of the two-body problem as suggested by Sundman [62] uses the transformation of the form

$$d\tau = \frac{dt}{d}, \tag{1.5}$$

where d is the distance between two bodies. This equation shows the new time τ depends on the original time t and distance d.

This technique is useful for the change of the step size during numerical integration. When d becomes smaller, the time-step of integration, Δt, also decreases in order to accommodate the large changes occurring on the right-hand side of the equations to be integrated. But changing the step size of integration does not eliminate the singularity, because when bodies encounter a singularity the integration steps increase beyond a limit. Bettis and Szebehely also discussed that instead of distance $g = d$ some other choices can be made for the function g and found that the $g = d^{3/2}$ is the most advantageous choice for a transformation as compared to $g = d^2$ and $g = d$ [6].

Later, many choices of the function g were suggested by investigators. Szebehely [68] used the inversion of the velocity vector as the function

of g. Aarseth and Zare [1, 36, 3] considered the function g of the form

$$g = \prod_{i<j} q_{ij}, \quad q_{ij} = \mathbf{r}_i - \mathbf{r}_j, \quad i = 1, 2, ..., N. \tag{1.6}$$

The choice of function g as the inverse of potential $g = 1/U$ and inverse of Lagrangian $g = 1/L, \quad L = T - U$ was also explored [6, 3], where T is the kinetic energy of the system.

Heggie [23] proposed a transformation for the simultaneous collision of the N-body problem in the form

$$g = \frac{\prod_{i<j} q_{ij}}{\left(\sum_{i<j} q_{ij}\right)^{\alpha}}, \quad \alpha = \frac{N(N-1) - 3}{2}, \quad i = 1, 2, ..., N. \tag{1.7}$$

It was also recognized in [6] that regularizations involving only the transformation of independent variables do not offer the best formulation for numerical work. In contrast, transformations with both independent and dependent variables are more useful to obtain regular differential equations. The standard regularization technique that is used to regularize the singularity that appears in the equations of motion during the collision of bodies is based on three steps [11]. These three steps involve the canonical transformation of both independent and dependent variables and are explained in Figure 1.1.

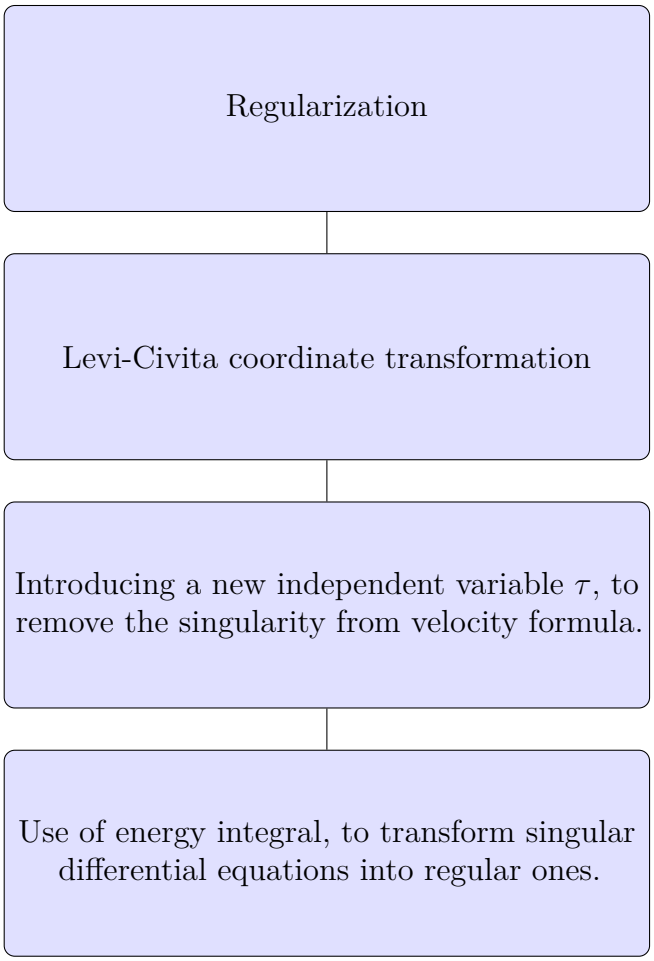

Figure 1.1 Three basic steps of a standard regularization scheme.

In 1920, Levi-Civita introduced regularization in the plane by defining the coordinate transformation of the form [10]

$$u + iv = (Q_1 + iQ_2)^2 = Q_1^2 - Q_2^2 + 2iQ_1Q_2.$$

After simplification

$$\begin{aligned} u(Q_1, Q_2) &= Q_1^2 - Q_2^2, \\ v(Q_1, Q_2) &= 2Q_1Q_2. \end{aligned}$$

Consider the Hamiltonian that describes the two-body problem

$$H = \frac{1}{2}(p_1^2 + p_2^2) - \frac{1}{\sqrt{q_1^2 + q_2^2}}.$$

The canonical transformation was made using the generating function of the form

$$F(p_1, p_2, Q_1, Q_2) = p_1(Q_1^2 - Q_2^2) + 2p_2Q_1Q_2,$$

where the generating function F (see for detail Section 2.1.1 of Chapter 2) describes the transformation between the old and new coordinates of the system. Now a relation between old and new coordinates associated with generating function F was given by

$$\begin{aligned} q_1 &= \frac{\partial F}{\partial p_1} = Q_1^2 - Q_2^2, \\ q_2 &= \frac{\partial F}{\partial p_2} = 2Q_1Q_2, \\ P_1 &= \frac{\partial F}{\partial q_1} = 2p_1Q_1 + 2p_2Q_2, \\ P_2 &= \frac{\partial F}{\partial q_2} = -2p_1Q_2 + 2p_2Q_1, \end{aligned} \tag{1.8}$$

where p_1, p_2, q_1, q_2 and Q_1, Q_2, P_1, P_2 are physical and regularised coordinates.

Another important property of the Levi-Civita regularization is that it halves the angles in the regularised coordinates. If we represent the angle between the position vector and origin by θ in physical coordinates and in regularised coordinates by ϕ, we have

$$\tan\theta = \frac{q_2}{q_1} = \frac{2Q_1Q_2}{Q_1^2 - Q_2^2} = \frac{2.\frac{Q_2}{Q_1}}{1 - (\frac{Q_2}{Q_1})^2} = \frac{2\tan\phi}{1 - \tan^2\phi} = \tan 2\phi.$$

The Levi-Civita transformation can be expressed in matrix notation

$$\begin{pmatrix} q_1 \\ q_2 \end{pmatrix} = \begin{pmatrix} Q_1 & -Q_2 \\ Q_2 & Q_1 \end{pmatrix} \begin{pmatrix} Q_1 \\ Q_2 \end{pmatrix}. \tag{1.9}$$

The 2×2-matrix on the right-hand side $L = \begin{pmatrix} Q_1 & -Q_2 \\ Q_2 & Q_1 \end{pmatrix}$ is a Levi-Civita matrix and has the following properties

- The matrix L is an orthogonal matrix
- The elements of this matrix L are linear and homogeneous functions of the regularised coordinates Q_1 and Q_2.
- The first column of matrix L is the Q-vector.

Following the Levi-Civita coordinate transformation, Waldvogel [71] proposed a new regularization scheme to study the planar three-body problem. He performed the coordinate transformation using a polynomial of degree four together with a suitable time transformation to regularize the three binary collisions so that the triple collision can only be approached asymptotically. Later, Hénon [25, 26] used this regularization technique to explore the families of planar three-body orbits.

In 1933, Hurwitz showed that the Levi-Civita transformation can not be generalized to three dimensions because no 3×3-matrix exists that satisfies all three properties of the Levi-Civita matrix, However, this transformation can be extended to four dimensions [6]. Later, Kustaanheimo and Stiefel introduced a new regularization scheme that uses a transformation from four dimensions to three dimensions. Using this transformation Kustaanheimo and Stiefel generalized the Levi-Civita coordinate transformation to three dimensions by defining two four-

dimensional vectors [60] as follows

$$\begin{aligned} q_1 &= Q_1^2 - Q_2^2 - Q_3^2 + Q_4^2, \\ q_2 &= 2(Q_1 Q_2 - Q_3 Q_4), \\ q_3 &= 2(Q_1 Q_3 + Q_2 Q_4), \\ q_4 &= 0. \end{aligned}$$

This was found very useful and is widely used to study the N-body problem.

Aarseth and Zare [1, 2] extended the K-S transformation to a three-body problem. Later, it was extended to the N-body problem by Mikkola and Aarseth [37] and is known as the chain method. This method is based on the fact that for N-body systems a chain of shortest interbody distance vectors can be made in such a way that all the interactions that require regularization are included in the chain. The chained vectors are regularised using the K-S regularization scheme and a time transformation. After every integration step, it is checked if non-chained vectors become smaller in magnitude compared to the chained vectors, and a new chain is made that includes these smaller magnitude vectors.

Heggie [23] discovered a global regularization scheme for the N-body problem. This method simultaneously regularizes all possible two-body collisions. In this method, all the interbody distance vectors are regularised using the K-S transformation. However, this makes the original formulation more complex by increasing the number of differential equations. In 1985, Mikkola [34] introduced a modified notation for the coordinates. This made the use of the Heggie global regularisation more straightforward.

Sivasankaran, Steves, and Sweatman [56] used the Levi-Civita regu-

larization to integrate the Caledonian symmetric four-body problem along with a time transformation similar to the one proposed by Heggie described earlier in equation (1.5). Their regularization scheme allowed them to study close encounters and collision events. It was tested on a range of orbits of the Caledonian symmetric four-body problem, they concluded this scheme has good energy conservation properties.

Alexander [3] conducted a comparison of different regularization schemes, including Zare [1], Aarseth-Zare formulation [36, 37], and Heggie with Mikkola's modification [23, 34], with different time transformations for integrating the three-body and four-body systems. He found the Heggie global regularization together with the time transformation as the inverse of the Lagrangian $1/L$, and the chain regularization scheme both are good. However, the chain regularization scheme is more efficient because it has fewer equations than the Heggie global regularization.

We present here a very simple example to explain how the regularization technique helps to remove the singularity from the differential equations of the system [10]. Consider a two-body system, where two bodies with masses m_1 and m_2 move on a straight line and interact with each other through Newton's law of gravitation. The equation of motion of this system is

$$\ddot{r} + \frac{K}{r^2} = 0, \quad K = G(m_1 + m_2). \tag{1.10}$$

The corresponding energy integral is given by

$$H = \frac{K}{r} - \frac{1}{2}\dot{r}^2. \tag{1.11}$$

It can be seen from the equation (1.10), the distance between two bodies becomes zero ($r = 0$) at the collision and the velocity $\dot{r} = \pm\sqrt{2(\frac{K}{r} - H)}$ becomes infinite. To remove this singularity we perform Levi-Civita

coordinate transformation (a change of coordinates) by introducing $r = Q^2$ together with a time transformation $dt = rd\tau = Q^2 d\tau$.

The equation of motion after the transformations takes the form

$$Q^{''} - \frac{1}{Q}Q^{'2} + \frac{K}{2Q} = 0, \tag{1.12}$$

where $Q^{'} = \frac{dQ}{d\tau}$, $\dot{Q} = \frac{dQ}{dt} = \frac{dQ}{d\tau}\frac{d\tau}{dt} = \frac{1}{Q^2}Q^{'}$ and similarly, $\ddot{Q} = \frac{1}{Q^4}Q^{''} - \frac{2}{Q^5}Q^{'2}$. While the energy integral is given by

$$H = \frac{K}{Q^2} - \frac{2Q^{'2}}{Q^2}. \tag{1.13}$$

The new velocity takes the form

$$Q^{'} = \pm\sqrt{\frac{K}{2} - \frac{HQ^2}{2}} \tag{1.14}$$

It follows from the equation (1.14) that the transformations removed the singularity from the velocity equation but the equation of motion is still singular. To remove the singularity from the equation of motion we finally make use of energy integral.

Rewrite the equation of motion (1.12)

$$Q^{''} + \frac{1}{2}\left(\frac{K}{Q^2} - \frac{2Q^{'2}}{Q^2}\right)Q \;\; = \;\; 0. \tag{1.15}$$

Making use of equation 1.13 in the above equation, we have

$$Q^{''} + \frac{H}{2}Q = 0. \tag{1.16}$$

which is the equation of a harmonic oscillator with frequency $w = \sqrt{\frac{H}{2}}$. Relating this to the original two-body system (equation (1.11)), the negative values of H, $H < 0$, correspond to elliptic motion, and $H = 0$, corresponds to parabolic motion. Thus we conclude that the above regularizing technique helped to obtain a regular differential equation and the solution of this differential equation is a periodic function of τ.

1.3 Poincaré map

Poincaré was the first who proposed a classical technique now known as the Poincaré map to visualize the periodic trajectories of dynamical systems. The Poincaré map, also known as the first recurrence map, is a discrete dynamical system that represents the periodic flow of a continuous dynamical system.

The usefulness of the Poincaré map lies in the fact that it analyzes the original continuous dynamical system in a simpler way by replacing the continuous dynamical system of Nth order with a lower-dimensional $(N-1)th$ order discrete dynamical system.

Consider an example of an N-dimensional system [61]

$$\dot{r} = f(r). \tag{1.17}$$

To find the Poincaré map P a lower dimensional $(N-1)th$ order surface of section Σ is defined that is transverse to the flow, meaning the flow is not along the direction of the section as shown in Figure 1.2. The Poincaré map is a mapping from Σ to itself, found by following the trajectories from one intersection r_n of Σ to the next intersection r_{n+1}. So, it can be written as

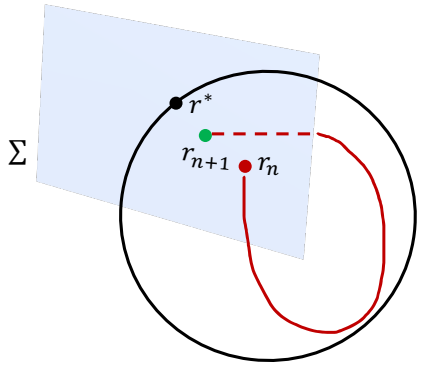

Figure 1.2 Projection of different points by a Poincaré map.

$$r_{n+1} = P(r_n). \tag{1.18}$$

This map tells us if one starts at some point r_n of this section and moves forward in time it will next intersect the section at point r_{n+1}, similarly, it sends the point r_{n+1} to r_{n+2} and so on as shown in Figure 1.2. If r^* is a fixed point of P, then a trajectory that starts at point r^* returns back to the same point after some time, that is

$$r^* = P(r^*). \tag{1.19}$$

We compute a Poincaré map for the six-body problem with aligned triangles from a 10×18 grid of initial values as presented in Figure 2.14. This map helps to characterize the possible types of motion in the aligned case of the six-body problem with equal masses. Some typical and non-typical orbits are explored using the Poincaré map and are presented in Chapter 2.

Chapter summary

In this chapter, we provided a description of our project, the computational study of the planar symmetric six-body problem. Most of the chapter is dedicated to a review of the research on few-body problems. This primarily consists of the search and existence of the Schubart orbit and searches for the family of periodic orbits. We mostly focus on symmetric problems.

The collisions and near-collision events between any two bodies correspond to a singularity in the equations of motion. Therefore, it is necessary to discuss the techniques to transform singular equations into regular ones. We, therefore, dedicated another part of this review to the types of regularization techniques for the equations of motion of the few-body problem.

We presented a simple definition and explanation of the Poincaré map in the last section of this chapter. This map is a helpful tool for analyzing the periodic, quasiperiodic, and their neighbouring orbits in few-body problems.

In the next chapter, we will introduce and analyze the six-body problem with aligned triangles.

Chapter 2

The symmetric six-body problem with aligned triangles

In this chapter, we analyze a six-body system with aligned triangles following the approach of Hietarinta and Mikkola for the one-dimensional Newtonian three-body problem [38–40] and Winston Sweatman for the symmetrical one-dimensional Newtonian four-body problem [63, 64].

The study of the six-body system with aligned triangles is much simpler than the general six-body problem. The analytical and numerical analysis of general N-body problems has proved to be very complicated. Understanding simpler few-body systems, for example, six-body systems with aligned and non-aligned triangles can provide useful information and ideas for analyzing the general problem.

In the first section of this chapter, we describe the initial configuration of our system, where the system is symmetrically distributed about the centre of mass. We use Levi-Civita regularisation for our equations of motion. The transformed equations are integrated using a Runge-Kutta method. In subsection 2.1.2 we describe the initial conditions of the six-body system. As in the three-body and four-body cases, the selection of initial values can be reduced to a two-dimensional space, which is

explored using a 100×180 grid.

In the second section, we present some typical and special orbits of which an important one is the Schubart orbit.

We use the results of the aligned case to initiate the search for the family of periodic orbits in the non-aligned case, which is presented in Chapters 4 and 5. Starting from the collinear motion of the Schubart orbit, an equal mass family of periodic orbits is generated and presented in Chapter 5.

2.1 Six-body system

2.1.1 Derivation of equations

Figure 2.1 below shows a system of six bodies, which are placed at the vertices of two aligned concentric equilateral triangles. The bodies are labelled as b_1, b_2, b_3, b_4, b_5 and b_6, where the outer triangle (black) carries the bodies b_1, b_3 and b_5 with masses m_1, m_3 and m_5, and the inner equilateral triangle (yellow) has the bodies b_2, b_4 and b_6 with masses m_2, m_4 and m_6. The system remains symmetrically distributed about the centre of mass D. Let x_1 and x_2 be the distances from the centre of mass D to b_1 and b_2, respectively. We calculate distance x_3 between the bodies b_1 and b_3 and distance x_4 between the bodies b_1 and b_4 in terms of x_1 and x_2. The remaining distances are symmetric about the centre of mass. This implies that if we know the position of b_1 and b_2 then we can specify the positions of all other bodies because of the symmetry.

The total energy of the planar symmetric six-body problem is constant and is fixed as $E = K + U = -1$, where

$$K = \frac{3}{2} m_1 \dot{x}_1^2 + \frac{3}{2} m_2 \dot{x}_2^2, \tag{2.1}$$

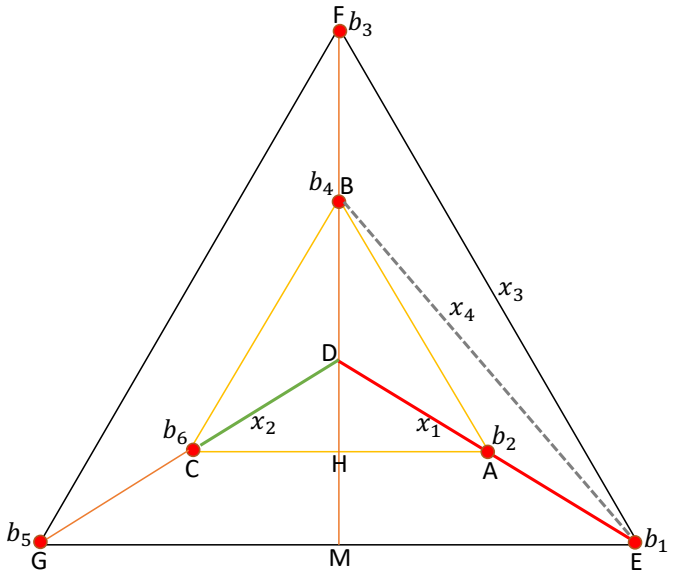

Figure 2.1 Six-body system: b_i are bodies and x_i are distances between the bodies and from the centre of mass.

is the kinetic energy of the system, and

$$U = -\frac{3m_1^2}{|EF|} - \frac{3m_2^2}{|AB|} - \frac{3m_1m_2}{|AE|} - \frac{6m_1m_2}{|EB|}, \tag{2.2}$$

is the potential energy of the six-body system with interbody distances $|EF|$, $|AB|$, $|AE|$, and $|EB|$. We are dealing with equal masses, so, we choose $m_1 = m_2 = 1$ in equations 2.1 and 2.2. The resulting equations are

$$K = \frac{3}{2}\dot{x}_1^2 + \frac{3}{2}\dot{x}_2^2, \tag{2.3}$$

and

$$U = -\frac{3}{|EF|} - \frac{3}{|AB|} - \frac{3}{|AE|} - \frac{6}{|EB|}. \tag{2.4}$$

The negative sign of potential energy indicates that for gravitational systems, the reference point or zero of potential energy is at infinite separation. The potential energy is the work done in bringing an object

from an infinite distance to a finite distance r, so, when an object moves from infinity to distance r its kinetic energy increases at the expense of the potential energy. So if the potential energy was zero at infinite separation, it must decrease from zero at a finite distance r.

The reason for fixing the total energy of our system $E = -1$ is that we require our system to have more potential energy in magnitude than kinetic energy. In general, this makes sure that at least one pair of bodies stays bound for all time. Otherwise, the system possesses enough kinetic energy to move toward infinity, and therefore the system would not be bounded. If the total energy has a positive value, the system will fall apart with at least one of the bodies moving away. Mikkola and Hietarinta discussed the possible motion of bodies in the case of positive energies for the collinear three-body problem [39].

Now we calculate the interbody distances for our six-body system. First, we calculate the distances $AH = \frac{\sqrt{3}}{2}x_2$ and $DM = \frac{1}{2}x_1$ using the right-angle triangles AHD and EMD, respectively with $\angle E = \angle A = 30°$, $AD = x_2$ and $ED = x_1$.
The distance between the bodies b_1 and b_2, AE, is $x_1 - x_2 = ED - AD$.
The distance between the bodies b_2 and b_4 is $AB = \sqrt{3}x_2$, which is calculated using the right-angle triangle AHB with $\angle B = 60°$ and $AH = \frac{\sqrt{3}}{2}x_2$.
The distance between b_1 and b_3, EF, is $x_3 = \sqrt{3}x_1$, which is computed using the right-angle triangle EMF with $\angle E = 60°$ and $FM = \frac{3}{2}x_1 = FD + DM$.
The distance between b_1 and b_4, EB, is $x_4 = \sqrt{x_1^2 + x_1x_2 + x_2^2}$, that is computed by making use of the right-angle triangle EMB.

These calculations show that the symmetric six-body system has the

Hamiltonian

$$H = \frac{w_1^2}{6} + \frac{w_2^2}{6} - \frac{\sqrt{3}}{x_1} - \frac{\sqrt{3}}{x_2} - \frac{3}{x_1 - x_2} - \frac{6}{\sqrt{x_1^2 + x_1 x_2 + x_2^2}}, \qquad (2.5)$$

where w_1 and w_2 are the conjugate momenta to x_1 and x_2 and these are calculated using the Lagrangian ($L = T - U$), where $w_i = 3\dot{x}_i = \frac{\partial L}{\partial \dot{x}_i}$ for $i = 1, 2$. To overcome the singularity in Eq.(2.5), we introduce two new coordinates relating to the interbody distances

$$q_1 = x_1 - x_2, \quad q_2 = x_2. \qquad (2.6)$$

The corresponding conjugate momenta p_i are found using a generating function. The generating function F is defined such that the transformation from old coordinates to new coordinates is a canonical transformation. Indeed, the generating function F is helpful for describing the exact form of canonical transformation only if F is a function of the old plus new variables, where old and new coordinates are separately independent (Goldstein [19], pp.371−375 and Cline [17] pp.15.3.1−15.3.3).

The generating function of the six-body system is

$$F = \sum p_i q_i(x_i) \quad = \quad p_1(x_1 - x_2) + p_2 x_2, \qquad (2.7)$$

and, the required conjugate momenta are (see Appendix A for detail)

$$w_i = \frac{\partial F_2}{\partial x_i}, \qquad (2.8)$$

$$w_1 = p_1, \quad w_2 = p_2 - p_1. \qquad (2.9)$$

This results in a new form for the Hamiltonian

$$H = \frac{p_1^2}{3} + \frac{p_2^2}{6} - \frac{p_1 p_2}{3} - \frac{3}{q_1} - \frac{\sqrt{3}}{q_2} - \frac{\sqrt{3}}{q_1 + q_2} - \frac{6}{\sqrt{q_1^2 + 3q_1 q_2 + 3q_2^2}}. \qquad (2.10)$$

The system (2.10) is regularised using a Levi-Civita regularisation by setting $q_i = Q_i^2$. This regularisation removes two- and three-body singularities of the equations of motion.

To find the canonical momenta corresponding to Q_i, we choose the generating function

$$G = \sum p_i q_i(Q_i) \quad = \quad p_1 Q_1^2 + p_2 Q_2^2. \tag{2.11}$$

which gives us the new canonical momenta

$$P_i = \frac{\partial G}{\partial Q_i} = 2 p_i Q_i. \tag{2.12}$$

Now the Hamiltonian takes the form

$$\begin{aligned} H &= \frac{P_1^2}{12Q_1^2} + \frac{P_2^2}{24Q_2^2} - \frac{P_1 P_2}{12 Q_1 Q_2} - \frac{3}{Q_1^2} - \frac{\sqrt{3}}{Q_2^2} - \frac{\sqrt{3}}{Q_1^2 + Q_2^2} \\ &- \frac{6}{\sqrt{Q_1^4 + 3Q_1^2 Q_2^2 + 3Q_2^4}}. \end{aligned} \tag{2.13}$$

We also perform the time transformation from t to τ given by

$$\frac{dt}{d\tau} = q_1 q_2 = Q_1^2 Q_2^2. \tag{2.14}$$

Now the regularised Hamiltonian can be calculated using the expression

$$\Gamma = \frac{dt}{d\tau}(H - E). \tag{2.15}$$

The resulting Hamiltonian is

$$\begin{aligned} \Gamma &= \frac{P_1^2 Q_2^2}{12} + \frac{P_2^2 Q_1^2}{24} - \frac{P_1 P_2 Q_1 Q_2}{12} - \sqrt{3} Q_1^2 - 3 Q_2^2 - \frac{\sqrt{3} Q_1^2 Q_2^2}{Q_1^2 + Q_2^2} \\ &- \frac{6 Q_1^2 Q_2^2}{\sqrt{Q_1^4 + 3Q_1^2 Q_2^2 + 3Q_2^4}} - Q_1^2 Q_2^2 E, \end{aligned} \tag{2.16}$$

where E is the energy − the constant numerical value of the Hamiltonian. For the six-body system, we have four equations of motion to combine with the time equation by using the formulae

$$\frac{dQ_i}{d\tau} = \frac{\partial \Gamma}{\partial P_i}. \tag{2.17}$$

$$\frac{dP_i}{d\tau} = -\frac{\partial \Gamma}{\partial Q_i}. \tag{2.18}$$

The equations (2.17) and (2.18) are the equations of motion corresponding to the regularised Hamiltonian 2.16.

The resulting equations are

$$\frac{dQ_1}{d\tau} = \frac{P_1 Q_2^2}{6} - \frac{Q_1 Q_2 P_2}{12}, \tag{2.19}$$

$$\frac{dQ_2}{d\tau} = \frac{P_2 Q_1^2}{12} - \frac{Q_1 Q_2 P_1}{12}, \tag{2.20}$$

$$\begin{aligned}\frac{dP_1}{d\tau} &= \frac{-P_2^2 Q_1}{12} + \frac{Q_2 P_1 P_2}{12} + \frac{2\sqrt{3}Q_1 Q_2^2}{Q_1^2+Q_2^2} - \frac{2\sqrt{3}Q_1^3 Q_2^2}{(Q_1^2+Q_2^2)^2} + 2\sqrt{3}Q_1 \\ &+ \frac{12Q_1Q_2^2}{\sqrt{Q_1^4+3Q_1^2Q_2^2+3Q_2^4}} - \frac{12Q_1^5Q_2^2}{\sqrt{(Q_1^4+3Q_1^2Q_2^2+3Q_2^4)^3}} \\ &- \frac{18Q_1^3Q_2^4}{\sqrt{(Q_1^4+3Q_1^2Q_2^2+3Q_2^4)^3}} + 2Q_1Q_2^2E,\end{aligned} \tag{2.21}$$

$$\begin{aligned}\frac{dP_2}{d\tau} &= \frac{-P_1^2 Q_2}{6} + \frac{Q_1 P_1 P_2}{12} + \frac{2\sqrt{3}Q_1^2 Q_2}{Q_1^2+Q_2^2} - \frac{2\sqrt{3}Q_1^2 Q_2^3}{(Q_1^2+Q_2^2)^2} + 6Q_2 \\ &+ \frac{12Q_1^2Q_2}{\sqrt{Q_1^4+3Q_1^2Q_2^2+3Q_2^4}} - \frac{18Q_1^4Q_2^3}{\sqrt{(Q_1^4+3Q_1^2Q_2^2+3Q_2^4)^3}} \\ &- \frac{36Q_1^2Q_2^5}{\sqrt{(Q_1^4+3Q_1^2Q_2^2+3Q_2^4)^3}} + 2Q_1^2Q_2E,\end{aligned} \tag{2.22}$$

$$\frac{dt}{d\tau} = Q_1^2 Q_2^2. \tag{2.23}$$

The four equations of motion and that of time are integrated using ode45 in MATLAB.

2.1.2 Selection of initial values

To characterize the orbit we use four parameters: x_1, x_2, $\dot{x_1}$, $\dot{x_2}$. By using the scaling invariances of the Hamiltonian we choose $E = -1$, reducing the parameters to three, and then choose the origin of time so that the ratio $\frac{x_2}{x_1}$ takes a fixed value at $t = 0$. The quantity $\frac{x_2}{x_1}$ takes all possible values in the interval $[0, 1]$ in the case of ordinary trajectories. But we note that there exists a special solution, a so-called homothetic solution, for which the quantity $\frac{x_2}{x_1}$ is independent of time and has a fixed value

$$\frac{x_2}{x_1} = \alpha.$$

To find this orbit and value of α, we substitute $x_2 = \alpha x_1$ and $w_2 = \alpha w_1$ into the equations of motion obtained from the Hamiltonian 2.5 [27] and require that both pairs of equations, for x_1 and w_1, are consistent. These lead to the one-dimensional two-body problem $\ddot{x} = -\frac{\tilde{R}}{x^2}$, where $\tilde{R}$ is a function of α. This is analytically solvable and yields a periodic orbit, called the homothetic sextuple collision orbit of the six-body system as represented in Figure 2.11 in Section 2.2.1. This sextuple collision orbit is regular but an orbit close to it can have a very different outcome. The consistency condition yields the equation

$$\begin{aligned}(\sqrt{3}\alpha^5 - 2\sqrt{3}\alpha^4 + (\sqrt{3}+3)\alpha^3 + (-\sqrt{3}+3)\alpha^2 + 2\sqrt{3}\alpha - \sqrt{3}) \times \\ (\alpha^2+\alpha+1)^{3/2} + 3\alpha^6 - 6\alpha^5 + 6\alpha^3 - 3\alpha^2 = 0, \qquad (2.24)\end{aligned}$$

which has one real root which is approximately $\alpha = 0.3977437537$.

We choose $\frac{x_2}{x_1} = \alpha$ at time $t = 0$ that ensures that every orbit crosses the surface of the Poincaré section at least once. We choose new coordinates R (sum of distances q_1, q_2) and θ (related to kinetic energy between particles) as done previously by Hietarinta and Mikkola [27].

The position coordinate on the section is

$$R = x_1 = q_1 + q_2, \tag{2.25}$$

and the corresponding energy, when $\frac{x_2}{x_1} = \alpha$, is

$$E = T - \frac{1}{R}\left(\sqrt{3} + \frac{\sqrt{3}}{\alpha} + \frac{3}{1-\alpha} + \frac{6}{\sqrt{1+\alpha+\alpha^2}}\right). \tag{2.26}$$

The maximum value $R_{\max}$ of R for the fixed total energy $E = -1$ is obtained from equation (2.26) when the velocities vanish in equation (2.26). The maximum value of R is

$$R_{\max} = \frac{1}{|E|}\left(\sqrt{3} + \frac{\sqrt{3}}{\alpha} + \frac{3}{1-\alpha} + \frac{6}{\sqrt{1+\alpha+\alpha^2}}\right). \tag{2.27}$$

To find the remaining coordinate θ, we choose something related to momenta but we want the kinetic energy independent of this quantity and we also impose another condition that the homothetic sextuple collision orbit is located on the line $\theta = 0$. Thus, we diagonalize the kinetic energy part T in H by writing it as the sum of squares

$$T = (a_{11}\dot{x_1} + a_{12}\dot{x_2})^2 + (a_{21}\dot{x_1} + a_{22}\dot{x_2})^2, \tag{2.28}$$

noting that $\dot{x_i}$ can be parametrised as follows

$$\sqrt{T}\cos(\theta) = a_{11}\dot{x_1} + a_{12}\dot{x_2}, \tag{2.29}$$

$$\sqrt{T}\sin(\theta) = a_{21}\dot{x_1} + a_{22}\dot{x_2}. \tag{2.30}$$

We find the constants a_{ij} such that $\frac{\dot{x_2}}{\dot{x_1}} = \frac{x_2}{x_1} = \alpha$, at $\theta = 0$ and making use of equations 2.3, 2.28, 2.29 and 2.30, which give $a_{11} = a_{22} = \frac{\sqrt{3}}{\sqrt{2(1+\alpha^2)}}$,

$a_{12} = \frac{\sqrt{3}\alpha}{\sqrt{2(1+\alpha^2)}}$ and $a_{21} = -a_{12}$.

Substituting the values of a_{ij} into equations 2.29 and 2.30 gives

$$\theta = \arctan\left(\frac{\dot{x}_2 - \alpha\dot{x}_1}{\dot{x}_1 + \alpha\dot{x}_2}\right), \tag{2.31}$$

where θ takes values from the interval $0 \leq \theta < \pi$. It should be noted that by replacing θ with $\pi - \theta$, we find the same orbit but with opposite directions of velocities.

2.2 Results and analysis

The equations of motion for our six-body system $(2.19 - 2.23)$ are integrated using the standard MATLAB's ode45 integrator with the initial conditions described in Section 2.1.2. The ode45 integrator uses a combination of 4th and 5th-order Runge-Kutta methods in order to calculate the stepsize for error reduction. We compute a Poincaré map using the event location option in ode45. This helps us find some typical and non-typical trajectories of which an important one is the Schubart orbit, presented in Figure 2.13.

2.2.1 Characterization of trajectories

A selection of different trajectories is shown in Figure 2.2. To find these trajectories we integrated our six-body system both forward and backward in time from an initial condition (described in Section 2.1.2). The orbits found for our six-body system can be roughly grouped into two main classes: one is those that stay bound (Bounded orbits) and the other is those that break up (If the orbit is not bounded for all times the system breaks up in the past and in the future.)

1. **Bounded orbits:** These are the orbits where the system stays together at all times and bodies do not escape as subsystems. Bounded orbits may be further subdivided into

   (a) Quasiperiodic orbits: These orbits are close to but not quite periodic.

   (b) Periodic orbits: The special one is the Schubart orbit.

2. **Scattering orbits:** These are trajectories where the system breaks up, which means the bodies are heading away from each other and escape as distinct subsystems such as binaries, single stars, or trinaries. The system still possesses constant negative energy, $E = -1$, because of the potential energy within each of the bound multi-body subsystems. When this potential energy is large in magnitude, then the velocity of the escaping entity may also be large. For the scattering orbits possible types of motion can be divided into the following groups,

   (a) When $x_1 \to \infty$ and x_2 is finite (where x_1 and x_2 are the distances of the bodies b_1 and b_2 from the centre of mass), we observe a central trinary with three single bodies moving independently

   (b) Three separate binaries moving independently when $x_1 \to \infty$, $x_2 \to \infty$ and $x_1 - x_2$ is finite.

In our case, most of the orbits are of the type described in points 2(a) and 2(b). The full ionization case, where the system breaks up into six separate bodies is only possible with positive total energy [39]. As the total energy in our case is $E = -1$, the full ionization case does not occur.

In a more detailed classification scattering orbits can be further categorized as fast-scattering orbits where bodies escape as subsystems after a

single close interaction of the whole system; and chaotic scattering orbits where the six bodies come together multiple times. In between these close encounters in the chaotic scattering orbit, the system temporarily divides into subsystems.

Figures 2.2− 2.13 show some examples of general and periodic orbits in the aligned case. It should be noted bodies b_1 and b_2 do not swap their position. In other words, the bodies preserve their order on the line and we always have $q_1 > q_2$ in this case. In the collinear limit of the two-body interaction, the bodies behave as if they undergo a perfect elastic bounce. Consequently, we get a reflection where the bodies cannot change their initial order on the line.

Figures 2.2−2.5 show plots of fast-scattering orbits. In Figure 2.2 a fast-scattering orbit begins as a central trinary with three single bodies and finishes as three separate binaries. Figure 2.3 represents a fast-scattering orbit that starts and finishes as three separate binaries. The start and end structure of the system is the same in Figure 2.4, a central trinary with three single bodies, while in Figure 2.5 the system starts as three separate binaries and escapes as three single bodies with a central trinary.

Chaotic scattering orbits are shown in Figures 2.6−2.10. The homothetic sextuple collision orbit is shown in Figure 2.11. This orbit has an essential singularity at both sides that can not be regularized. If we perturb the system, then on one side it separates as a tightly bound binary, and on the other side it separates as a single body with a central trinary, as shown in Figures 2.9 and 2.10.

Figures 2.9 and 2.10 illustrate orbits that pass close to homothetic sextuple collision. The contraction of a system increases the binding

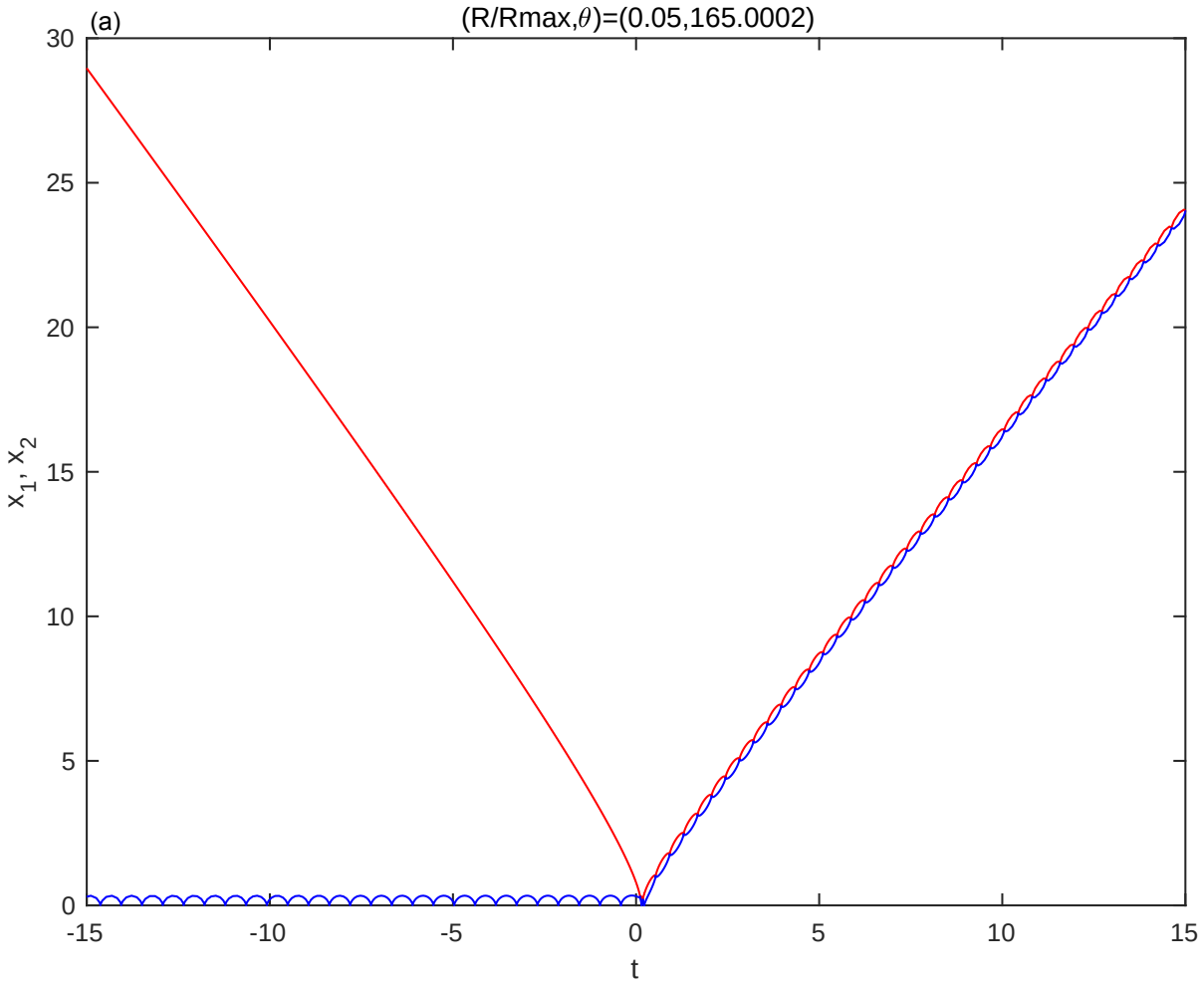

Figure 2.2 Fast scattering orbit: The system begins as three single bodies with a central trinary and finishes as three separate binaries. The initial value for this plot is $(R/R_{\max}, \theta) = (0.05, 165.0002)$. The total energy $E = -1$, $m_i = 1$ for $i = 1, 2, ...6$ and the system is symmetric about the centre of mass. Red and blue lines represent the bodies b_1 and b_2, respectively.

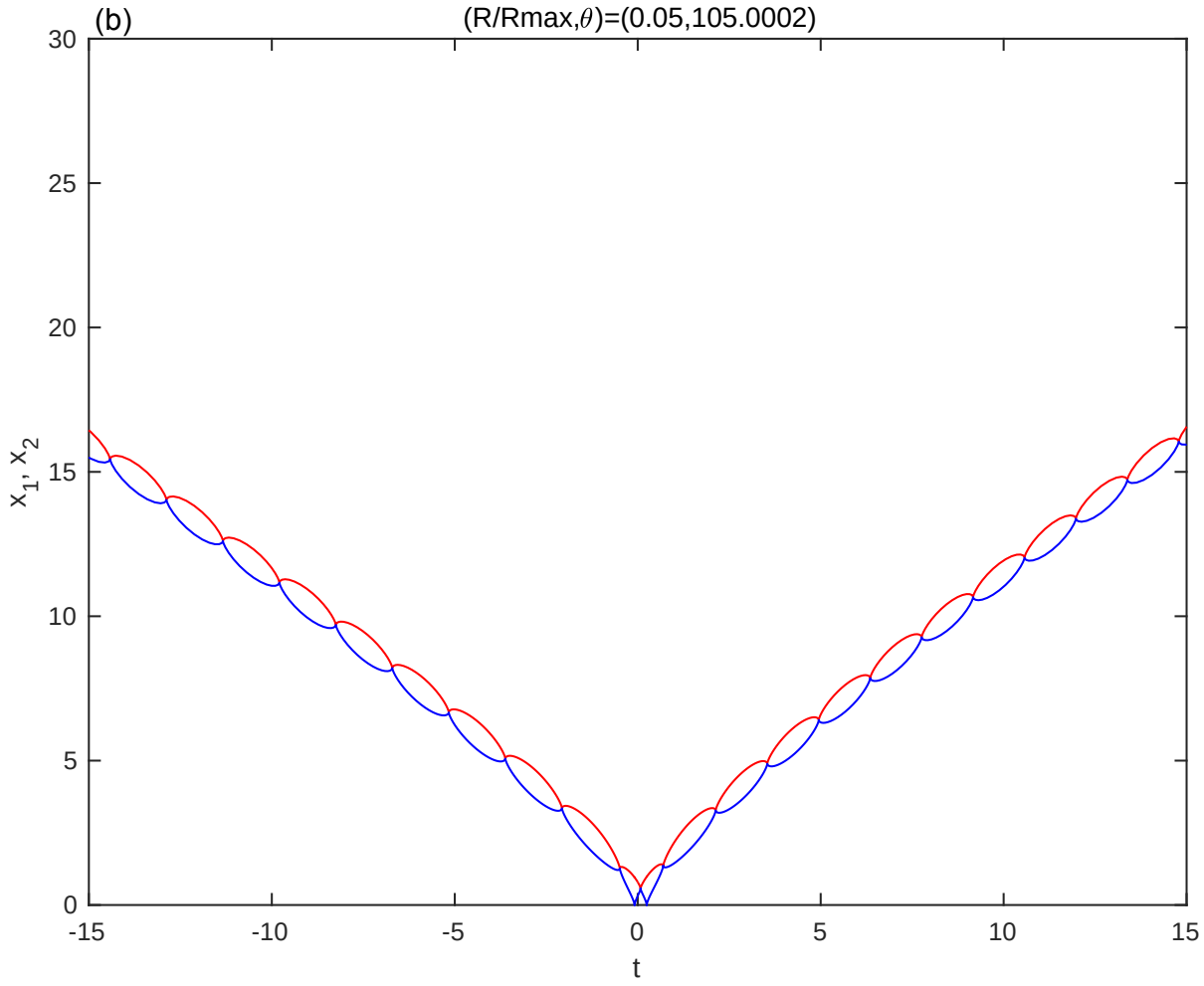

Figure 2.3 Fast scattering orbit: The system starts and finishes as three separate binaries. The initial value for this orbit is $(R/R_{\max}, \theta) = (0.05, 105.0002)$. Red and blue lines represent the bodies b_1 and b_2, respectively.

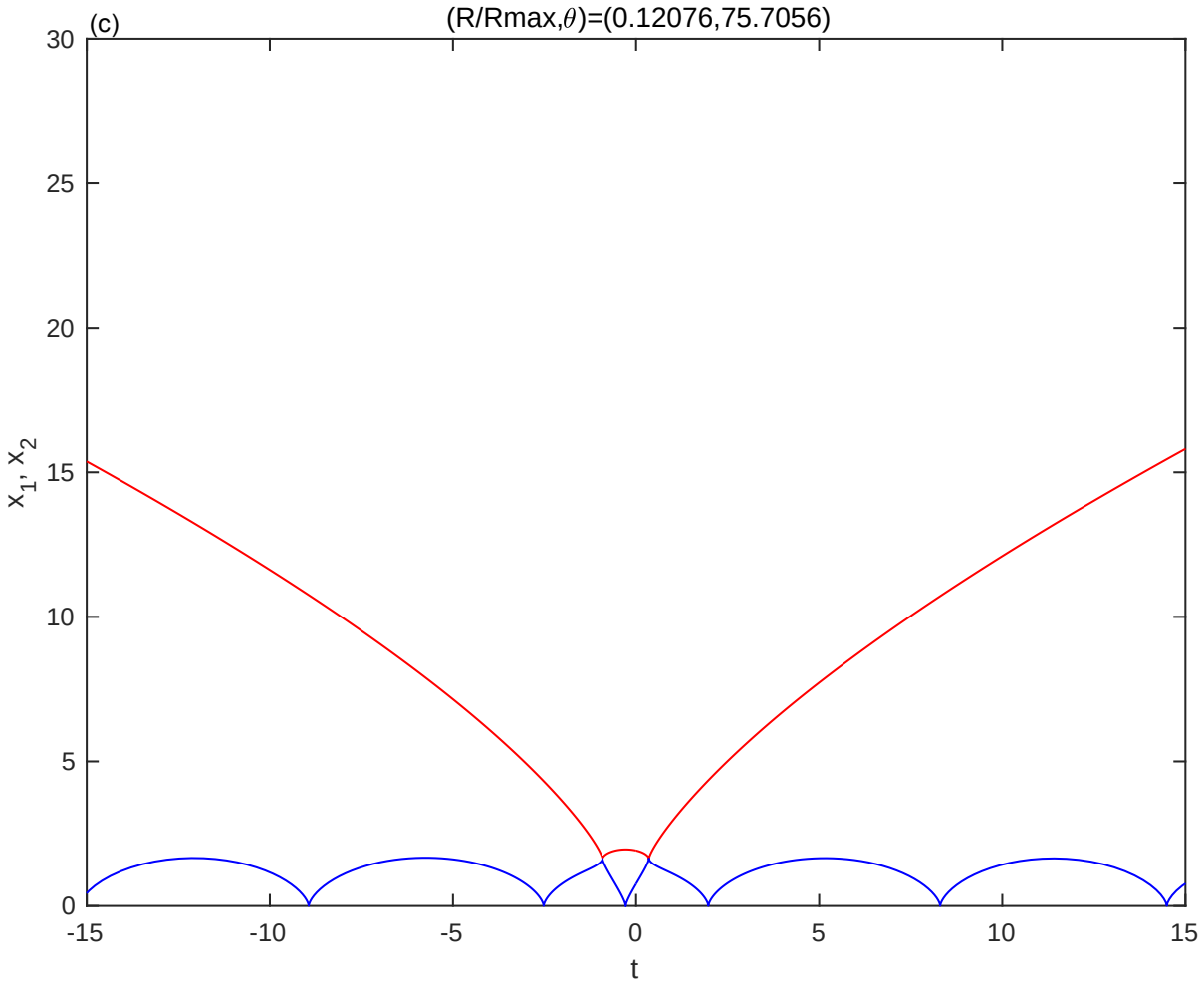

Figure 2.4 Fast scattering orbit: The system starts and finishes as a central trinary with three single bodies. The initial value for this orbit is $(R/R_{\max}, \theta) = (0.12076, 75.7056)$. Red and blue lines represent the bodies b_1 and b_2, respectively.

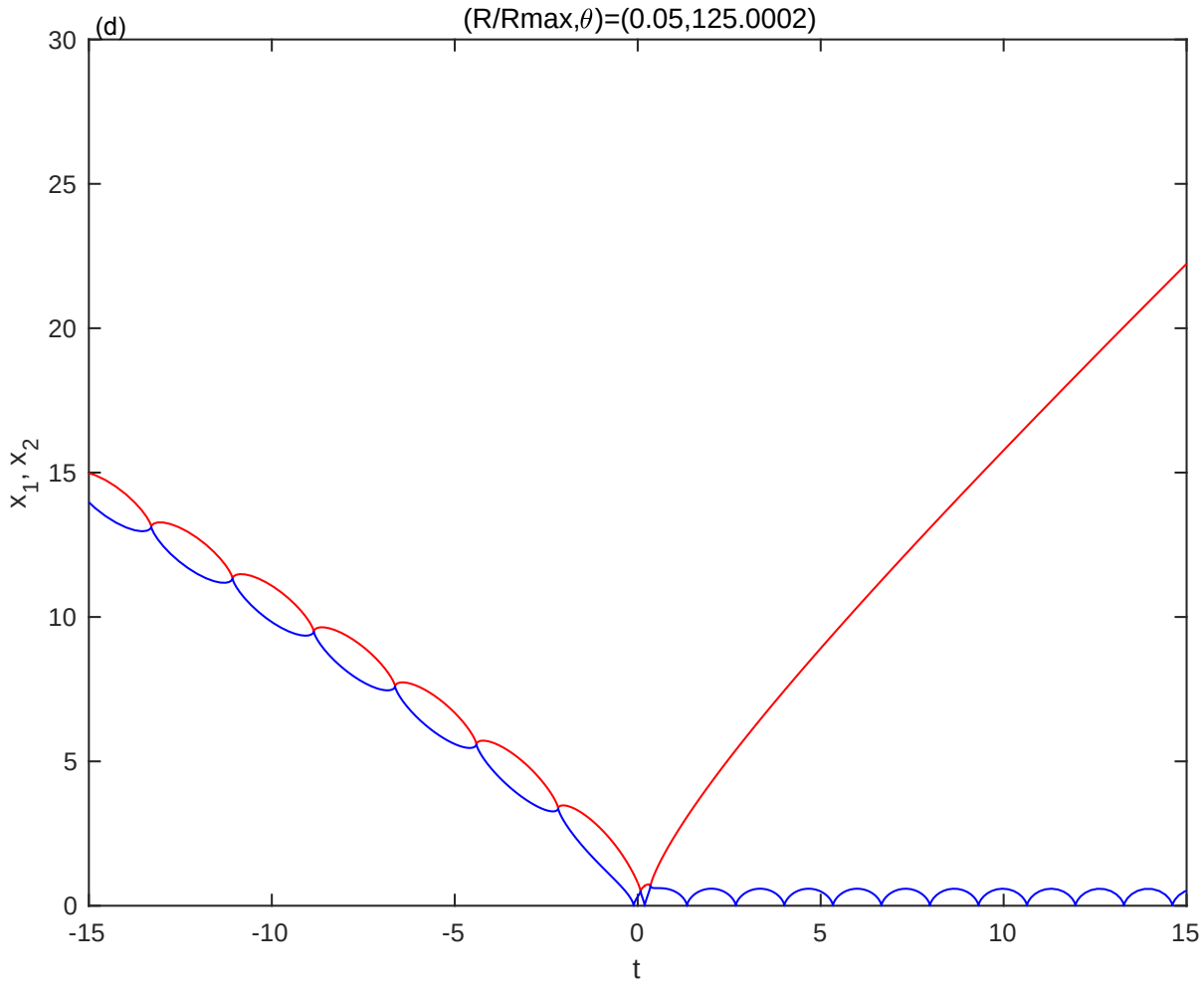

Figure 2.5 Fast scattering orbit: The system starts as three separate binaries and finishes as three single bodies with a central trinary. The initial value for this orbit is $(R/R_{\max}, \theta) = (0.05, 125.0002)$. Red and blue lines represent the bodies b_1 and b_2, respectively.

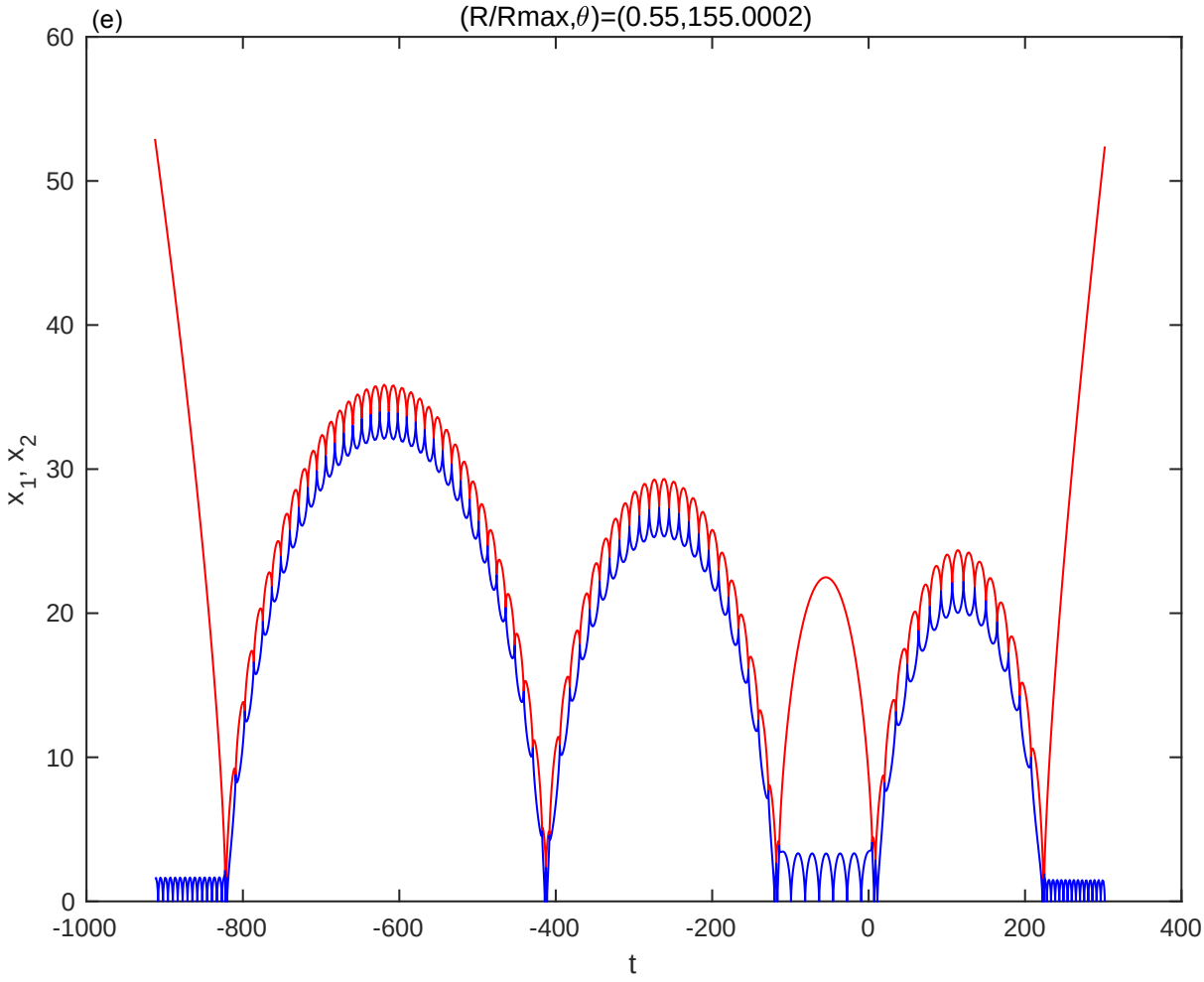

Figure 2.6 Chaotic scattering orbit: Three single bodies make a long detour before interacting with the central trinary. The final outcome of the chaotic scattering orbits is highly sensitive to the initial values, that is, even a small change in initial values drastically changes the final outcome of the system (see the final outcome of Figures 2.6 and 2.7). The initial value for this orbit is $(R/R_{\max}, \theta) = (0.55, 155.0002)$. Red and blue lines represent the bodies b_1 and b_2, respectively.

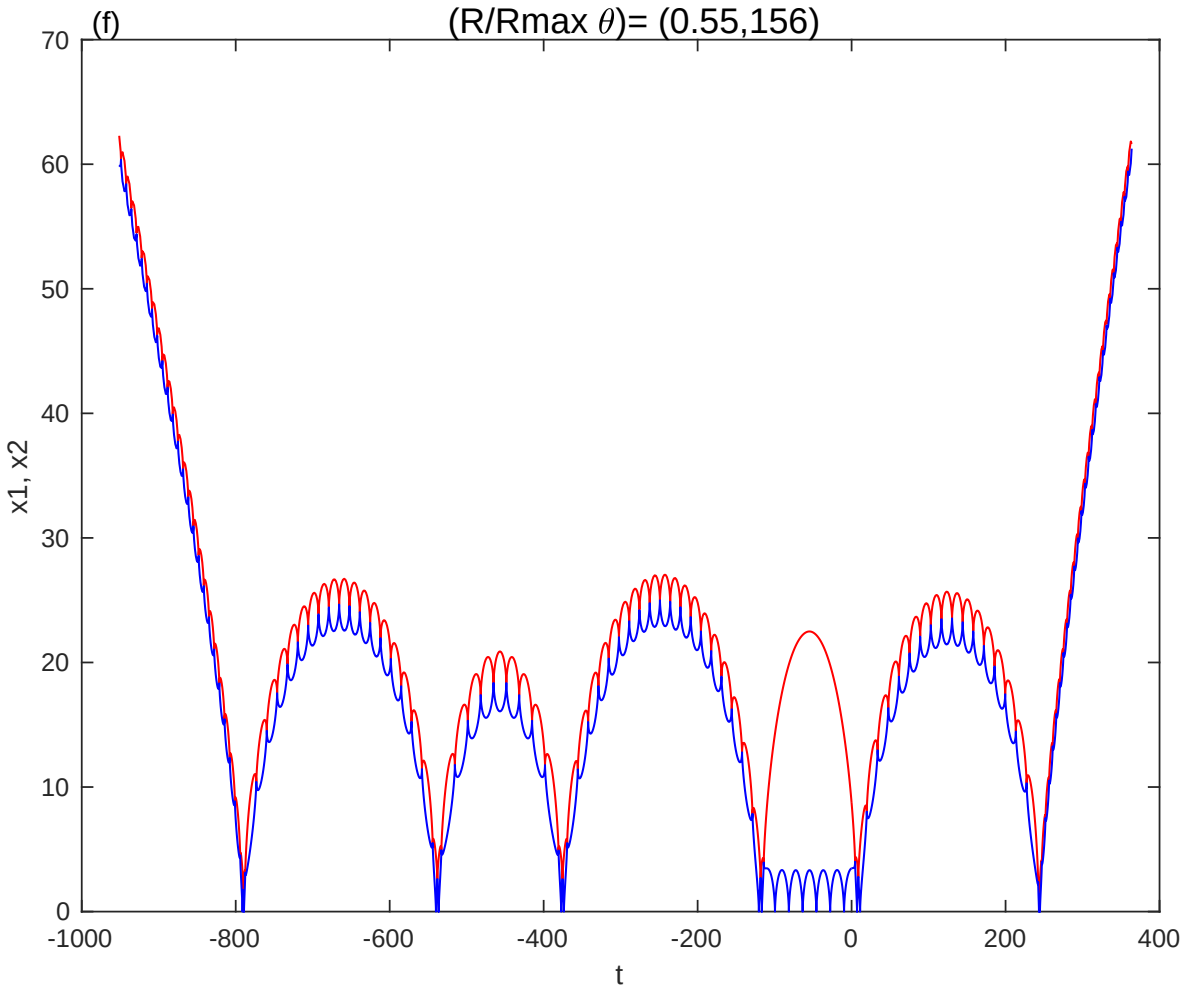

Figure 2.7 Chaotic scattering orbit: The six-body system breaks up as three separate tight binaries. The initial value for this orbit is $(R/R_{\max}, \theta) = (0.55, 156)$. Red and blue lines represent the bodies b_1 and b_2, respectively.

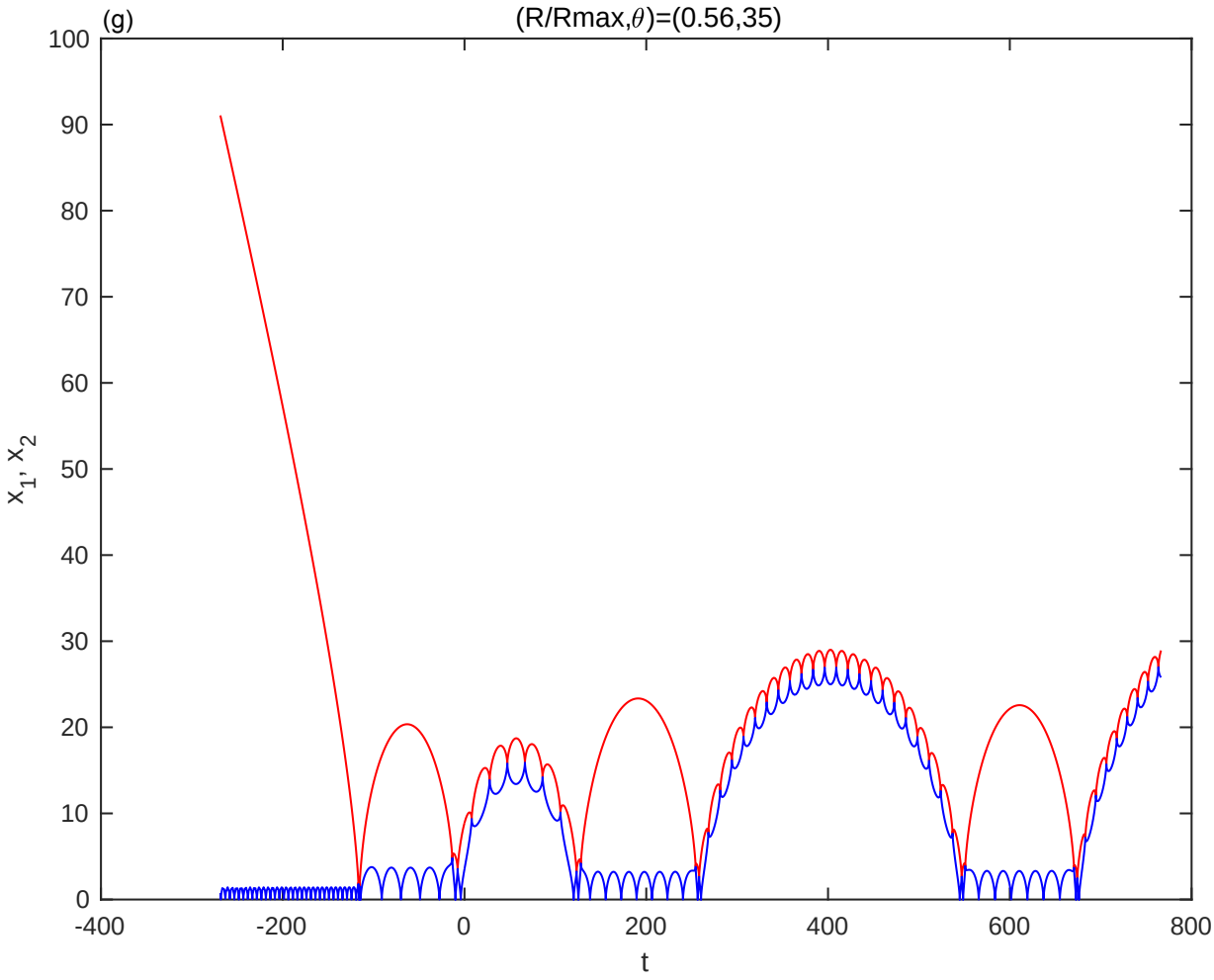

Figure 2.8 Chaotic scattering orbit: The bodies come together a number of times before separating as a subsystem. The initial value for this orbit is $(R/R_{\max}, \theta) = (0.56, 35)$. Red and blue lines represent the bodies b_1 and b_2, respectively.

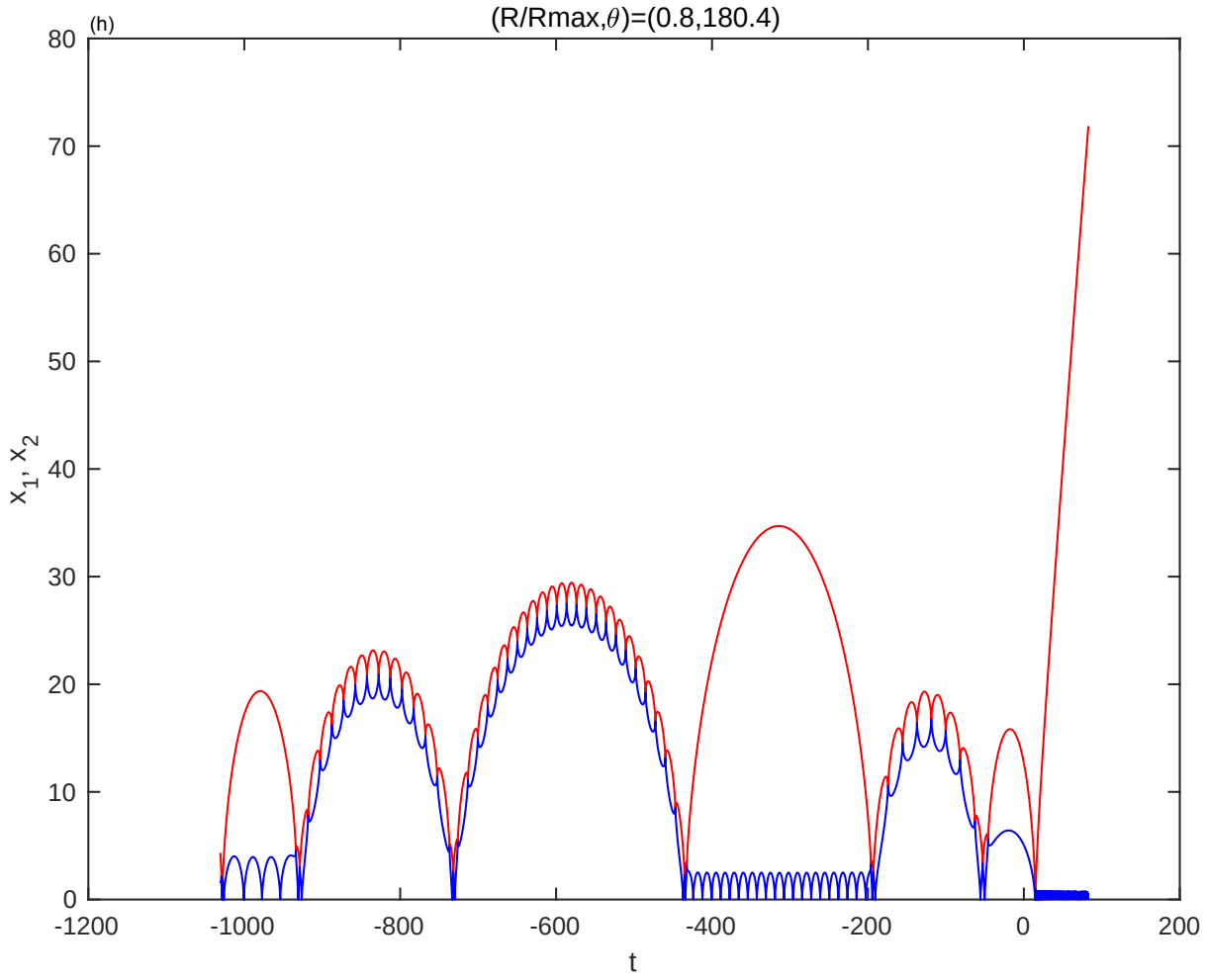

Figure 2.9 Chaotic scattering orbit: This orbit passes close to the homothetic sextuple collision. The initial value for this orbit is $(R/R_{\max}, \theta) = (0.8, 180.4)$. Red and blue lines represent the bodies b_1 and b_2, respectively.

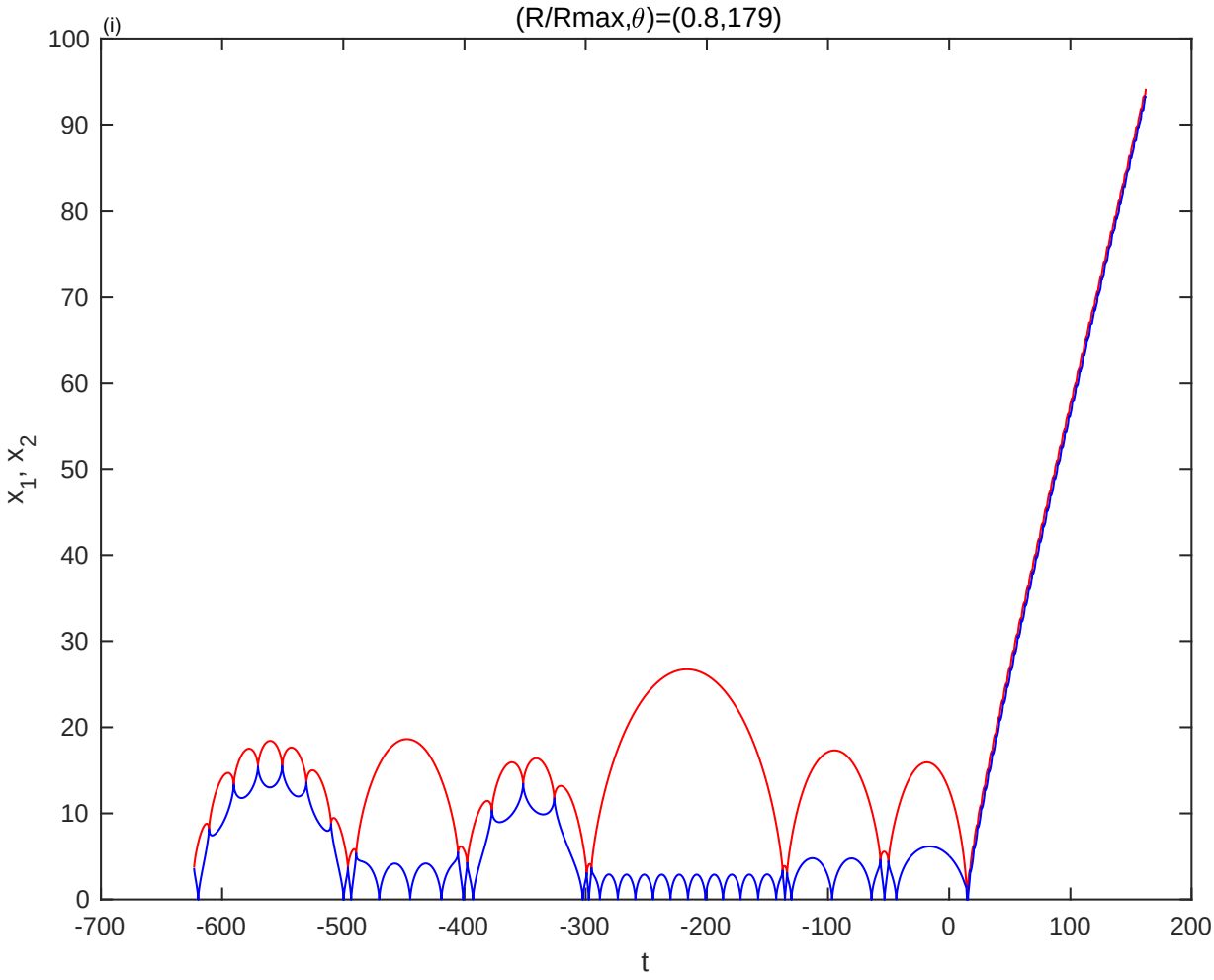

Figure 2.10 Chaotic scattering orbit: Another example of a chaotic scattering orbit that passes close to the homothetic sextuple collision. The initial value for this orbit is $(R/R_{\max}, \theta) = (0.8, 179)$. Red and blue lines represent the bodies b_1 and b_2, respectively.

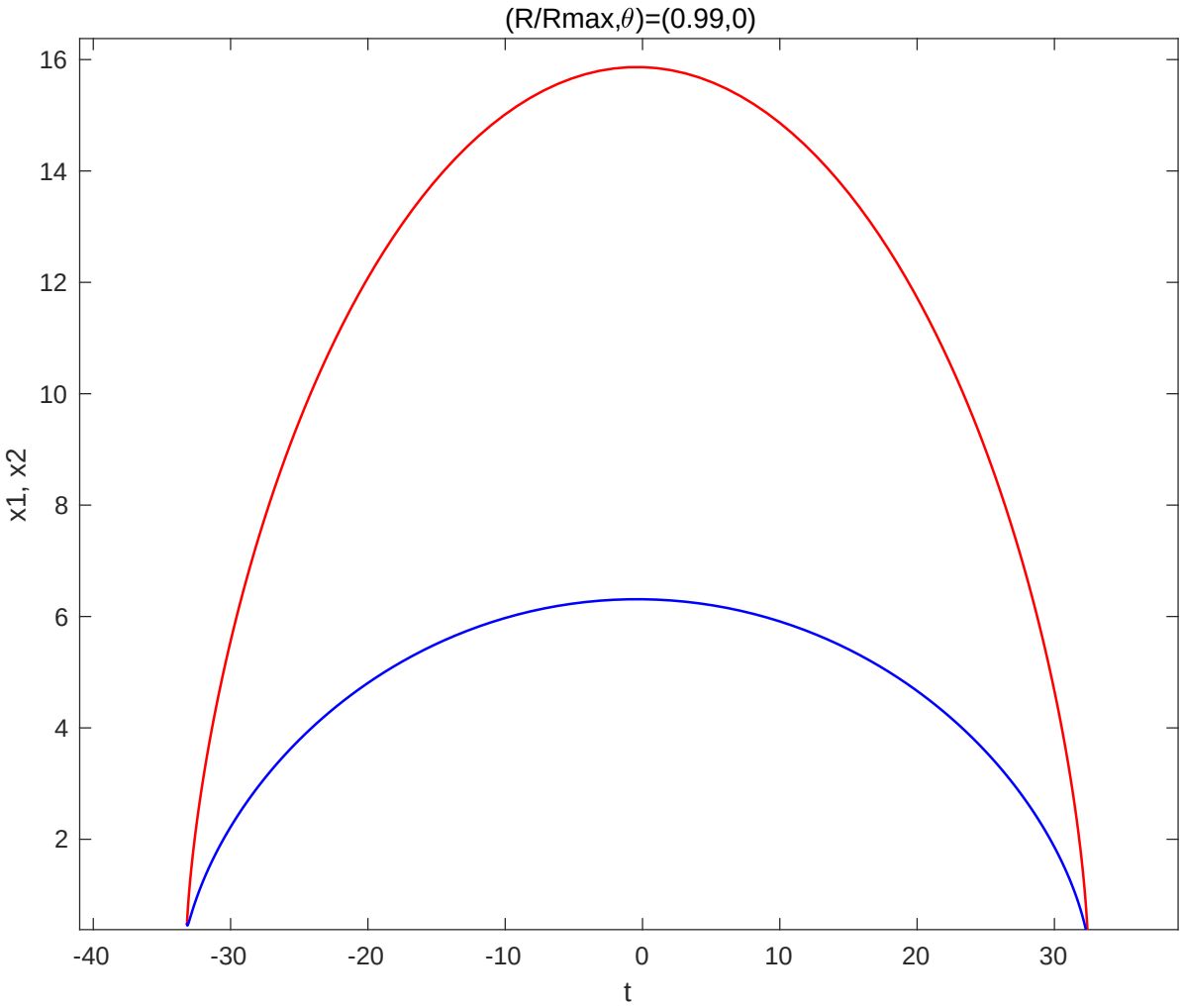

Figure 2.11 Homothetic sextuple collision orbit: The initial value for this orbit is $(R/R_{\max}, \theta) = (0.99, 0)$. Red and blue lines represent the bodies b_1 and b_2, respectively.

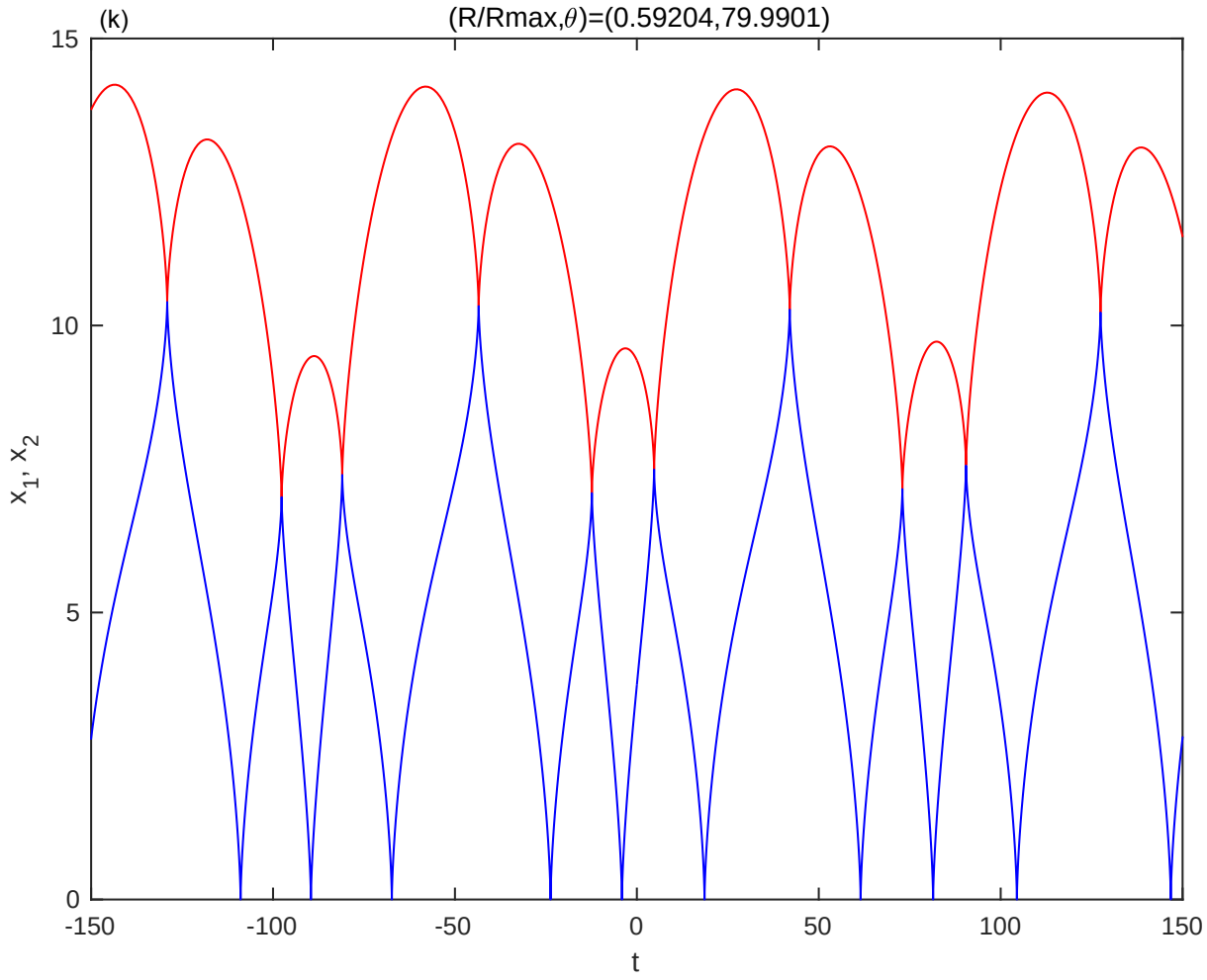

Figure 2.12 Quasi-periodic orbit: These orbits consist of a sequence of alternate interactions at irregular intervals. The initial value for this orbit is $(R/R_{\max}, \theta) = (0.59204, 79.9901)$. Red and blue lines represent the bodies b_1 and b_2, respectively.

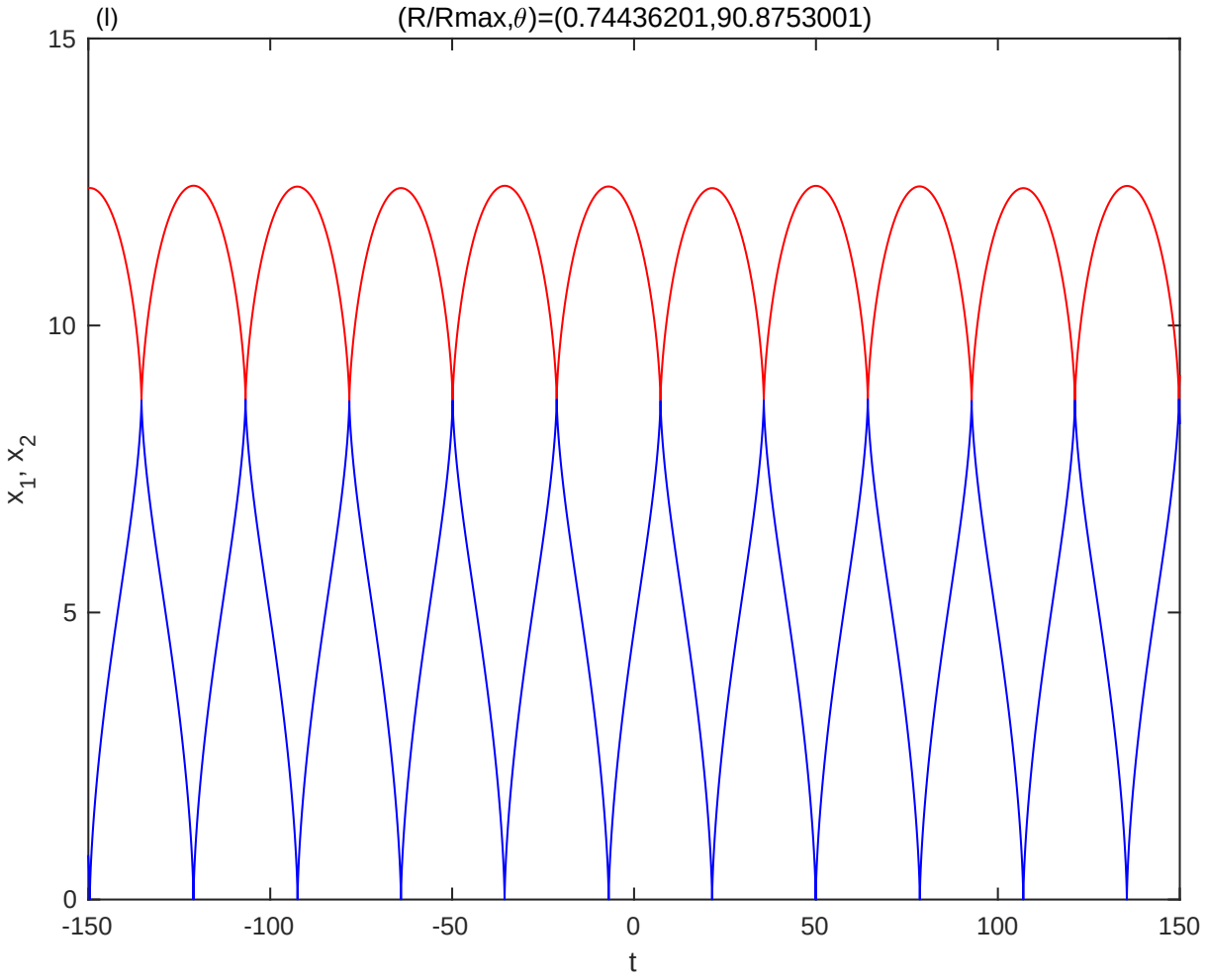

Figure 2.13 The Schubart periodic orbit. This orbit consists of a sequence of alternate interactions at regular intervals. The initial value for this orbit is $(R/R_{\max}, \theta) = (0.74436201, 90.8753001)$. Red and blue lines represent the bodies b_1 and b_2, respectively.

energy of its subsystems which results in the increase of relative velocities of subsystems. As a result the subsystem rapidly escapes as tightly bound bodies. The subsystems of those orbits that pass close to the homothetic sextuple collision have higher binding energy. The system finishes with a tightly bound central trinary and three high-velocity single bodies in Figure 2.9, while in Figure 2.10 it finishes as three tightly bound high-velocity binaries.

Figures 2.12 and 2.13 are examples of quasiperiodic and periodic orbits respectively. In both these orbits, we observe a pattern of alternate interactions between the pairs of bodies. The Schubart orbit for the six-body problem is shown in Figure 2.13, which is similar to the periodic orbit found by Schubart in 1956 for the three-body problem. The Schubart orbit consists of a regular sequence of alternating collisions. (For further details see Chapter 3.)

As described earlier, the final state of a system can be quasiperiodic orbits that stay bounded or orbits that break up. We use a criterion to check when a breakup has occurred, which is based on the previous method used by Mikkola and Hietarinta for the one-dimensional three-body problem [38, 39], and Sweatman for the one-dimensional four-body problem [63]. This criterion for the break up of the subsystems requires

- Total binding energy, which is the energy required to disperse the particles of all the subsystems of binaries or trinary must be greater than $|E|$.
- The distance between subsystems moving apart must be greater than 100 times the semi-major axis of the corresponding binary or trinary.

2.2.2 Poincaré map

We have generated a Poincaré map for our six-body system as shown in Figure 2.14 using the grid

$$R/R_{\max} = 0.05, 0.15, ..., 0.95, \tag{2.32}$$

$$\theta = 5, 10, ...175. \tag{2.33}$$

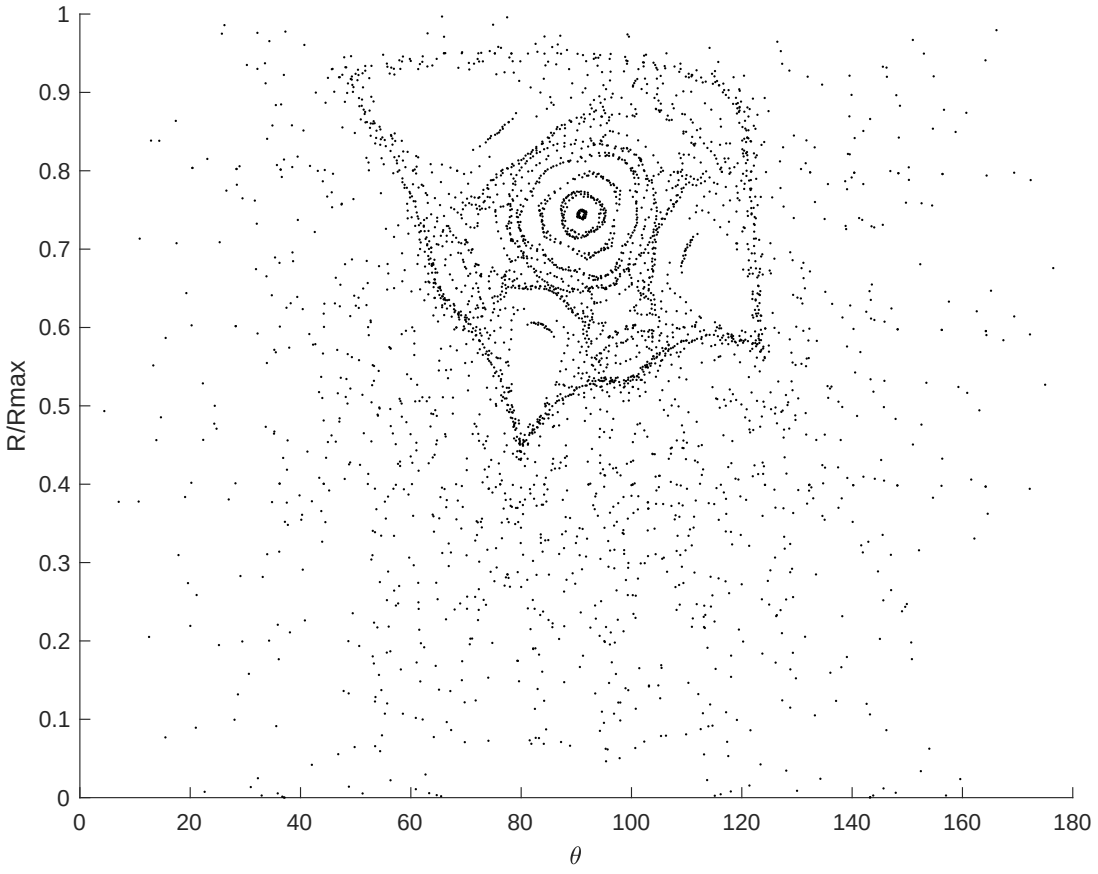

Figure 2.14 The Poincaré section. Black dots represent the section crossing of orbits.

The results are found by integrating both forward and backward in time and marking every crossing of the Poincaré section. The quasi-periodic orbits occupy the region around the Schubart orbit that is represented

by a circular structure in Figure 2.14. These orbits always stay in their region. The fast scattering orbits are found at the base of the Poincaré section near $R/R_{\max} = 0$. This region has fewer crossings as compared to the chaotic region because these orbits rapidly split into subsystems. The chaotic scattering orbits occupy the space around the quasi-periodic region. These orbits cross the section many times and separate into subsystems after entering the fast-scattering region.

2.2.3 The Schubart orbit

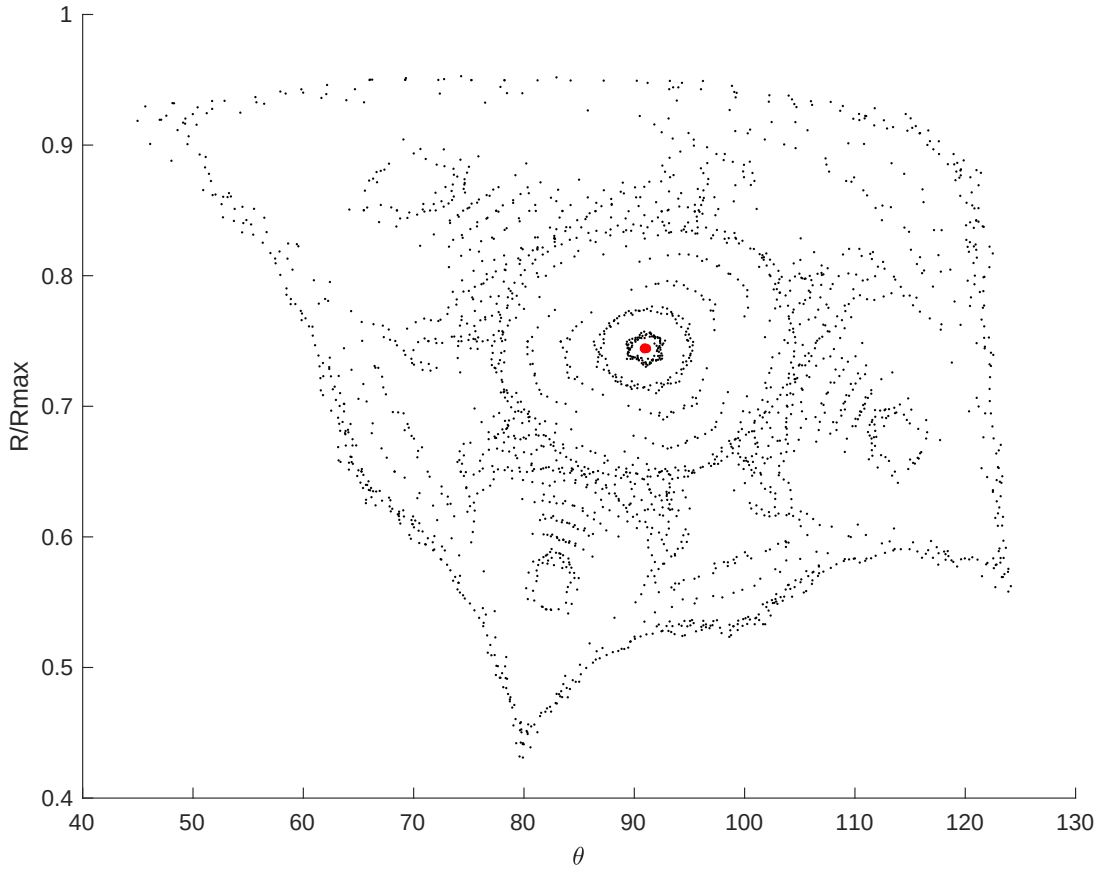

Figure 2.15 The quasiperiodic region of Poincaré map 2.14. The Schubart orbit is located in the heart of the quasiperiodic region highlighted by a red dot.

Figure 2.13 shows the Schubart orbit for the six-body system while the location of the Schubart orbit inside the quasiperiodic region is shown in Figure 2.15. We have computed the coordinates for the Schubart orbit, which are given by

$R/R_{max} \in [0.74436201, 0.74436204]$ and $\theta \in [90.8753001, 90.8753004]$.

These values are found by repeatedly refining the grid used to generate the Poincaré sections. These correspond to approximate values

$$\begin{aligned} x_1 &= 11.81025563, \\ x_2 &= 4.72410255, \\ v_1 &= -0.184573623, \\ v_2 &= 0.441502411. \end{aligned}$$

The approximate period of the Schubart orbit is 28.3946.

2.3 Non-linear stability check of the Schubart orbit

The non-linear stability of the Schubart orbit is performed by a simple approach used by Mikkola and Hietarinta [40] and Sweatman [63, 64]. We start the integration of the Schubart orbit from its initial conditions over a large number of periods. If instability is present then the numerical errors that appear during the integration of the system will gradually lead to the break up of the system. The simulations are done using the simple code of a six-body problem with aligned triangles and planar symmetric code.

The first simulation is performed when the system lies along the x-axis. It is observed during the integration that the system does not deviate from the x-axis and the orbit remains unchanged after 10000 periods as

shown in Figures 2.16a and 2.16b.

We performed another simulation using the planar symmetric code developed for the non-aligned case (see Chapter 4). We first rotate the initial conditions of the Schubart orbit off the x-axis into the plane before integration. The initial rotation is made by an arbitrary angle $\pi/5$. The system again does not show any deviation and the orbit appears unchanged after 10000 periods. The system is apparently stable along the x-axis and in the plane to a symmetrical perturbation.

Figures 2.17 and 2.18 show the behaviour of the x and y-coordinates of the Schubart orbit against time. Figures 2.17 and 2.18 are produced by rotating the initial conditions of the Schubart orbit by an arbitrary angle $\pi/5$. Figures 2.17a and 2.18a illustrate the behaviour of the orbit for about the first 11 orbits. The simulations after about 10000 orbits are shown in Figures and 2.17b and 2.18b. It is clear from Figures 2.17 and 2.18 that the system does not deviate from its regular pattern under the symmetric perturbations after about 10000 periods.

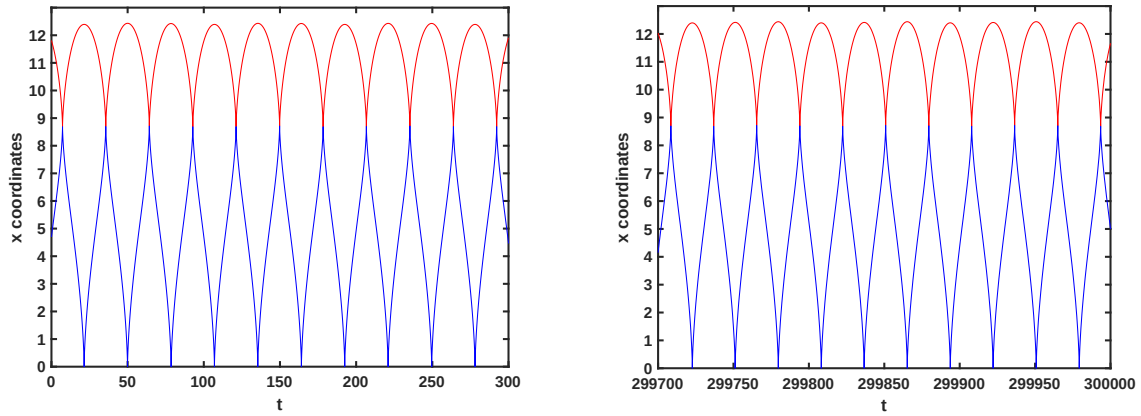

(a) Behaviour of the Schubart orbit at the start of the simulation.

(b) Behaviour of the Schubart orbit after about 10000 periods.

Figure 2.16 The Schubart six-body orbit with x coordinate against time t, which is plotted using the code developed for the aligned triangles.

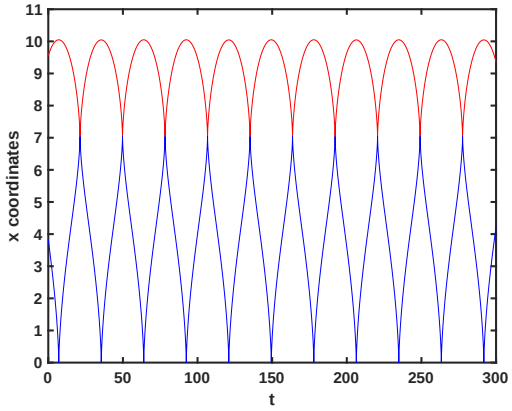

(a) Behaviour of the Schubart orbit at the start of the simulation.

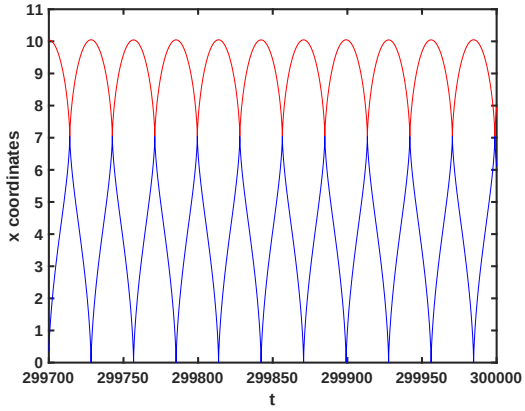

(b) Behaviour of the Schubart orbit after about 10000 periods.

Figure 2.17 The Schubart six-body orbit with x coordinate against time t, which is plotted using the planar symmetric code developed for the non-aligned triangles.

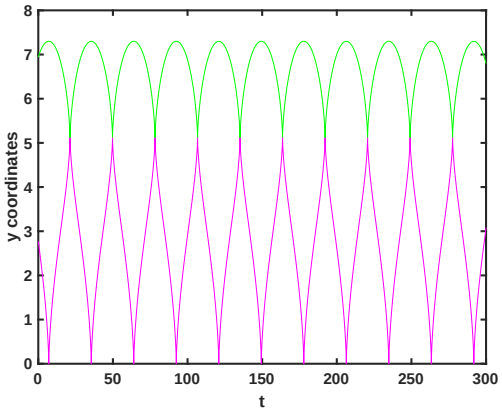

(a) Behaviour of the Schubart orbit at the start of the simulation.

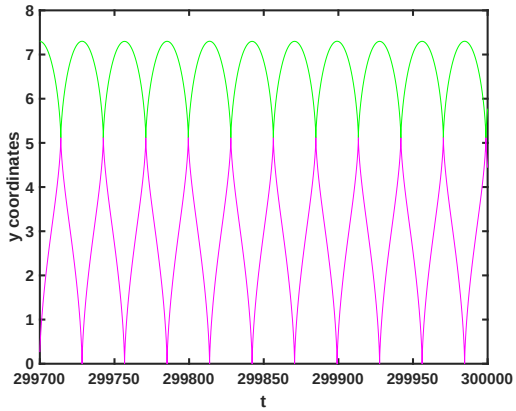

(b) Behaviour of the Schubart orbit after about 10000 periods.

Figure 2.18 The Schubart six-body orbit with y coordinate against time t, which is plotted using the planar symmetric code developed for the non-aligned triangles.

Chapter summary

In this chapter, we have explored the six-body problem with aligned triangles. We started with the description of the initial configuration and calculation of the equations of motion for the six-body system. The system is initially characterized by six initial values which are reduced to two: scaled sum of distances, $R/R_{\max}$, and angle of rotation, θ. The equations of motion are integrated using ode45 in MATLAB with the two initial conditions $R/R_{\max}$ and θ to find the general and periodic orbits of the system. We computed a Poincaré map that helped us to find the positions of different orbits for example, quasiperiodic orbits, Schubart orbit, fast scattering orbits, and chaotic scattering orbits. In the next chapter, we will prove the analytic existence of the Schubart orbit.

Chapter 3

Theoretical Proof of the Schubart orbit

In this chapter, we present an analytical proof of the existence of a Schubart orbit for our six-body system. The Schubart six-body orbit is a periodic orbit with the following properties:

1. First a triple collision occurs between the central bodies which is shown in Figure 3.1 and in this chapter we take this triple collision as the initial condition at $t = 0$

$$x_1(0) = S, \quad x_2(0) = 0, \quad \dot{x}_1(0) = 0, \quad \dot{x}_2(0) = \infty. \tag{3.1}$$

2. Then there occurs a simultaneous double collision of the central bodies with the corresponding outer bodies, see Figure 3.2,

3. After this the bodies return to their initial configuration as represented in Figure 3.1 and repeat the steps (1) and (2), repeatedly, therefore the Schubart orbit is a periodic orbit.

The existence of the Schubart orbit is proved using the approach used by Ouyang and Yan [47] for the collinear four-body problem and Yan [73] for the collinear three-body problem.

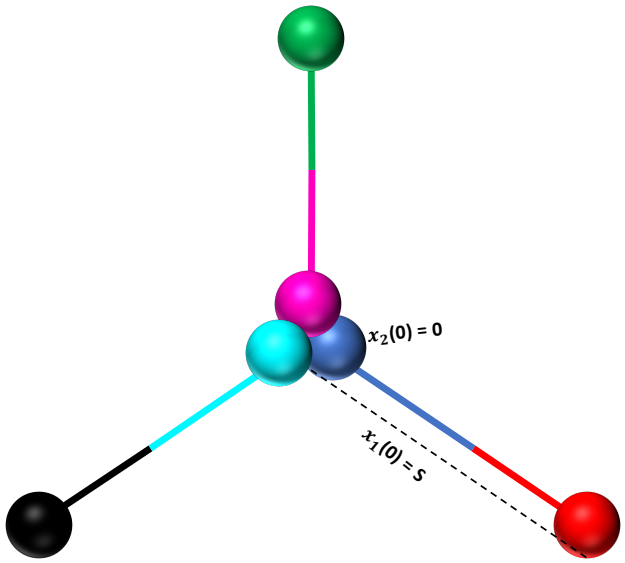

Figure 3.1 Triple collision of the inner bodies at the centre of mass: $x_1(0) = S$, $x_2(0) = 0$, $\dot{x}_1(0) = 0$ and $\dot{x}_2(0) = \infty$ are the initial distances and momenta of the bodies b_1 and b_2 at $t = 0$.

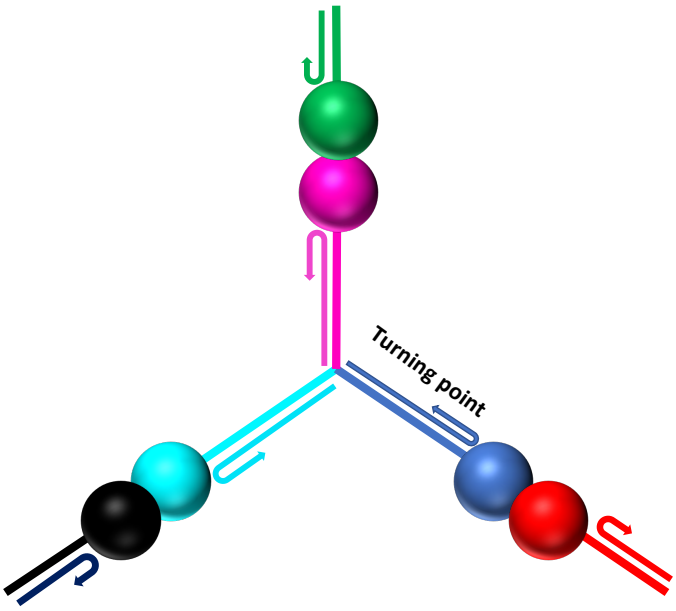

Figure 3.2 Simultaneous double collision of inner bodies with the corresponding outer body. The arrows indicate the turning point of the bodies after the simultaneous double collision.

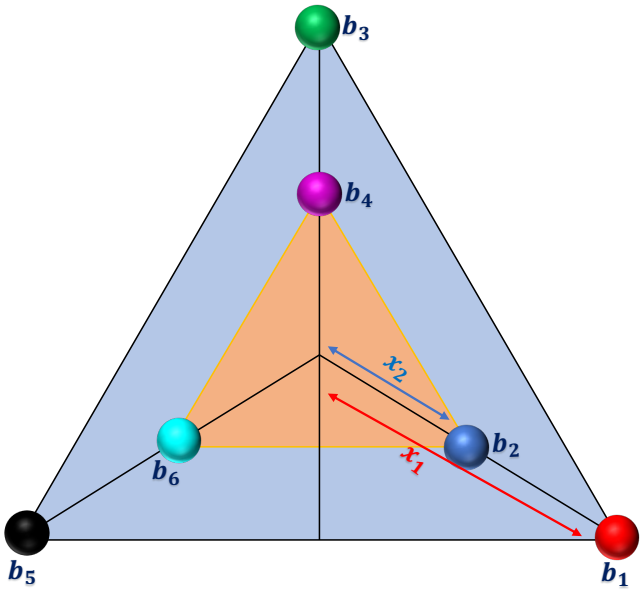

Figure 3.3 Six-body system: The bodies are placed on the points of two concentric equilateral triangles: x_1 and x_2 are the distances of the bodies b_1 and b_2 from the centre of mass, respectively.

Figure 3.3 shows the configuration of the bodies at some time t, while the motion of the bodies during one period of the Schubart orbit is represented in Figures 3.1 and 3.2. As described earlier, in the Schubart orbit the inner bodies first collide at the centre of mass, where $x_2(0) = 0$, which is the distance of the inner body from the centre of mass at triple collision and $x_1(0) = S$, where S is the starting distance of the outer body at $t = 0$ from the centre of mass. This collision is followed by another collision of the inner bodies with the corresponding outer body, after which the inner bodies turn back again for a triple collision at the centre and the outer bodies return to the maximum distance $x_1(0) = S$, the turning points of the bodies are shown in Figure 3.2. If the starting distance S of the outer body is sufficiently large, then the inner bodies come back from the turning point before the first simultaneous double collision happens as shown in Figure 3.4, so, before the first simultaneous

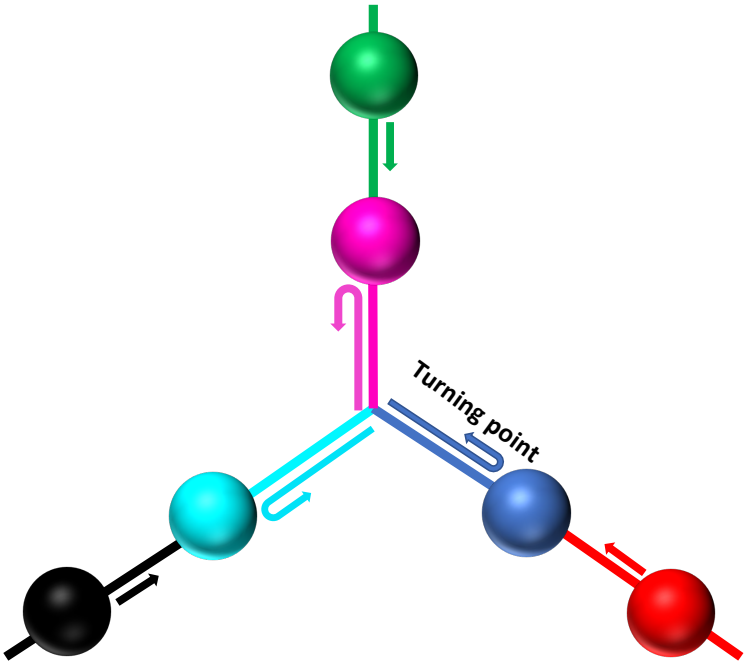

Figure 3.4 The inner bodies are turning back to the centre of mass without the simultaneous double collision in the case of sufficiently large S.

double collision there will be multiple triple collisions at the centre of mass.

To prove the existence of the Schubart periodic orbit we use a continuity argument. In order to prove that the orbit is exactly the Schubart orbit we need to estimate the value of the maximum distance of the outer bodies S for which there is no extra triple collision of inner bodies between every two connected collisions: a triple collision where b_2, b_4 and b_6 interact at the centre and a simultaneous double collision that occurs between three pairs of bodies (b_1, b_2), (b_3, b_4) and (b_5, b_6). The value of the maximum distance S of the outer bodies is estimated by a turning point technique.

Definition of turning point: Consider the six-body problem $(3.2 - 3.8)$ and suppose that $t_a < t_b$ and there exists a time $t = t^*$ in the interval

$t_a < t^* < t_b$ such that the velocity of the body b_2 is zero at this time that is $\dot{x}_2(t^*) = 0$.

$$\begin{aligned} &\text{If} \quad \dot{x}_2(t) > 0, \text{ for } t_a \leq t < t^* \quad \text{and} \quad \dot{x}_2(t) < 0, \text{ for } t^* < t \leq t_b \\ &\text{or} \quad \dot{x}_2(t) < 0, \text{ for } t_a \leq t < t^* \quad \text{and} \quad \dot{x}_2(t) > 0, \text{ for } t^* < t \leq t_b, \end{aligned}$$

then the body b_2 has a turning point at t^*, where t^* is the turning time and $x_2(t^*)$ is the turning point.

In Section 3.1 we regularize the Hamiltonian for our six-body system. A turning point technique is used in Section 3.2 to estimate the value of S so that the possibility of an "extra triple collision" can be excluded. In Section 3.3 we prove the existence of the Schubart periodic orbit using continuity arguments in the regularised Hamiltonian system. Our proof is of the general symmetric mass case rather than just a simpler equal masses case.

3.1 The Hamiltonian for the six-body system

The initial configuration of our six-body system is shown in Figure 3.3. As discussed earlier in Chapter 2.1.1 our system is symmetric about the centre of mass.

The six-body system has the Hamiltonian (This is described earlier in the equal mass case in Equation (2.5))

$$H = \frac{w_1^2}{6m_1} + \frac{w_2^2}{6m_2} - \frac{\sqrt{3}m_1^2}{x_1} - \frac{\sqrt{3}m_2^2}{x_2} - \frac{3m_1m_2}{x_1 - x_2} - \frac{6m_1m_2}{\sqrt{x_1^2 + x_1x_2 + x_2^2}}. \quad (3.2)$$

The Newtonian equations for the six-body system can be derived using the relation (1.1) or alternatively, we can use Hamilton's equations of

motion [19]

$$m_i \frac{d^2 x_i}{dt^2} = \frac{dp_i}{dt} = -\frac{\partial H}{\partial x_i}, \quad i = 1, 2, ..., N. \tag{3.3}$$

For the six-body system, we can write using (3.2)

$$\begin{aligned} m_1 \ddot{x}_1 = & -\frac{\partial H}{\partial x_1}, \\ m_2 \ddot{x}_2 = & -\frac{\partial H}{\partial x_2}. \end{aligned} \tag{3.4}$$

Using (3.2) and (3.4), we get the Newtonian equations of the six-body system

$$\ddot{x}_1 = -\frac{m_1}{\sqrt{3}x_1^2} - \frac{m_2}{(x_1 - x_2)^2} - \frac{m_2(2x_1 + x_2)}{\sqrt{(x_1^2 + x_1 x_2 + x_2^2)^3}}, \tag{3.5}$$

$$\ddot{x}_2 = -\frac{m_2}{\sqrt{3}x_2^2} + \frac{m_1}{(x_1 - x_2)^2} - \frac{m_1(2x_2 + x_1)}{\sqrt{(x_1^2 + x_1 x_2 + x_2^2)^3}}. \tag{3.6}$$

The regularized Hamiltonian is

$$\begin{aligned} \Gamma = & \frac{P_1^2 Q_2^2}{24 m_1} + \frac{P_1^2 Q_2^2}{24 m_2} + \frac{P_2^2 Q_1^2}{24 m_2} - \frac{P_1 P_2 Q_1 Q_2}{12 m_2} - \sqrt{3} m_2^2 Q_1^2 - 3 m_1 m_2 Q_2^2 \\ - & \frac{\sqrt{3} m_1^2 Q_1^2 Q_2^2}{Q_1^2 + Q_2^2} - \frac{6 m_1 m_2 Q_1^2 Q_2^2}{\sqrt{Q_1^4 + 3 Q_1^2 Q_2^2 + 3 Q_2^4}} - Q_1^2 Q_2^2 E, \end{aligned} \tag{3.7}$$

where the energy E is the constant numerical value of the Hamiltonian, which is described by the relations (2.1) and (2.2).

We consider the following initial conditions at a triple collision:

$$x_1(0) = S, \quad x_2(0) = 0, \quad \dot{x}_1(0) = 0, \quad \dot{x}_2(0) = \infty, \tag{3.8}$$

which is a singularity. To analyze the motion in the neighbourhood, we need to regularise this singularity. The first three initial conditions in

the regularised Hamiltonian system at $\tau = 0$ can be calculated using the relations $q_1 = x_1 - x_2$, $q_2 = x_2$, $q_i = Q_i^2$, $\omega_i = 3\dot{x}_i$, $\omega_1 = p_1, \omega_2 = p_2 - p_1$ and $P_i = 2p_iQ_i$ for $i = 1, 2$, that are described in Section 2.1.1.

$$\begin{aligned} Q_2(0) &= & x_2(0) &= 0, \\ Q_1(0) &= & \sqrt{x_1(0) - x_2(0)} &= \sqrt{S}, \\ P_1(0) &= 2p_1(0)Q_1(0) = 6\dot{x}_1(0)Q_1(0) & &= 0. \end{aligned} \tag{3.9}$$

The value of $P_2(0)$ is computed using the fact that $\Gamma = 0$ at $t = 0$, which can be seen from Equation (2.15). From the relations (3.7)−(3.9), we have

$$\Gamma = 0 = \frac{P_2(0)^2 Q_1(0)^2}{24m_2} - \sqrt{3}m_2^2 Q_1(0)^2.$$

We obtain

$$P_2(0) = \sqrt{24\sqrt{3}m_2^3}.$$

Thus the singular initial point becomes a regular point in the regularised Hamiltonian system. The new initial conditions in the regularized coordinates are

$$Q_1(0) = \sqrt{S} = R, \quad Q_2(0) = 0, \quad P_1(0) = 0, \quad P_2(0) = \sqrt{24\sqrt{3}m_2^3}.$$

From (3.5), we write

$$-\ddot{x}_1(t) = \frac{1}{x_1^2(t)}\left(\frac{m_1}{\sqrt{3}} + \frac{m_2}{(1 - \frac{x_2}{x_1})^2} + \frac{m_2(2 + \frac{x_2}{x_1})}{\sqrt{(1 + \frac{x_2}{x_1} + \frac{x_2^2}{x_1^2})^3}}\right).$$

Setting $\frac{x_2}{x_1} = y$, we have

$$-\ddot{x}_1 = \frac{1}{x_1^2}\left(\frac{m_1}{\sqrt{3}} + \frac{m_2}{(1 - y)^2} + \frac{m_2(2 + y)}{\sqrt{(1 + y + y^2)^3}}\right). \tag{3.10}$$

Now we show that the function $f(y)$ defined below is an increasing function in (0,1).

Lemma 1: The function $f(y)$ defined by

$$f(y) = \left(\frac{m_1}{\sqrt{3}} + \frac{m_2}{(1-y)^2} + \frac{m_2(2+y)}{\sqrt{(1+y+y^2)^3}} \right),$$

is an increasing function in the interval (0,1).

Proof. The derivative of the function $f(y)$ with respect to y is given by

$$\begin{aligned} f'(y) &= \frac{2m_2}{(1-y)^3} - \frac{m_2(4y^2+13y+4)}{2(1+y+y^2)^{5/2}} \\ &= \frac{4m_2(1+y+y^2)^{5/2} - m_2(4y^2+13y+4)(1-y)^3}{2(1-y)^3(1+y+y^2)^{5/2}}. \end{aligned}$$

The function $f(y)$ has critical points $-0.212215, -4.71219, 0, 1$ and $f'(y) \geq 0$ in the interval $(0,1)$. So, $f(y)$ is an increasing function in the interval $(0,1)$. □

3.2 Calculation of S

In the present section, our task is to estimate the value of S such that there will be no triple collision for $t \in [0, t_1]$ where t_1 is the time when the first simultaneous double collision happens. We first prove that, if the body b_2 has a turning point before it collides with the body b_1 for the first time, then there exists a positive lower bound of S.

Lemma 2: Let t_1 be the time when the first simultaneous double collision occurs. If the body b_2 has a turning point for $t \in [0, t_1]$. Then

$$S \geq \sqrt{3}m_1^2 + \frac{3m_1m_2a^2}{(a-1)^2} + \frac{3m_1m_2a^2(2a+1)}{(a^2+a+1)^{3/2}}, \tag{3.11}$$

where $\frac{x_1(t^*)}{x_2(t^*)} = a$, with $a > 1$ (because $x_1(t^*) > x_2(t^*) > 0$).

Proof. We consider the case when the body b_2 has a turning point that is not the result of the simultaneous double collision. So, the body b_2 is changing direction at time $t = t^* < t_1$. Then by definition of turning point, at $t = t^*$, $\dot{x}_2 = 0$ and $\ddot{x}_2 \leq 0$ for $t \in (0, t^*]$. Moreover $\dot{x}_2(t) > 0$ for $t \in (0, t^*)$ and $\dot{x}_2(t) < 0$ for $t \in (t^*, t_1)$. Also $x_1(t^*) > x_2(t^*) > 0$.

Since $\ddot{x}_2 \leq 0$, using (3.6) a must satisfy

$$\ddot{x}_2(t^*) = \frac{1}{x_2^2(t^*)}\left(-\frac{m_2}{\sqrt{3}} + \frac{m_1}{(a-1)^2} - \frac{m_1(2+a)}{\sqrt{(a^2+a+1)^3}}\right) \leq 0.$$

Simplification of the above expression gives

$$-m_2(a-1)^2(a^2+a+1)^{3/2} + \sqrt{3}m_1(a^2+a+1)^{3/2} \\ -\sqrt{3}m_1(2+a)(a-1)^2 \leq 0.$$

So, we have

$$(a^2+a+1)^{3/2}(\sqrt{3}m_1 - m_2(a-1)^2) \leq \sqrt{3}m_1(2+a)(a-1)^2. \quad (3.12)$$

Also taking $\dot{x}_1(t) < 0$ and $\dot{x}_2(t) \geq 0$ for $t \in (0, t^*]$, we have

$$\frac{x_1(t)}{x_2(t)} \geq \frac{x_1(t^*)}{x_2(t^*)} = a.$$

Further, notice that $\frac{x_2}{x_1} = y \leq \frac{1}{a}$ and $\frac{1}{a} < 1$. So, we have $y \leq \frac{1}{a} < 1$. This implies $f(y) \leq f(\frac{1}{a})$ because by Lemma 1 $f(y)$ is an increasing function in the interval $(0, 1)$.

Now from (3.10), we have

$$\begin{aligned} -\ddot{x}_1 &= \frac{1}{x_1^2}\left(\frac{m_1}{\sqrt{3}} + \frac{m_2}{(1-y)^2} + \frac{m_2(2+y)}{\sqrt{(1+y+y^2)^3}}\right), \\ &\leq \frac{1}{x_1^2}\left(\frac{m_1}{\sqrt{3}} + \frac{m_2}{(1-\frac{1}{a})^2} + \frac{m_2(2+\frac{1}{a})}{\sqrt{(1+\frac{1}{a}+\frac{1}{a^2})^3}}\right), \quad \text{since } f(y) \leq f(\tfrac{1}{a}) \\ &= \frac{1}{x_1^2}\left(\frac{m_1}{\sqrt{3}} + \frac{m_2 a^2}{(a-1)^2} + \frac{m_2 a^2(2a+1)}{\sqrt{(a^2+a+1)^3}}\right). \end{aligned}$$

Therefore for $t \in (0, t^*]$

$$-\ddot{x}_1(t) \leq \frac{1}{x_1^2(t)}\left(\frac{m_1}{\sqrt{3}} + \frac{m_2 a^2}{(a-1)^2} + \frac{m_2 a^2(2a+1)}{\sqrt{(a^2+a+1)^3}}\right). \tag{3.13}$$

Let us consider $x_1(0) = S$ and $x_1(t^*) = S_1 < S$. By multiplying inequality (3.13) with $-\dot{x}_1(t)$ because $\dot{x}_1(t) < 0$ for $t \in (0, t^*]$, we have

$$\dot{x}_1(t)\ddot{x}_1(t) \leq -\dot{x}_1(t)\frac{1}{x_1^2(t)}\left(\frac{m_1}{\sqrt{3}} + \frac{m_2 a^2}{(a-1)^2} + \frac{m_2 a^2(2a+1)}{\sqrt{(a^2+a+1)^3}}\right).$$

Integrating the above inequality from $t = 0$ to t^* gives

$$\frac{\dot{x}_1^2(t)}{2}\bigg|_0^{t^*} \leq \left(\frac{m_1}{\sqrt{3}} + \frac{m_2 a^2}{(a-1)^2} + \frac{m_2 a^2(2a+1)}{\sqrt{(a^2+a+1)^3}}\right)\left(\frac{1}{x_1(t)}\bigg|_0^{t^*}\right).$$

As we have $\dot{x}_1(0) = 0$, $x_1(0) = S$ and $x_1(t^*) = S_1$, this becomes

$$\frac{\dot{x}_1^2(t^*)}{2} \leq \left(\frac{1}{S_1} - \frac{1}{S}\right)\left(\frac{m_1}{\sqrt{3}} + \frac{m_2 a^2}{(a-1)^2} + \frac{m_2 a^2(2a+1)}{\sqrt{(a^2+a+1)^3}}\right). \tag{3.14}$$

We have taken $E = -1$. Now we calculate the Hamiltonian (3.7) at time $t = t^*$

$$\begin{aligned} -1 &= \frac{3m_1\dot{x}_1^2(t^*)}{2} + \frac{3m_2\dot{x}_2^2(t^*)}{2} - \frac{\sqrt{3}m_1^2}{x_1(t^*)} - \frac{\sqrt{3}m_2^2}{x_2(t^*)} - \frac{3m_1m_2}{x_1(t^*) - x_2(t^*)} \\ &- \frac{6m_1m_2}{\sqrt{x_1^2(t^*) + x_1(t^*)x_2(t^*) + x_2^2(t^*)}}, \end{aligned}$$

Also we have $x_1(t^*) = S_1$, $x_2(t^*) = S_1/a$ (from $x_1(t^*) = ax_2(t^*)$) and $\dot{x}_2(t^*) = 0$. The above equation takes the form

$$-1 = \frac{3m_1\dot{x}_1^2(t^*)}{2} - \frac{1}{S_1}\left(\sqrt{3}m_1^2 + \sqrt{3}am_2^2 + \frac{3am_1m_2}{a-1} + \frac{6am_1m_2}{\sqrt{a^2+a+1}}\right).$$

Using inequality (3.14), we have

$$\begin{aligned} -1 &\leq \left(\frac{1}{S_1} - \frac{1}{S}\right)\left(\sqrt{3}m_1^2 + \frac{3m_1m_2a^2}{(a-1)^2} + \frac{3m_1m_2a^2(2a+1)}{\sqrt{(a^2+a+1)^3}}\right) \\ &- \frac{1}{S_1}\left(\sqrt{3}m_1^2 + \sqrt{3}am_2^2 + \frac{3am_1m_2}{a-1} + \frac{6am_1m_2}{\sqrt{a^2+a+1}}\right). \end{aligned}$$

This simplifies to

$$\begin{aligned} -1 &\leq \frac{\sqrt{3}am_2}{S_1(a-1)^2(a^2+a+1)^{3/2}}\Bigg((a^2+a+1)^{3/2}(\sqrt{3}m_1 - m_2(a-1)^2) \\ &- \sqrt{3}m_1(a-1)^2(a+2)\Bigg) - \frac{1}{S}\left(\sqrt{3}m_1^2 + \frac{3m_1m_2a^2}{(a-1)^2} + \frac{3m_1m_2a^2(2a+1)}{\sqrt{(a^2+a+1)^3}}\right). \end{aligned}$$

Applying inequality (3.12) to this equation, we find

$$-1 \leq -\frac{1}{S}\left(\sqrt{3}m_1^2 + \frac{3m_1m_2a^2}{(a-1)^2} + \frac{3m_1m_2a^2(2a+1)}{\sqrt{(a^2+a+1)^3}}\right).$$

This implies

$$S \geq \sqrt{3}m_1^2 + \frac{3m_1m_2a^2}{(a-1)^2} + \frac{3m_1m_2a^2(2a+1)}{(a^2+a+1)^{3/2}}. \tag{3.15}$$

Hence, from inequality (3.15) it is clear if the body b_2 has a turning point in the interval $(0, t_1)$ then $S \geq \sqrt{3}m_1^2 + \frac{3m_1m_2a^2}{(a-1)^2} + \frac{3m_1m_2a^2(2a+1)}{(a^2+a+1)^{3/2}}$. □

Now we consider a set ψ= {S|there is at least one turning point for the body b_2 in the interval $(0, t_1)$}. Next we will show that the set ψ is non-empty.

On the contrary, if we suppose ψ is empty then for all $S > 0$ the body b_2 has no turning point for $t \in (0, t_1)$. So that the velocity of b_2 at any time t is positive, that is, $\dot{x}_2(t) > 0$ when $t \in (0, t_1)$. Therefore, we can write

$$\lim_{S\to+\infty} \dot{x}_2(t) \geq 0 \quad \text{for } t \in (0, t_1). \tag{3.16}$$

However, in the limit $\lim_{S\to+\infty}$, the Newtonian equations (3.5) and (3.6) of the six-body system become

$$\ddot{x}_1 = 0, \tag{3.17}$$

$$\ddot{x}_2 = -\frac{m_2}{\sqrt{3}x_2^2}, \tag{3.18}$$

where (3.18) indicates that the motion of the body b_2 is the pure Kepler motion and its solution is a closed orbit, given by

$$x = \frac{K^2}{4\omega^2}(1 - \cos 2\omega\tau),$$

$$t = \frac{K^2}{8\omega^3}(2\omega\tau - \sin 2\omega\tau),$$

where $K^2 = \frac{m_2}{\sqrt{3}}$ and $\omega = \frac{1}{2}E$ with $E = -1$. Since our system reduces to pure kepler motion with negative energy, so its solution is bounded.

Therefore, there must be at least one turning point for the body b_2, which contradicts (3.16). Therefore, the set ψ can not be empty.

Consider $S_0 = \inf \psi$, then from Lemma (2), we have

$$S_0 \geq \sqrt{3}m_1^2 + \frac{3m_1m_2a^2}{(a-1)^2} + \frac{3m_1m_2a^2(2a+1)}{(a^2+a+1)^{3/2}}. \tag{3.19}$$

We know from the definition of S_0, that the body b_2 is free of turning points for $S < S_0$. But, for each $S \in \psi$, $\dot{x}_2(t^*) = 0$ and $\ddot{x}_2(t^*) \leq 0$ for some $t^* > 0$.

Next we prove that when S is equal to S_0, then $\dot{x}_2(t^*) = 0 = \ddot{x}_2(t^*)$.

Theorem 1: Consider the six-body system (3.2−3.7). Let t_1 be the time when the first simultaneous double collision occurs and t^* be the turning time of the body b_2.
Then S_0 is the unique value such that:

1. When $S = S_0$, then $\dot{x}_2(t^*) = 0 = \ddot{x}_2(t^*)$ for $t^* \in (0, t_1)$.
2. If $0 < S \leq S_0$ then the body b_2 has no turning point for $t \in (0, t_1)$.

Proof. We first show that when $S = S_0$, there exists a unique t^* in the interval $(0, t_1)$, such that $\dot{x}_2(t^*) = 0 = \ddot{x}_2(t^*)$.

If for a given value of $S > 0$ with $x_1(0) = S$ and $x_2(0) = 0$, the solution $x_2(t)$ has a turning point in $(0, t_1)$, then by continuity of the solution with respect to the initial conditions, if we slightly change S, the solution $x_2(t)$ will still have a turning point in the interval $(0, t_1)$. But body b_2 has no turning point (by definition of S_0) in the interval $(0, t_1)$. This implies $x_2(t)$ is increasing in the interval $(0, t_1)$. In other words $\dot{x}_2(t) \geq 0$ for $t \in (0, t_1)$.

To show $\ddot{x}_2(t^*) = 0$ for $S = S_0$, we consider

$$g(z) = -\frac{m_2}{\sqrt{3}} + \frac{m_1}{(z-1)^2} - \frac{m_1(2+z)}{(z^2+z+1)^{3/2}}.$$

which is a decreasing function for $z > 1$. Let us have a unique value $a > 1$ for which $g(a) = 0$. Also note that $\frac{x_1(t)}{x_2(t)}$ is a decreasing function for $S = S_0$ in the interval $(0, t_1)$ and for some $t^* \in (0, t_1)$, we have $\frac{x_1(t^*)}{x_2(t^*)} = a$. By (3.6), $\ddot{x}_2(t^*)$ has the same sign as $g(a)$. Therefore, we can write $\ddot{x}_2(t^*) = 0$. Moreover in the interval $(0, t^*)$, we have $\ddot{x}_2(t^*) < 0$ and $\ddot{x}_2(t^*) > 0$ for (t^*, t_1).

As $\dot{x}_2(t) \geq 0$ in the interval $(0, t_1)$ for $S = S_0$, if we choose $\dot{x}_2(t^*) > 0$, then we will get relative minimum of $\dot{x}_2(t)$ at t^* because of the sign of $\ddot{x}_2(t)$. Hence $\dot{x}_2(t) \geq \dot{x}_2(t^*) > 0$ for all $t \in (0, t_1)$. By the continuity with respect to the initial conditions, this preserves the slight change of S, so the solution would be free of a turning point when S and S_0 are close. This contradicts the definition of S_0, therefore, at $S = S_0$

$$\dot{x}_2(t^*) = 0 = \ddot{x}_2(t^*).$$

Now, the proof can be ended with the following lemma.

Lemma 3: For some $t^* < t_1$, $\dddot{x}_2(t^*) \geq 0$.

Proof. Taking the derivative of equation (3.6), we get

$$\begin{aligned}
\dddot{x}_2(t^*) &= \frac{2m_2\dot{x}_2(t^*)}{\sqrt{3}x_2^3(t^*)} - \frac{2m_1(\dot{x}_1(t^*) - \dot{x}_2(t^*))}{(x_1(t^*) - x_2(t^*))^3} \\
&- \frac{2\dot{x}_2(t^*) + \dot{x}_1(t^*)}{(x_1^2(t^*) + x_1(t^*)x_2(t^*) + x_2^2(t^*))^{3/2}} \\
&+ \frac{(2x_2(t^*) + x_1(t^*))(2\dot{x}_1(t^*) + x_1(t*)\dot{x}_2(t^*) + \dot{x}_1(t^*)x_2(t^*) + 2\dot{x}_2(t^*))}{(x_1^2(t^*) + x_1(t^*)x_2(t^*) + x_2^2(t^*))^{5/2}}.
\end{aligned}$$

We have, $\dot{x}_2(t^*) = 0 = \ddot{x}_2(t^*)$ at $S = S_0$. Furthermore, $\dot{x}_1(t^*) < 0$ and $x_1(t^*) > x_2(t^*) > 0$. Therefore,

$$\dddot{x}_2(t^*) = \dot{x}_1(t^*)\left[\frac{2m_1}{(x_1(t^*) - x_2(t^*))^3} - \frac{1}{(x_1^2(t^*) + x_1(t^*)x_2(t^*) + x_2^2(t^*))^{3/2}} + \right.$$
$$\left. + \frac{(2x_2(t^*) + x_1(t^*))(2 + x_2(t^*))}{(x_1^2(t^*) + x_1(t^*)x_2(t^*) + x_2^2(t^*))^{5/2}}\right] > 0.$$

□

Lemma 3 shows that when time passes beyond t^* the body b_2 keeps moving towards the body b_1. In other words, the body b_2 does not turn back when $S = S_0$. Therefore, when $S \leq S_0$ the body b_2 has no turning point and there is no additional collision between a triple collision and simultaneous double collision.

□

In the next section, we prove the existence of the Schubart orbit using the implicit function theorem and a continuity argument on the differential equations of the regularized Hamiltonian.

3.3 Existence of the Schubart orbit

In this section, we prove the existence of the Schubart orbit. First, we need to find the initial coordinates at $\tau = \tau_1$, where τ_1 is the time when the first simultaneous double collision occurs.

The regularized Hamiltonian and equations of motion (derived in Chapter 2.1.1) for our six-body system are

$$\begin{aligned}
\Gamma &= \frac{P_1^2Q_2^2}{24m_1} + \frac{P_1^2Q_2^2}{24m_2} + \frac{P_2^2Q_1^2}{24m_2} - \frac{P_1P_2Q_1Q_2}{12m_2} - \sqrt{3}m_2^2Q_1^2 - 3m_1m_2Q_2^2 \\
&- \frac{\sqrt{3}m_1^2Q_1^2Q_2^2}{Q_1^2+Q_2^2} - \frac{6m_1m_2Q_1^2Q_2^2}{\sqrt{Q_1^4+3Q_1^2Q_2^2+3Q_2^4}} - Q_1^2Q_2^2E. \qquad (3.20)
\end{aligned}$$

$$\frac{dQ_1}{d\tau} = \frac{P_1Q_2^2}{12m_1} + \frac{P_1Q_2^2}{12m_2} - \frac{Q_1Q_2P_2}{12m_2}. \qquad (3.21)$$

$$\frac{dQ_2}{d\tau} = \frac{P_2Q_1^2}{12m_2} - \frac{Q_1Q_2P_1}{12m_2}. \qquad (3.22)$$

$$\begin{aligned}
\frac{dP_1}{d\tau} &= \frac{-P_2^2Q_1}{12m_2} + \frac{Q_2P_1P_2}{12m_2} + \frac{2\sqrt{3}m_1^2Q_1Q_2^2}{Q_1^2+Q_2^2} - \frac{2\sqrt{3}m_1^2Q_1^3Q_2^2}{(Q_1^2+Q_2^2)^2} + 2\sqrt{3}m_2^2Q_1 \\
&+ \frac{12m_1m_2Q_1Q_2^2}{\sqrt{Q_1^4+3Q_1^2Q_2^2+3Q_2^4}} - \frac{12m_1m_2Q_1^5Q_2^2}{\sqrt{(Q_1^4+3Q_1^2Q_2^2+3Q_2^4)^3}} \\
&- \frac{18m_1m_2Q_1^3Q_2^4}{\sqrt{(Q_1^4+3Q_1^2Q_2^2+3Q_2^4)^3}} + 2Q_1Q_2^2E. \qquad (3.23)
\end{aligned}$$

$$\begin{aligned}
\frac{dP_2}{d\tau} &= \frac{-P_1^2Q_2}{12m_1} - \frac{P_1^2Q_2}{12m_2} + \frac{Q_1P_1P_2}{12m_2} + \frac{2\sqrt{3}m_1^2Q_1^2Q_2}{Q_1^2+Q_2^2} - \frac{2\sqrt{3}m_1^2Q_1^2Q_2^3}{(Q_1^2+Q_2^2)^2} \\
&+ 6m_1m_2Q_2 + \frac{12m_1m_2Q_1^2Q_2}{\sqrt{Q_1^4+3Q_1^2Q_2^2+3Q_2^4}} - \frac{18m_1m_2Q_1^4Q_2^3}{\sqrt{(Q_1^4+3Q_1^2Q_2^2+3Q_2^4)^3}} \\
&- \frac{36m_1m_2Q_1^2Q_2^5}{\sqrt{(Q_1^4+3Q_1^2Q_2^2+3Q_2^4)^3}} + 2Q_1^2Q_2E. \qquad (3.24)
\end{aligned}$$

We know from Theorem 1 that $Q_2^2 = x_2$ is increasing from $\tau = 0$ to $\tau = \tau_1$ for $0 < S \leq S_0$. The initial conditions are given by

$$Q_1(0) = \sqrt{S} = R, \quad Q_2(0) = 0, \quad P_1(0) = 0, \quad P_2(0) = \sqrt{24\sqrt{3}m_2^3},$$

where $R^2 = S$. As τ_1 is the time when the first simultaneous double collision happens, at τ_1 both bodies (b_1 and b_2) are at the same distance from the centre of mass (that is $x_1(t_1) = x_2(t_1)$). Thus the coordinates at τ_1 are

$$Q_1(\tau_1) = \sqrt{q_1} = \sqrt{x_1 - x_2} = 0, \quad Q_2(\tau_1) = R_1, \quad P_1(\tau_1) = -\frac{6\sqrt{2}m_1m_2}{\sqrt{m_1 + m_2}},$$

where P_1 is calculated using that $\Gamma = 0$ at $\tau = \tau_1$. Now to show the existence of a Schubart orbit we need to find a suitable value of R such that

$$P_2(\tau_1) = P_2(\tau_1, R) = 0.$$

We first show that $P_2(\tau_1, R)$ is a continuous function of R.

Lemma 4 If τ_1 is the time for the first simultaneous double collision, then $P_2(\tau_1, R)$ is a continuous function of R.

Proof. As the Hamiltonian for the six-body system is regularised the solutions $P_1(\tau, R)$ and $Q_2(\tau, R)$ are continuous functions of τ and R. So, to prove the continuity of $P_2(\tau_1, R)$ it is enough to show that $\tau_1(R)$ is continuous. This is proved using the implicit function theorem (See Appendix D for details). We know that, $Q_2(\tau_1) > 0$, $Q_1(\tau_1) = 0$ (as the first simultaneous double collision happens at τ_1) and also $Q_2(\tau) > 0$ for $0 < \tau \leq \tau_1$.

To apply the implicit function theorem for $Q_1 = Q_1(\tau_1, R) = 0$, we have

to show that the derivative of Q_1 with respect to τ at (τ_1, R) is non zero.

$$\begin{aligned}\left.\frac{\partial Q_1}{\partial \tau}\right|_{(\tau_1,R)} &= \left.\frac{\partial \Gamma}{\partial P_1}\right|_{(\tau_1,R)} = \left.\left[\frac{(m_1+m_2)P_1Q_2^2}{12m_1m_2} - \frac{Q_1Q_2P_2}{12m_2}\right]\right|_{(\tau_1,R)} \\ &= -\sqrt{\frac{m_1+m_2}{2}}R_1 \quad \text{(using values of } Q_1(\tau_1),\ P_1(\tau_1) \text{ and } Q_2(\tau_1)) \\ &\neq 0.\end{aligned}$$

Hence by the implicit function theorem $\tau_1(R)$ is continuous which implies $P_2(\tau_1, R)$ is a continuous function. □

Lemma 5: Consider the six-body system (3.20−3.24). Suppose the initial conditions for the differential equations of the system (3.20−3.24) are

$$Q_1(0) = \sqrt{S} = R, \quad Q_2(0) = 0, \quad P_1(0) = 0, \quad P_2(0) = \sqrt{24\sqrt{3}m_2^3},$$

where $R \in (0, \sqrt{S_0})$. Then there exists some R such that $P_2(\tau_1) = P_2(\tau_1, R) = 0$.

Proof. To prove that there exists a value of R such that $P_2(\tau_1, R) = 0$ we use the intermediate value theorem (See Appendix D). For this, we need to prove two simple cases

- $P_2(\tau_1, R) > 0$ for some $R > 0$, and
- $P_2(\tau_1, R) < 0$ for $R^2 = S_0$,

  where $P_2(\tau_1, R)$ is a continuous function of R by Lemma (4).

Case 1: Using (3.21−3.24), we have

$$\begin{aligned}\frac{\partial(P_1Q_1+P_2Q_2)}{\partial\tau} &= Q_1\frac{\partial P_1}{\partial\tau}+P_1\frac{\partial Q_1}{\partial\tau}+Q_2\frac{\partial P_2}{\partial\tau}+P_2\frac{\partial Q_2}{\partial\tau},\\ &= 2\sqrt{3}m_2^2Q_1^2+6m_1m_2Q_2^2+2Q_1^2Q_2^2\Bigg[\frac{\sqrt{3}m_1^2}{Q_1^2+Q_2^2}\\ &+ \frac{18m_1m_2Q_2^2(Q_1^2-Q_2^2)}{(Q_1^4+Q_1^2Q_2^2+Q_2^4)^{3/2}}+\frac{12m_1m_2}{\sqrt{Q_1^4+Q_1^2Q_2^2+Q_2^4}}\\ &- \frac{6m_1m_2Q_1^4}{(Q_1^4+Q_1^2Q_2^2+Q_2^4)^{3/2}}-2\Bigg]. \qquad (3.25)\end{aligned}$$

For some time $t\in[0,t_1]$, $x_1(t)$ and $x_2(t)$ are decreasing and increasing, respectively, and $S\geq x_1(t)>x_2(t)\geq 0$. Hence

$$0\leq Q_1=\sqrt{x_1(t)-x_2(t)}\leq\sqrt{S}=R. \qquad (3.26)$$

Also note that for some $\tau\in[0,\tau_1]$, we have

$$x_1(t_1)=x_2(t_1)=Q_2^2(\tau_1)=R_1^2<2S=2R^2. \qquad (3.27)$$

Thus from equations (3.25)−(3.27), we obtain

$$\begin{aligned}&\frac{\sqrt{3}m_1^2}{Q_1^2+Q_2^2}+\frac{18m_1m_2Q_2^2(Q_1^2-Q_2^2)}{(Q_1^4+Q_1^2Q_2^2+Q_2^4)^{3/2}}+\frac{12m_1m_2}{\sqrt{Q_1^4+Q_1^2Q_2^2+Q_2^4}}\\ &-\frac{6m_1m_2Q_1^4}{(Q_1^4+Q_1^2Q_2^2+Q_2^4)^{3/2}}\geq\frac{m_1^2}{\sqrt{3}R^2}+\frac{6m_1m_2}{\sqrt{7}R^2}>0.\end{aligned}$$

Choosing a particular value for R, we have

$$\begin{aligned}&\frac{\sqrt{3}m_1^2}{Q_1^2+Q_2^2}+\frac{18m_1m_2Q_2^2(Q_1^2-Q_2^2)}{(Q_1^4+Q_1^2Q_2^2+Q_2^4)^{3/2}}+\frac{12m_1m_2}{\sqrt{Q_1^4+Q_1^2Q_2^2+Q_2^4}}\\ &-\frac{6m_1m_2Q_1^4}{(Q_1^4+Q_1^2Q_2^2+Q_2^4)^{3/2}}-2\geq\frac{12\sqrt{3}m_2}{\sqrt{7}m_1}>0.\end{aligned}$$

So for $\tau \in [0, \tau_1]$ $(P_1Q_1+P_2Q_2)' \geq 0$ this means $P_1Q_1+P_2Q_2$ is increasing on the interval $[0, \tau_1]$. It can be seen from the initial conditions $P_1Q_1 + P_2Q_2 = 0$ at $\tau = 0$. So, $(P_1Q_1 + P_2Q_2)|_{\tau=\tau_1} = R_1P_2(\tau_1) > 0$. It follows that $P_2(\tau_1)$ is positive for $R = \frac{m_1}{2^{1/2}3^{1/4}}$.

Case 2: Now we prove that for some $R = \sqrt{S_0}$, $P_2(\tau_1) < 0$.

It is clear from Theorem 1 that at $S = S_0$ for some time $t^* < t_1$, we have $\dot{x}_1(t^*) < 0$ and $\dot{x}_2(t^*) = 0$. Therefore $3m_1\dot{x}_1(t^*) + 3m_2\dot{x}_2(t^*)$ is negative. The addition of the Newtonian equations gives

$$\begin{aligned} 3m_1\ddot{x}_1(t^*) + 3m_2\ddot{x}_2(t^*) &= -\frac{\sqrt{3}m_1^2}{x_1^2} - \frac{\sqrt{3}m_2^2}{x_2^2} \\ &- \frac{9m_1m_2(x_1+x_2)}{(x_1^2+x_1x_2+x_2^2)^{3/2}} < 0. \end{aligned}$$

From the above expression, it is clear $3m_1\dot{x}_1(t)+3m_2\dot{x}_2(t)$ is a decreasing function with respect to t. Therefore,

$$\lim_{t\to t_1}[3m_1\dot{x}_1(t) + 3m_2\dot{x}_2(t)] \leq 3m_1\dot{x}_1(t^*) + 3m_2\dot{x}_2(t^*) < 0.$$

Now we consider

$$\frac{P_2(\tau_1)}{2Q_2(\tau_1)} = \lim_{t\to t_1} p_2(t) = \lim_{t\to t_1}[3m_1\dot{x}_1(t) + 3m_2\dot{x}_2(t)] < 0. \tag{3.28}$$

As we know $Q_2(\tau_1) = R_1 > 0$, so, $P_2(\tau_1) < 0$. Hence by the intermediate value theorem, there exists some value of R in the interval $[0, \sqrt{S_0}]$ for which $P_2(\tau_1) = 0$. □

Theorem 2: If $P_2(\tau_1) = P_2(\tau_1, R) = 0$ for some R then the solution of the ordinary differential equations is a Schubart orbit.

Proof. This theorem is proved by using the uniqueness of the solution of the ordinary differential equations.

At time $\tau = 0$, a triple collision occurs between the inner bodies b_2, b_4 and b_6, and at $\tau = \tau_1$ a simultaneous double collision happens between three pairs of bodies (b_1, b_2),(b_3, b_4) and (b_5, b_6). Note that the solution P_i, Q_i for $i = 1, 2$ is continuous because our system is regularized. The boundary conditions at $\tau = 0$ and $\tau = \tau_1$ are given, respectively, by

$$Q_1(0) = \sqrt{A} = R, \quad Q_2(0) = 0, \quad P_1(0) = 0, \quad P_2(0) = \sqrt{24\sqrt{3}m_2^3},$$

and

$$\begin{aligned} Q_1(\tau_1) &= 0, \quad Q_2(\tau_1) = R_1 > 0, \quad P_1(\tau_1) = -\frac{6\sqrt{2}m_1m_2}{\sqrt{m_1+m_2}}, \\ P_2(\tau_1) &= 0. \end{aligned}$$

From equations (3.21) and (3.22), we have $Q_1'(\tau_1) = -\frac{R_1^2\sqrt{m_1+m_2}}{\sqrt{2}} < 0$ and $Q_2'(\tau_1) = \frac{Q_1(P_2Q_1 - Q_2P_1}{12m_2} = 0$. But $Q_2''(\tau_1) = -\frac{R_1^3m_1}{2} < 0$. So, by the second derivative test of relative extrema $Q_2(\tau_1)$ is a relative maximum of Q_2. In other words, we can say that Q_2 starts decreasing after the time τ_1. Now, by the uniqueness of the solution of our ordinary differential equations, the orbit from τ_1 to $2\tau_1$ is the same orbit as from 0 to τ_1 but with the reversed direction of velocities (see Figure 3.5), where $2\tau_1$ is the time when a second triple collision occurs

$$Q_1(2\tau_1) = -R, \quad Q_2(2\tau_1) = 0, \quad P_1(2\tau_1) = 0, \quad P_2(2\tau_1) = -\sqrt{24\sqrt{3}m_2^3}.$$

Again by symmetry and the uniqueness property at $\tau = 3\tau_1$, we have

$$\begin{aligned} Q_1(3\tau_1) &= 0, \quad Q_2(3\tau_1) = -R_1, \quad P_1(3\tau_1) = \frac{6\sqrt{2}m_1m_2}{\sqrt{m_1+m_2}}, \\ P_2(3\tau_1) &= 0. \end{aligned}$$

At $\tau = 4\tau_1$, we have

$$Q_1(4\tau_1) = R, \quad Q_2(4\tau_1) = 0, \quad P_1(4\tau_1) = 0, \quad P_2(4\tau_1) = \sqrt{24\sqrt{3}m_2^3}.$$

We can see that initial coordinates at $\tau = 0$ and $\tau = 4\tau_1$ are exactly the same (see Figure 3.5). So, this means that one complete period of the regularized system will be generated from $\tau = 0$ and $\tau = 4\tau_1$.

Also note that in real time t, the period is $2t_1$ instead of $4t_1$ because we have $q_i = Q_i^2$ and $P_i = 2Q_iP_i$ for $i = 1, 2$. □

Figure 3.5 shows the periodic solution with $m_1 = m_2 = 1$ in terms of regularized coordinates Q_1, Q_2, P_1 and P_2. The initial condition for this solution is calculated below in Remark 1.

Remark 1: As we know from Theorem 1 that at $S = S_0$ $\dot{x}_2(t^*) = 0 = \ddot{x}_2(t^*)$, if we take $m_1 = m_2 = 1$, then equation (3.12) can be written as

$$\begin{aligned} a^{10} - a^9 - 2\sqrt{3}a^8 - (3 + 2\sqrt{3})a^7 + (3 - 2\sqrt{3})a^6 + (9 + 4\sqrt{3})a^5 \\ +(39 + 4\sqrt{3})a^4 + (6 + 4\sqrt{3})a^3 - (9 + 2\sqrt{3})a^2 + (44 - 2\sqrt{3})a \\ -(8 + 2\sqrt{3}) = 0. \end{aligned}$$

With $a > 1$, we have $a \approx 2.521842784516267$, for which

$$S \geq \sqrt{3}m_1^2 + \frac{3m_1m_2a^2}{(a-1)^2} + \frac{3m_1m_2a^2(2a+1)}{(a^2+a+1)^{3/2}} \geq 13.682098128470169.$$

Thus the initial condition in the regularised coordinates takes the form

$$Q_1(0) \approx 3.58, \quad Q_2(0) = 0, \quad P_1(0) = 0, \quad P_2(0) = \sqrt{24\sqrt{3}}.$$

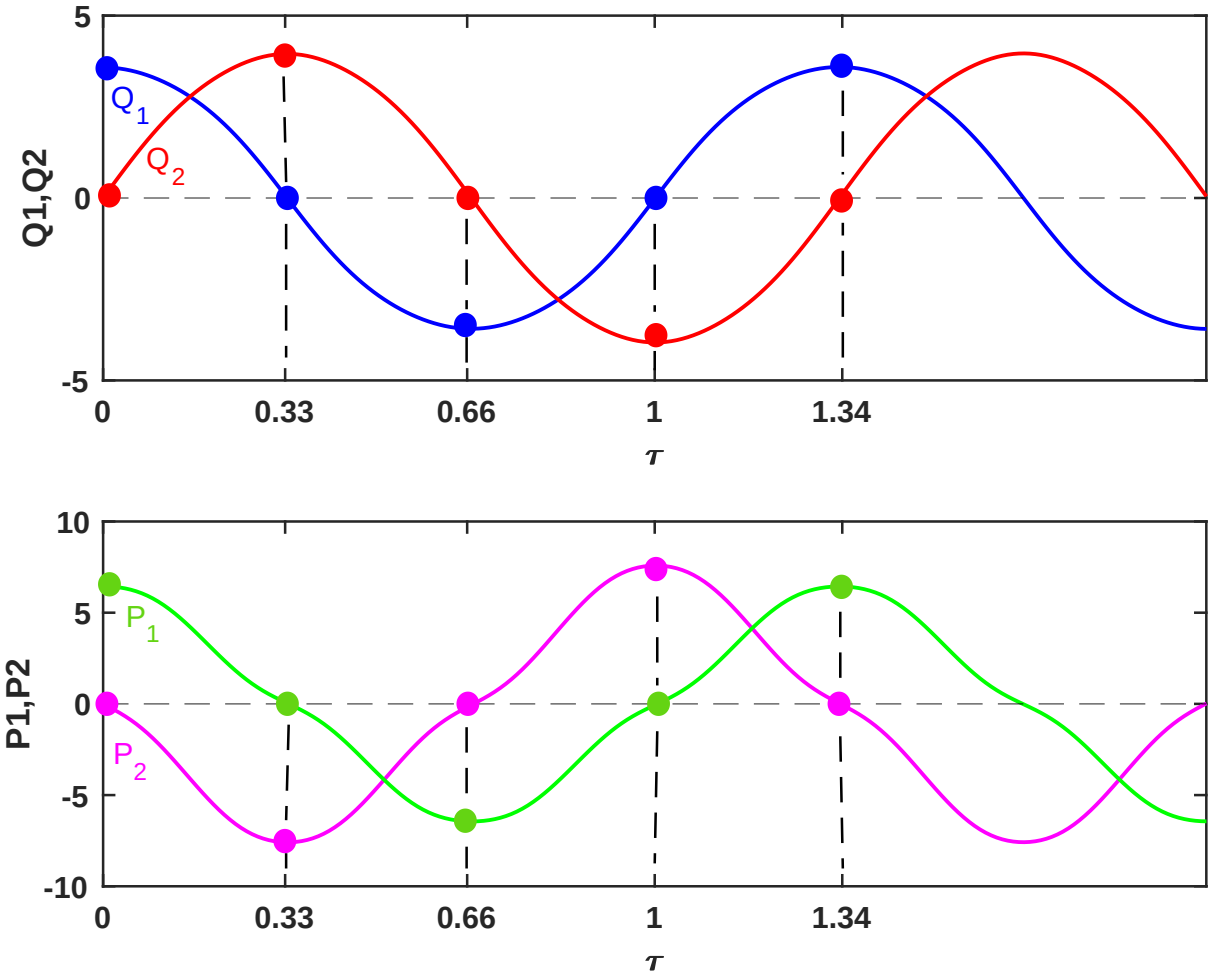

Figure 3.5 Plot of Q_1, Q_2, P_1 and P_2 against τ. The motion starts at $\tau = 0$, which is a triple collision between the inner bodies (b_2, b_4 and b_6). Coloured filled circles represent the values of Q_1, Q_2, P_1 and P_2 at $\tau_1 = 0.33, 2\tau_1 = 0.66, 3\tau_1 = 1.0$ and $4\tau_1 = 1.34$.

3.4 Chapter summary

In this chapter, we proved the analytic existence of the Schubart orbit. We first restricted the initial value to a proper interval, such that there were no additional collisions between every two connected collisions: a triple collision and an alternate binary collision. The interval is estimated by a turning point technique that guarantees the shape of the Schubart orbit. Then the existence is shown using the intermediate value theorem. The six-body problem is investigated further with non-aligned triangles in the next chapter.

Chapter 4

The planar symmetric six-body problem with non-aligned triangles

In this chapter, we present a description of the planar symmetric six-body problem with non-aligned triangles and an explanation of various techniques and methods used to find the solutions of this system.

The first and second sections are devoted to deriving the equations of motion of the six-body system that involves six point-masses moving about their centre of mass in a fixed plane. The simplifications reduce the general six-body problem with 42 parameters (36 for the velocities and positions and 6 for masses) to 30 parameters of which only six act as initial parameters (for more detail see Section 5). The symmetry and restrictions applied to the general six-body problem reduce its complexity, but the reduced system, despite its simplification, provides ideas and insights to understand the more general six-body system.

In order to regularise our system we follow the approach described by Sivasankaran, Steves and Sweatman [56] for the Caledonian symmetric four-body problem. We used the Levi-Civita coordinate transformation along with a time transformation which is based upon that proposed by Heggie [23].

Sections 3 and 4 outline some useful definitions and formulae which play a key role in the numerical techniques and procedures that we use in Chapter 5 to search for the family of periodic orbits.

The last section provides the algorithm and procedure used in the search for periodic solutions of our six-body system.

4.1 Equations of motion

The configuration of the six-body system at some time t with non-aligned triangles is shown in Figure 4.1. The six bodies b_i with coordinates (x_{2i-1}, x_{2i}) for $i = 1, 2, 3, 4, 5, 6$ are located at the vertices of two non-aligned equilateral triangles and interact with each other under their mutual Newtonian gravitational force. We consider that the bodies located on the same triangle have equal masses that is $m_1 = m_3 = m_5$ and $m_2 = m_4 = m_6$ and they are moving about the centre of mass in a fixed plane. The centre of mass is fixed at the origin: since the system experiences no external force, the centre of mass of the system can be taken to be at rest. The motion of each mass is described by two coordinates x_{2i-1}, x_{2i} for position and two coordinates $\omega_{2i-1}, \omega_{2i}$ for momenta with $i = 1, 2, 3, 4, 5, 6$, where x_{2i-1}, ω_{2i-1} and x_{2i}, ω_{2i} are along the x-axis and the y-axis, respectively for $i = 1, 2, 3, 4, 5, 6$.

We consider that the bodies b_1, b_3, b_5 are located on the vertices of the same equilateral triangle (blue triangle), while the remaining bodies b_2, b_4, b_6 are located on another triangle (orange triangle) as shown in Figure 4.1. When bodies move they change their relative position to bodies on the other triangle but we label them according to their configuration at some time $t = t_0$.

The planar six-body problem has some symmetric restrictions: the

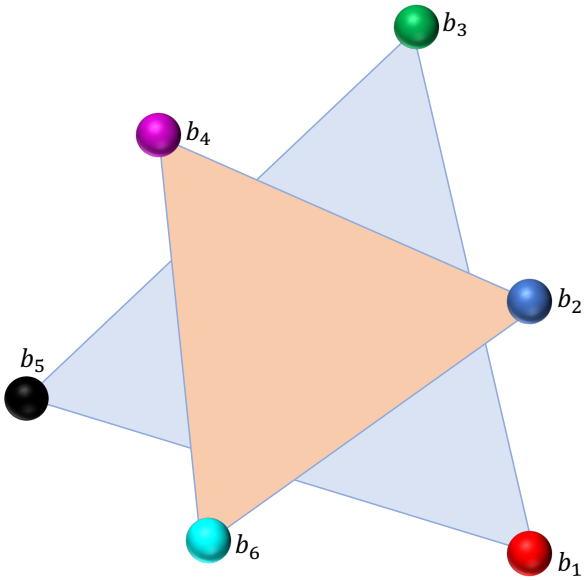

Figure 4.1 Six-body system with non-aligned triangles: (filled circles stand for bodies b_i for $i = 1, 2, ...6$, located at the vertices of two non-aligned triangles).

symmetry about the centre of mass which is fixed at the origin and the time symmetry. We apply symmetry about the centre of mass at the origin in such a way that the dynamical evolution of the bodies placed at the vertices of the same triangle are a rotational image of each other. For example, the bodies b_1, b_3 and b_5 are located at the vertices of an equilateral triangle moving about the centre of mass. So, there is rotational symmetry of 120° about the origin. This implies that the bodies b_3 and b_5 are rotational images of the body b_1. Similarly, the bodies b_4 and b_6 are rotational images of the body b_2. Thus b_1 and b_2 move symmetrically to b_3, b_4 and b_5, b_6, respectively.

The six-body system satisfies the Mirror theorem [51]: "if N point masses are acted upon by their mutual gravitational forces only, and at a certain epoch, each radius vector from the centre of mass of the system is perpendicular to every velocity vector, then the orbit of each mass after

that epoch is a mirror image of its orbit prior to that epoch."

The time symmetry of the six-body system implies that, if we start at time $t = t_0$, the certain epoch of the Mirror theorem, then the dynamical behaviour of the six-body system at time $t_1 = t_0 + \Delta t_0$ is a mirror image of its behaviour at $t_{-1} = t_0 - \Delta t_0$, where t_{-1} and t_1 are the times before and after t_0, respectively. In other words, if we integrate our six-body system backwards in time it will not make any change in the description of the system's behaviour.

The position coordinates of the two bodies b_1 and b_2 can be taken to be $\mathbf{r_1} = (x_1, x_2)$, $\mathbf{r_2} = (x_3, x_4)$. However, the position coordinates of the remaining bodies can be computed using the rotational symmetric property described above. We calculate the position coordinate $\mathbf{r_3} = (x_5, x_6)$ of body b_3 using the rotational matrix with $\theta = 120^\circ$

$$\begin{aligned} \mathbf{r_3} &= \begin{pmatrix} \cos 120^\circ & -\sin 120^\circ \\ \sin 120^\circ & \cos 120^\circ \end{pmatrix} \begin{pmatrix} x_1 \\ x_2 \end{pmatrix}, \\ &= \left(\frac{-x_1}{2} - \frac{\sqrt{3}x_2}{2}, \frac{-x_2}{2} + \frac{\sqrt{3}x_1}{2} \right). \end{aligned}$$

The position coordinates of b_5 are calculated using the rotational matrix with $\theta = -120^\circ$ or 240°

$$\begin{aligned} \mathbf{r_5} &= \begin{pmatrix} \cos 240^\circ & -\sin 240^\circ \\ +\sin 240^\circ & \cos 240^\circ \end{pmatrix} \begin{pmatrix} x_1 \\ x_2 \end{pmatrix}, \\ &= \left(\frac{-x_1}{2} + \frac{\sqrt{3}x_2}{2}, \frac{-x_2}{2} - \frac{\sqrt{3}x_1}{2} \right). \end{aligned}$$

Similarly, we can find the position coordinates $\mathbf{r_4}$ and $\mathbf{r_6}$ of bodies b_4 and b_6 given by

$$\begin{aligned}\mathbf{r_4} &= \left(\frac{-x_3}{2} - \frac{\sqrt{3}x_4}{2}, \frac{-x_4}{2} + \frac{\sqrt{3}x_3}{2}\right),\\ \mathbf{r_6} &= \left(\frac{-x_3}{2} + \frac{\sqrt{3}x_4}{2}, \frac{-x_4}{2} - \frac{\sqrt{3}x_3}{2}\right).\end{aligned}$$

The corresponding momenta of b_1 and b_2 are

$$(\omega_1, \omega_2) = 3m_1(\dot{x}_1, \dot{x}_2), \quad (\omega_3, \omega_4) = 3m_2(\dot{x}_3, \dot{x}_4).$$

Similarly,

$$\begin{aligned}(\omega_5, \omega_6) &= 3m_1\left(\frac{-\dot{x}_1}{2} - \frac{\sqrt{3}\dot{x}_2}{2}, \frac{-\dot{x}_2}{2} + \frac{\sqrt{3}\dot{x}_1}{2}\right),\\ (\omega_7, \omega_8) &= 3m_2\left(\frac{-\dot{x}_3}{2} - \frac{\sqrt{3}\dot{x}_4}{2}, \frac{-\dot{x}_4}{2} + \frac{\sqrt{3}\dot{x}_3}{2}\right),\\ (\omega_9, \omega_{10}) &= 3m_1\left(\frac{-\dot{x}_1}{2} + \frac{\sqrt{3}\dot{x}_2}{2}, \frac{-\dot{x}_2}{2} - \frac{\sqrt{3}\dot{x}_1}{2}\right),\\ (\omega_{11}, \omega_{12}) &= 3m_2\left(\frac{-\dot{x}_3}{2} + \frac{\sqrt{3}\dot{x}_4}{2}, \frac{-\dot{x}_4}{2} - \frac{\sqrt{3}\dot{x}_3}{2}\right).\end{aligned}$$

For simplicity, we consider that at time $t = 0$, the start of integration, one pair of bodies (b_1 and b_2) is positioned on the x-axis, as shown in Figure 4.2. The initial velocities of these bodies are perpendicular to the x-axis and initially ($t = t_0 = 0$) have the opposite direction.

The units of our six-body system are the standard N-body units, based on the Heggie regularization technique [24] and chosen such that, the gravitational constant G, the total energy E, and the total mass M are

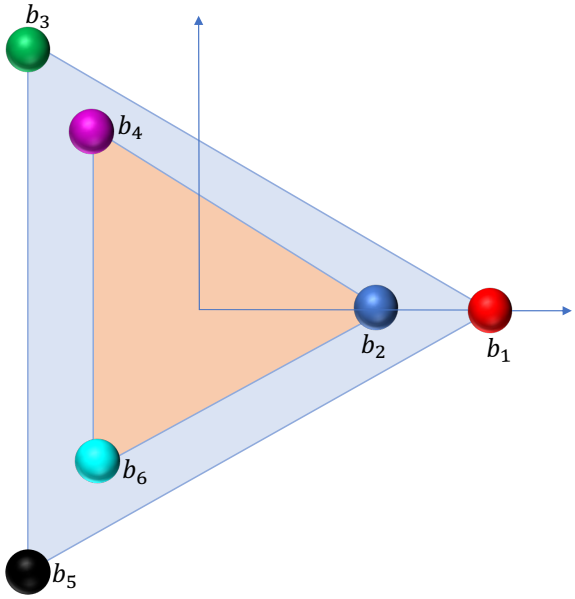

Figure 4.2 Arrangement of the six-body system at time $t = 0$.

fixed, respectively, as follows

$$G = 1, \quad E = -1, \quad M = \sum_{i=1}^{6} m_i = 6.$$

The planar six-body problem has six classical integrals of motion.

1. The four integrals for the centre of mass:

$$\begin{aligned} \frac{1}{M}\sum_{i=1}^{6} m_i x_{2i-1} &= x_0, \quad \frac{1}{M}\sum_{i=1}^{6} m_i x_{2i} = y_0, \\ \frac{1}{M}\sum_{i=1}^{6} m_i \dot{x}_{2i-1} &= \dot{x}_0, \quad \frac{1}{M}\sum_{i=1}^{6} m_i \dot{x}_{2i} = \dot{y}_0. \end{aligned} \tag{4.1}$$

2. Integral of angular momentum:

$$\sum_{i=1}^{6} m_i (x_{2i-1}\dot{x}_{2i} - x_{2i}\dot{x}_{2i-1}) = A. \tag{4.2}$$

3. Energy integral:

$$\sum_{i=1}^{6} \frac{1}{2} m_i (\dot{x}_{2i-1}^2 + \dot{x}_{2i}^2) - \sum_{1 \le i < j \le 6} \frac{m_i m_j}{r_{ij}} = E, \tag{4.3}$$

where r_{ij} is the interbody distance between the bodies b_i and b_j.

As described earlier, the centre of mass is fixed at the origin $(x_0, y_0) = (0, 0) = (\dot{x}_0, \dot{y}_0)$. So, the dynamical symmetry leaves only the last two integrals, the energy (E) integral and the angular momentum (A) integral after removing the centre of mass integrals.

The planar symmetric six-body system has fifteen interbody distances, we only calculate the following five distances

1. r_{12}, the distance between the bodies b_1 and b_2,
2. r_{13}, the distance between the bodies b_1 and b_3,
3. r_{14}, the distance between the bodies b_1 and b_4,
4. r_{16}, the distance between the bodies b_1 and b_6,
5. r_{24}, the distance between the bodies b_2 and b_4,

The remaining ten distances are symmetric about the centre of mass and are given by:

$$\begin{aligned} r_{12} &= r_{34} = r_{56}, \\ r_{13} &= r_{15} = r_{35}, \\ r_{14} &= r_{25} = r_{36}, \\ r_{16} &= r_{45} = r_{23}, \\ r_{24} &= r_{26} = r_{46}. \end{aligned}$$

The total energy of the six-body system is fixed as $E = K + U = -1$ as described earlier in Section 2.1.1 of Chapter 2. The kinetic energy (K)

and the potential energy (U) of the six-body system with non-aligned triangles are described, respectively, by the equations

$$\begin{aligned} K &= \frac{3m_1}{2}(\dot{x}_1^2+\dot{x}_2^2)+\frac{3m_2}{2}(\dot{x}_3^2+\dot{x}_4^2)=\frac{1}{6m_1}(\omega_1^2+\omega_2^2) \\ &+ \frac{1}{6m_2}(\omega_3^2+\omega_4^2), \\ U &= -\frac{3m_1m_2}{r_{12}}-\frac{3m_1m_2}{r_{14}}-\frac{3m_1m_2}{r_{16}}-\frac{3m_1^2}{r_{13}}-\frac{3m_2^2}{r_{24}}, \end{aligned}$$

with

$$\begin{aligned} r_{12} &= \sqrt{(x_1-x_3)^2+(x_2-x_4)^2}, \\ r_{14} &= \sqrt{(x_1+\frac{x_3}{2}+\frac{\sqrt{3}}{2}x_4)^2+(x_2+\frac{x_4}{2}-\frac{\sqrt{3}}{2}x_3)^2}, \\ r_{16} &= \sqrt{(x_1+\frac{x_3}{2}-\frac{\sqrt{3}}{2}x_4)^2+(x_2+\frac{x_4}{2}+\frac{\sqrt{3}}{2}x_3)^2}, \\ r_{13} &= \sqrt{(\frac{3}{2}x_1+\frac{\sqrt{3}}{2}x_2)^2+(\frac{3}{2}x_2-\frac{\sqrt{3}}{2}x_1)^2}, \\ r_{24} &= \sqrt{(\frac{3}{2}x_3+\frac{\sqrt{3}}{2}x_4)^2+(\frac{3}{2}x_4-\frac{\sqrt{3}}{2}x_3)^2}. \end{aligned}$$

The system is symmetrically distributed about the centre of mass and its Hamiltonian is defined as

$$\begin{aligned} H &= \frac{1}{6m_1}(w_1^2+w_2^2)+\frac{1}{6m_2}(w_3^2+w_4^2)-\frac{3m_1m_2}{r_{12}}-\frac{3m_1m_2}{r_{14}} \\ &- \frac{3m_1m_2}{r_{16}}-\frac{3m_1^2}{r_{13}}-\frac{3m_2^2}{r_{24}}. \end{aligned} \tag{4.4}$$

The differential equations for the Hamiltonian (Equation 4.4) are

$$\frac{dx_i}{dt} = \frac{\partial H}{\partial \omega_i}, \quad \frac{dx_j}{dt} = \frac{\partial H}{\partial \omega_j}, \quad \frac{d\omega_i}{dt} = -\frac{\partial H}{\partial x_i}, \quad \frac{d\omega_j}{dt} = -\frac{\partial H}{\partial x_j}, \tag{4.5}$$

for $i = 1, 3$ and $j = 2, 4$. The initial conditions at time $t = 0$, are that the bodies b_1 and b_2 are located on the x-axis with coordinates ($x_1(0)$,0), ($x_3(0)$, 0) and momenta (0, $\omega_2(0)$), (0, $\omega_4(0)$). We choose all the masses equal to unity.

4.2 Levi-Civita regularisation

It is very challenging to numerically solve the differential equations directly near the close encounter of bodies because of the singularity that appears in the equations of motion at collision events. The accuracy of numerical integration becomes poor near the collision event. The integration process becomes very long by decreasing the step size of the numerical integrator in order to compensate for the numerical error at each step. This results in the growth of round-off errors.

In order to handle such numerical difficulties, we regularise our singular differential equations using the Levi-Civita coordinate transformation along with a time transformation similar to the one proposed by Heggie (Equation 1.5). To perform the Levi-Civita coordinate transformation,

first, we introduce interbody coordinates q_i for $i = 1, 2, ...10$.

$$\begin{aligned}
q_1 &= x_1 - x_3, & q_2 &= x_2 - x_4, \\
q_3 &= x_1 + \frac{x_3}{2} + \frac{\sqrt{3}}{2}x_4, & q_4 &= x_2 + \frac{x_4}{2} - \frac{\sqrt{3}}{2}x_3, \\
q_5 &= x_1 + \frac{x_3}{2} - \frac{\sqrt{3}}{2}x_4, & q_6 &= x_2 + \frac{x_4}{2} + \frac{\sqrt{3}}{2}x_3, \\
q_7 &= x_3, & q_8 &= x_4, \\
q_9 &= x_1, & q_{10} &= x_2.
\end{aligned} \tag{4.6}$$

The corresponding conjugate momenta p_j are related to the original momenta ω_i by means of a generating function F given by

$$\omega_i = \frac{\partial F}{\partial x_i}, \quad F = \sum_{j=1}^{10} p_j q_j(x_i), \text{ for } i = 1, ...4, \tag{4.7}$$

where the generating function F (Goldstein [19], pp.371−375) is

$$\begin{aligned}
F &= p_1(x_1 - x_3) + p_2(x_2 - x_4) + p_3\left(x_1 + \frac{x_3}{2} + \frac{\sqrt{3}}{2}x_4\right) \\
&+ p_4\left(x_2 + \frac{x_4}{2} - \frac{\sqrt{3}}{2}x_3\right) + p_5\left(x_1 + \frac{x_3}{2} - \frac{\sqrt{3}}{2}x_4\right) \\
&+ p_6\left(x_2 + \frac{x_4}{2} + \frac{\sqrt{3}}{2}x_3\right) + p_7x_3 + p_8x_4 + p_9x_1 + p_{10}x_2.
\end{aligned} \tag{4.8}$$

Using (4.7) and (4.8) we get the following four relations between the original momenta and conjugate momenta

$$\begin{aligned}
\omega_1 &= p_1 + p_3 + p_5 + p_9. \\
\omega_2 &= p_2 + p_4 + p_6 + p_{10}. \\
\omega_3 &= -p_1 + \frac{p_3}{2} - \frac{\sqrt{3}}{2}p_4 + \frac{p_5}{2} + \frac{\sqrt{3}}{2}p_6 + p_9. \\
\omega_4 &= -p_2 + \frac{\sqrt{3}}{2}p_3 + \frac{p_4}{2} - \frac{\sqrt{3}}{2}p_5 + \frac{p_6}{2} + p_{10}.
\end{aligned} \tag{4.9}$$

In order to find the inverse transformation, we need another six relations. From the definition (4.6) of q_i , we can write the following six relations

$$\begin{aligned}
q_1 &= -q_7 + q_9, & q_2 &= -q_8 + q_{10}, \\
q_3 &= \frac{q_7}{2} + q_9 + \frac{\sqrt{3}}{2}q_8, & q_4 &= \frac{q_8}{2} + q_{10} - \frac{\sqrt{3}}{2}q_7, \\
q_5 &= \frac{q_7}{2} + q_9 - \frac{\sqrt{3}}{2}q_8, & q_6 &= \frac{q_8}{2} + q_{10} + \frac{\sqrt{3}}{2}q_7.
\end{aligned}$$

To remove the degeneracy found in the momentum coordinates, we make a choice to set a similar relation for the momenta [23]

$$\begin{aligned}
p_1 &= -p_7 + p_9, & p_2 &= -p_8 + p_{10}, \\
p_3 &= \frac{p_7}{2} + p_9 + \frac{\sqrt{3}}{2}p_8, & p_4 &= \frac{p_8}{2} + p_{10} - \frac{\sqrt{3}}{2}p_7, \\
p_5 &= \frac{p_7}{2} + p_9 - \frac{\sqrt{3}}{2}p_8, & p_6 &= \frac{p_8}{2} + p_{10} + \frac{\sqrt{3}}{2}p_7.
\end{aligned} \tag{4.10}$$

Applying (4.9) and (4.10), we find the conjugate momenta formulae:

$$\begin{aligned}
p_1 &= \frac{w_1}{4} - \frac{w_3}{4}, & p_2 &= \frac{w_2}{4} - \frac{w_4}{4},\\
p_3 &= \frac{w_1}{4} + \frac{w_3}{8} + \frac{\sqrt{3}}{8}w_4, & p_4 &= \frac{w_2}{4} - \frac{\sqrt{3}}{8}w_3 + \frac{w_4}{8},\\
p_5 &= \frac{w_1}{4} + \frac{w_3}{8} - \frac{\sqrt{3}}{8}w_4, & p_6 &= \frac{w_2}{4} + \frac{\sqrt{3}}{8}w_3 + \frac{w_4}{8},\\
p_7 &= \frac{w_3}{4}, & p_8 &= \frac{w_4}{4},\\
p_9 &= \frac{w_1}{4}, & p_{10} &= \frac{w_2}{4}.
\end{aligned}$$

Finally, we transform our system to Levi-Civita type coordinates (Q_k, P_k), such that

$$q_k = Q_k^2 - Q_{k+1}^2, \quad q_{k+1} = 2Q_kQ_{k+1} \quad k = 1, 3, 5, 7, 9.$$

We have

$$\begin{aligned}
q_1 &= Q_1^2 - Q_2^2, & q_2 &= 2Q_1Q_2,\\
q_3 &= Q_3^2 - Q_4^2, & q_4 &= 2Q_3Q_4,\\
q_5 &= Q_5^2 - Q_6^2, & q_6 &= 2Q_5Q_6,\\
q_7 &= Q_7^2 - Q_8^2, & q_8 &= 2Q_7Q_8,\\
q_9 &= Q_9^2 - Q_{10}^2, & q_{10} &= 2Q_9Q_{10}.
\end{aligned} \tag{4.11}$$

The inverse transformation of the above formulae is found by solving the equation $z = w^2$ or $w = \sqrt{z}$, where $z = q_1 + iq_2$ and $w = Q_1 + iQ_2$, $z, \omega \in \mathbb{C}$. Using polar coordinates, the complex solution can be represented as

$$w = \sqrt{re^{i\theta}} = \sqrt{r}\left(\cos\frac{\theta}{2} + i\sin\frac{\theta}{2}\right), \tag{4.12}$$

where $r = \sqrt{q_1^2 + q_2^2}$ and $\theta = \arctan(\frac{q_2}{q_1})$. Since $x_1 > x_3 > 0$ at $t = 0$, then $q_1 = x_1 - x_3$ is positive. Further $q_2 = x_2 - x_4$ is zero at $t = 0$. So, we choose to neglect the case of the negative square root. The resulting relation for inverse formulae is calculated using (4.12).

$$Q_1 = (q_1^2 + q_2^2)^{\frac{1}{4}} \cos\left(\frac{\arctan\frac{q_2}{q_1}}{2}\right), \quad Q_2 = (q_1^2 + q_2^2)^{\frac{1}{4}} \sin\left(\frac{\arctan\frac{q_2}{q_1}}{2}\right).$$

We apply the same assumption to calculate the remaining regularized position coordinates Q_k for $k = 3, 4, ..., 10$.

The corresponding conjugate momenta can be found using the generating function G

$$P_i \;=\; \frac{\partial G}{\partial Q_i}, \text{ where } G = \sum_{\substack{i=1 \\ i \text{ odd}}}^{11} p_i(Q_i^2 - Q_{i+1}^2) + \sum_{\substack{j=2 \\ j \text{ even}}}^{12} 2p_j Q_{j-1} Q_j.$$

That is for $j = 1, 3, 5, 7, 9$, we have

$$P_j \;=\; 2p_j Q_j + 2p_{j+1} Q_{j+1}, \quad P_{j+1} = -2p_j Q_{j+1} + 2p_{j+1} Q_j,$$

or, explicitly,

$$\begin{aligned}
P_1 &= 2p_1 Q_1 + 2p_2 Q_2, & P_2 &= -2p_1 Q_2 + 2p_2 Q_1, \\
P_3 &= 2p_3 Q_3 + 2p_4 Q_4, & P_4 &= -2p_3 Q_4 + 2p_4 Q_3, \\
P_5 &= 2p_5 Q_5 + 2p_6 Q_6, & P_6 &= -2p_5 Q_6 + 2p_6 Q_5, \\
P_7 &= 2p_7 Q_7 + 2p_8 Q_8, & P_8 &= -2p_7 Q_8 + 2p_8 Q_7, \\
P_9 &= 2p_9 Q_9 + 2p_{10} Q_{10}, & P_{10} &= -2p_9 Q_{10} + 2p_{10} Q_9.
\end{aligned}$$

For the inverse transformation, we use the formulae

$$
\begin{aligned}
p_1 &= -\frac{1}{2}\frac{P_2Q_2 - P_1Q_1}{Q_1^2+Q_2^2}, & p_2 &= \frac{1}{2}\frac{P_1Q_2 + P_2Q_1}{Q_1^2+Q_2^2},\\
p_3 &= -\frac{1}{2}\frac{P_4Q_4 - P_3Q_3}{Q_3^2+Q_4^2}, & p_4 &= \frac{1}{2}\frac{P_3Q_4 + P_4Q_3}{Q_3^2+Q_4^2},\\
p_5 &= -\frac{1}{2}\frac{P_6Q_6 - P_5Q_5}{Q_5^2+Q_6^2}, & p_6 &= \frac{1}{2}\frac{P_5Q_6 + P_6Q_5}{Q_5^2+Q_6^2},\\
p_7 &= -\frac{1}{2}\frac{P_8Q_8 - P_7Q_7}{Q_7^2+Q_8^2}, & p_8 &= \frac{1}{2}\frac{P_7Q_8 + P_8Q_7}{Q_7^2+Q_8^2},\\
p_9 &= -\frac{1}{2}\frac{P_{10}Q_{10} - P_9Q_9}{Q_9^2+Q_{10}^2}, & p_{10} &= \frac{1}{2}\frac{P_9Q_{10} - P_{10}Q_9}{Q_9^2+Q_{10}^2}.
\end{aligned}
$$

Following the general approach proposed by Heggie [23], we choose the rescaled time τ for the planar symmetric six-body problem defined by

$$
\frac{dt}{d\tau} = g = \frac{r_{12}r_{13}r_{14}r_{16}r_{24}}{(r_{12}+r_{13}+r_{14}+r_{16}+r_{24})^{\frac{7}{2}}},
$$

with

$$
\begin{aligned}
r_{12} &= Q_1^2 + Q_2^2,\\
r_{13} &= \sqrt{3}(Q_9^2 + Q_{10}^2),\\
r_{14} &= Q_3^2 + Q_4^2,\\
r_{16} &= Q_5^2 + Q_6^2,\\
r_{24} &= \sqrt{3}(Q_7^2 + Q_8^2).
\end{aligned}
$$

The final time-transformed Hamiltonian takes the form

$$
\Gamma = \frac{dt}{d\tau}(\tilde{H}(Q_k, P_k) - E), \tag{4.13}
$$

where $\tilde{H}$ is the original Hamiltonian, considered as a function of regu-

larised coordinates Q_k and P_k, and E represents the constant numerical value of $\tilde{H}$. The final regularised equations of motion together with the time equation are

$$\frac{dQ_i}{d\tau} = \frac{\partial \Gamma}{\partial P_i}, \quad \frac{dP_i}{d\tau} = -\frac{\partial \Gamma}{\partial Q_i}, \quad \frac{dt}{d\tau} = g. \tag{4.14}$$

From the implementation of the above equations, the results are presented in Chapter 5.

4.3 Periodic solutions and orbital period

Periodic orbits or periodic solutions play a key role in the rich structure of dynamical systems. Poincaré was the first to point out that the set of periodic cycles can be thought of as the skeleton of a dynamical system. We can find the standard definition of periodic solution in Poincaré ([48], pp.79-82 and 95-97).

Whittaker [72] defined a periodic orbit for the three-body problem. "In the problem of three bodies, a solution is said to be periodic if the mutual distances of the bodies are periodic functions of the time, although the bodies may not necessarily have the same orientation at the end of a period as at its beginning."

The periodicity criterion that we use for the orbits of the six-body system is expressed by two conditions explained by Broucke [8] for the three-body problem and later by Chopovda and Sweatman [15] for the four-body problem. These two conditions for the six-body system are explained below.

In our setting of the initial configuration, the bodies b_2, b_4, and b_6 are at

their maximum distance from the centre of mass at $t = 0$ so there is time symmetry. If we denote r_{24} as the distance between the bodies b_2 and b_4, then at $t = 0$ r_{24} has its maximum possible value and $\dot{r}_{24} = 0$. After a half period of the orbit $\dot{r}_{24}$ is again zero but r_{24} is minimal. When bodies complete one period, the distance r_{24} again has a maximum value, and so on. Thus we can use the relation $\dot{r}_{24} = 0$ to find the period of an orbit. In the regularised form it can be written as

$$Q_7\dot{Q}_7 + Q_8\dot{Q}_8 = 0. \tag{4.15}$$

Considering the symmetries of the planar symmetric six-body problem, we derive another relation to find the period of orbits. At the start of integration, $t = 0$, the bodies are on the same line. The bodies line up again in the same arrangements at the end of the period $t = T$. Now using the equation of a line through the origin $Y = kX$, we derive another relation to find the end of a period:

$$Y_1X_2 - X_1Y_2 = 0. \tag{4.16}$$

In regularised coordinates using equations (4.6) and (4.11), we have

$$(Q_7Q_{10} - Q_8Q_9)(Q_7Q_9 + Q_8Q_{10}) = 0. \tag{4.17}$$

Thus, when the above relations become true we can say that the bodies have completed one period. In actual computation, Equation (4.17) works well to compute the end of periods for the orbits of the six-body problem.

4.4 Motion in Rotating Coordinates

Following the approach described by Chopovda and Sweatman [15] (citing Hénon [26]), we express the motion of our six-body system in a rotating frame, which rotates with a constant angular velocity $\omega = \frac{\theta}{T}$ around the centre of mass, where T is the period of the orbit and θ is the angle by which the bodies deviate from their original positions during one period. Thus to transform the physical coordinates to rotating coordinates, we first track an orbit for one period T and then measure the angle θ between the x-axis and the line through the bodies and origin. The angular velocity can be calculated using the relation $\omega = \frac{\theta}{T}$, where θ is set in the region $[-\pi\ \pi]$. We then introduce rotating coordinates using the rotational matrix $R(t)$ for the time of integration $t \in [0, T]$

$$R(t) = \begin{bmatrix} \cos\omega t & \sin\omega t \\ -\sin\omega t & \cos\omega t \end{bmatrix}.$$

It is sometimes advantageous to use rotating coordinates during the search for an orbit. The rotating coordinates enable us to find the relative value by which a body deviates from its initial position when it moves along the orbit. This allows us to remove the rotation of the system and search for periodic orbits of the reduced system.

When the physical coordinates rotate by an angle $-\theta$ during one period around the origin, then rotating coordinates make all successive periods of orbits match with one another as shown in Figure 4.4. This makes the periodicity clearer because it is not obvious for some orbits that they are actually periodic in a relative sense. Note that the representation of orbits in a rotating frame is not unique, since the angle θ is defined modulo 2π, so θ can also be measured in regions $[0,\ 2\pi]$ and $[-2\pi,\ 0]$.

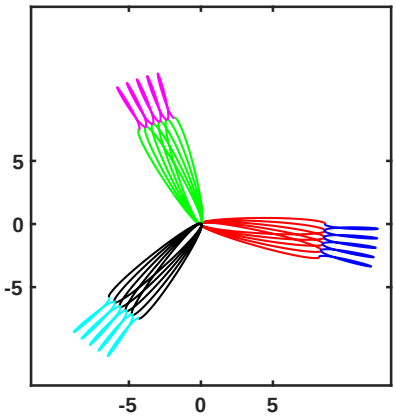

Figure 4.3 About five periods are shown of a periodic orbit plotted in fixed coordinates in a non-rotating frame.

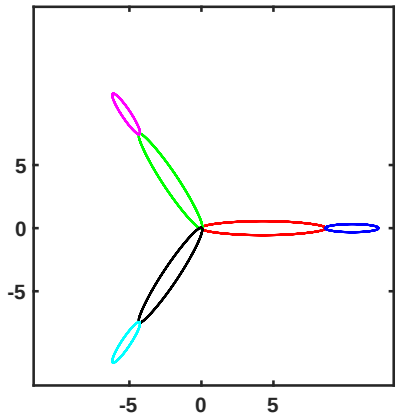

Figure 4.4 About five periods are shown of the same orbit plotted in rotating coordinates in a rotating frame.

4.5 Procedures to search the periodic orbits for the planar six-body system

This section provides an explanation of the procedure and algorithm that was used to explore the six-body system with non-aligned triangles. We used the differential correction method to search for the periodic orbits for our system by following the approach used by Broucke [7, 8] and Hénon [25, 26] to study three-body orbits and Chopovda and Sweatman [15] to explore four-body periodic orbits.

The implementation of the differential correction technique is performed in physical coordinates, but we can apply this procedure in different ways to different coordinates of the system. For example, the differential correction procedure can also be performed in regularised coordinates but it will result in an increased number of variables.

The next subsection outlines the differential correction procedure and

explains the idea of searching for the family of periodic orbits for the six-body system. The algorithm for the differential correction procedure is provided at the end of this chapter.

The methods and algorithms that are used during our study are implemented in MATLAB (Version R2019a). We used the standard MATLAB ode45 integrator based on Runge-Kutta $(4, 5)$ methods, to integrate the equations of motion of the six-body system. To find the orbits with good accuracy we fix the relative and absolute error tolerance as 10^{-12} during orbit integration.

4.5.1 Differential correction

The general six-body problem has a 36-dimensional phase space: where each body is described with three momentum coordinates and three position coordinates. In addition, each body has a specific mass $(m_i, i = 1, 2, ..., 6)$ and volume $(V_i, i = 1, 2, ..., 6)$. The latter quantity is neglected because we assume the masses of our six-body system are point masses. The motion of our six-body system is restricted to a plane, the momenta and the position coordinates corresponding to the third dimension are zero. Thus, when searching for a periodic orbit, we are left with a six-body system with 30 parameters.

In order to find the desired orbits, we reduce our system by applying some restrictions as described in Section 1 of Chapter 4. The system is symmetric about the centre of mass which reduces the number of parameters to 10. There are also six classical integrals of motion (discussed in section 1). The centre of mass is fixed at the origin, that is $(x_0, y_0) = 0 = (\dot{x}_0, \dot{y}_0)$.

The energy integral (E) is fixed by choosing $E = -1$. Thus five out of six integrals of motion are fixed. The last integral of angular momentum

(A) is used as a parameter in the search for orbits. Another parameter can be computed by fixing the total mass of the system

$$M = \sum_{i=1}^{6} m_i = 6.$$

We choose all the masses to be equal. So,

$$m_i = 1, \text{ for all } \quad i = 1, 2, ..., 6.$$

We choose the origin of the independent variable t in such a way that at the start of integration ($t = 0$) one of the bodies is on the x-axis. This means that at $t = 0$, the y-coordinate for the body located on the x-axis is zero. We also apply the initial configuration to restrict another four parameters ($x_2 = x_4 = \omega_1 = \omega_3 = 0$). If we do not fix the origin of the independent variable t, then we can trivially get an infinite number of periodic solutions just by changing the origin of time (initial point on the orbit) or by rotating the initial configuration about the centre of mass [25, 26].

We start our search for a periodic solution with particular properties for the specific values of the parameters A and m_1. We also need two more parameters x_1 and x_3 to characterize the initial state of the system. This is done by utilizing the technique of differential corrections, which we now describe.

The periodicity conditions can be defined as

$$\boldsymbol{x}(t) = \boldsymbol{x}(t + T), \qquad \dot{\boldsymbol{x}}(t) = \dot{\boldsymbol{x}}(t + T),$$

where the vector $\boldsymbol{x}$ contains the positions of all bodies in rotating coordinates, T is the period of the orbit and t is time. The above periodicity conditions imply that the difference between initial coordinates and final coordinates (coordinates after one period) should be zero.

However, if the required orbit is not quite periodic then we can find a periodic solution by introducing a small correction $\Delta\boldsymbol{x}_0$ to the initial coordinate vector $\boldsymbol{x}(0) = \boldsymbol{x}_0$ [9], so that

$$\boldsymbol{x}_0 + \Delta\boldsymbol{x}_0 = \boldsymbol{x}(T, \boldsymbol{x}_0 + \Delta\boldsymbol{x}_0). \tag{4.18}$$

In order to ensure that the linear theory is valid we take the correction $\Delta\boldsymbol{x}_0$ to be a very small quantity. We expand the right-hand side of this equation in $\Delta\boldsymbol{x}_0$ about the point $(T, \boldsymbol{x}_0)$, neglecting the higher order terms,

$$\boldsymbol{x}_0 + \Delta\boldsymbol{x}_0 = \boldsymbol{x}(T, \boldsymbol{x}_0) + \frac{\partial \boldsymbol{x}}{\partial \boldsymbol{x}_0}\Delta\boldsymbol{x}_0.$$

Simplification of this equation gives

$$\Delta\boldsymbol{x}_0 = \left[\frac{\partial \boldsymbol{x}}{\partial \boldsymbol{x}_0} - I\right]^{-1} (\boldsymbol{x}_0 - \boldsymbol{x}(T, \boldsymbol{x}_0)), \tag{4.19}$$

where $\frac{\partial \boldsymbol{x}}{\partial \boldsymbol{x}_0}$ is the matrix of partial derivatives and I is the identity matrix.

The solution of this linear system (Equation 4.19) provides the correction $\Delta\boldsymbol{x}_0$ which is applied to the initial coordinates. The matrix $\frac{\partial \boldsymbol{x}}{\partial \boldsymbol{x}_0}$ is obtained by applying the perturbation to each coordinate of the vector $\boldsymbol{x}$ by a small number (10^{-9} to 10^{-12} in our case). We solve the system

using an iterative method (Newton method) until the corrections applied are very close to zero.

The practical differential correction procedure is defined as follows: we apply the differential corrections to the initial values of the position coordinates x_1 and x_3. The initial momenta ω_2 and ω_4 are found using Newton's method from the angular momentum, A (4.2), and energy, E (4.3), equations with an accuracy of 10^{-14}

$$\begin{aligned} \omega_2^{i+1}(0) &= \omega_2^i(0) + \frac{H(x_1(0), x_3(0), \omega_2^i(0), \omega_4^i(0)) + 1}{\frac{\partial H(x_1(0), x_3(0), \omega_2^i(0), \omega_4^i(0))}{\partial \omega_2}}, \\ \omega_4^{i+1}(0) &= \frac{A - 3x_1(0)\omega_2^{i+1}(0)}{2x_3(0)}, \end{aligned}$$

where i is for the iteration counter. We generate the partial derivative matrix P after every iteration step, which can be numerically computed as follows. The four perturbed orbits are found by applying a small perturbation δ to the position coordinates as follows

1. The initial coordinate $x_1(0)$ is perturbed by δ.
2. The initial coordinate $x_1(0)$ is perturbed by $-\delta$.
3. The initial coordinate $x_3(0)$ is perturbed by δ.
4. The initial coordinate $x_3(0)$ is perturbed by $-\delta$.

To increase the accuracy the perturbation is applied in a symmetric manner. The coordinates at the end of the period are found by following the perturbed orbits for one period. Then the differential correction is applied using the central difference formula

$$\frac{\partial x_i(T)}{\partial x_j(0)} \approx \frac{dx_{i,x_{j+\delta}} - dx_{i,x_{j-\delta}}}{2\delta}, \quad i,j = 1,3,$$

where $dx_{i,x_{j+\delta}} = x_{i,x_{j+\delta}}(T) - x_{i,x_{j+\delta}}(0)$ and the i-th coordinate $x_{i,x_{j+\delta}}(t)$ is computed by applying the perturbation δ on the x_j coordinate.

The perturbation matrix B is given by

$$B = \begin{bmatrix} \frac{\partial x_1(T)}{\partial x_1(0)} & \frac{\partial x_1(T)}{\partial x_3(0)} \\ \\ \frac{\partial x_3(T)}{\partial x_1(0)} & \frac{\partial x_3(T)}{\partial x_3(0)} \end{bmatrix}.$$

We introduce the matrix P defined by

$$P = (B-I)^{-1} = \frac{1}{|B-I|} \begin{bmatrix} \frac{\partial x_1(T)}{\partial x_1(0)} - 1 & -\frac{\partial x_1(T)}{\partial x_3(0)} \\ \\ -\frac{\partial x_3(T)}{\partial x_1(0)} & \frac{\partial x_3(T)}{\partial x_3(0)} - 1 \end{bmatrix}.$$

We find the corrected values of x_1 and x_3 using the differential correction Equation 4.19.

$$\begin{pmatrix} x_1^{i+1} \\ x_3^{i+1} \end{pmatrix} = \begin{pmatrix} x_1^i \\ x_3^i \end{pmatrix} - P \begin{pmatrix} dx_1^i \\ dx_3^i \end{pmatrix}. \tag{4.20}$$

The whole process is repeated with new values of x_1 and x_3 until the

magnitude of the relative error $d\boldsymbol{X}$ which is the difference of distances between the initial coordinates ($t = 0$) and final coordinates ($t = T$) becomes smaller than 10^{-13}. The algorithm for the differential correction is provided at the end of this chapter.

The value of δ is usually chosen as 10^{-9}, but it can vary between 10^{-9} and 10^{-12}. The reason to vary the value of perturbation is that in some cases the initial coordinates of the bodies are very close to each other because of a close encounter. If we choose too big a value of the perturbation then there is a possibility for bodies to change their hierarchy which would lead to a different solution. Hierarchy means the particular arrangement of the system in which bodies are labelled according to their initial relative positions.

The differential correction technique can also be applied to different parameters of the system: for example, we can apply this technique to the momentum ω_1 and position x_1 coordinates of the body b_1. In this case, when a search of a near collision orbit starts, the position coordinate requires a very small value of perturbation but the perturbation value for the momentum coordinate can reach 10^3 because the velocities become infinite near collision.

In order to find the near-collision orbits, a variable size of perturbation is applied, depending on how far the bodies are apart, to overcome the difficulty of integrating close encounters. For this purpose we used a parameter d_{12} (difference between initial values of x_1 and x_3), and choose $\delta = 10^{-9}d_{12}$. Knowing the distance between the bodies, we can safely perturb them by a small distance.

Algorithm 1 The algorithm of the differential correction procedure

Step 1: Start a search for orbits with known values of m_1 and A.

Step 2: Guess the initial values of $x_1(0)$ and $x_3(0)$, accuracy $\xi = 10^{-13}$.

Step 3: Compute the corresponding $\omega_2^i(0)$, $\omega_4^i(0)$ for $i = 1$ from the integrals of A and E using Newton's method.

Step 4 : Find the differences $dx_1^i = x_1(T) - x_1(0)$, $dx_3^i = x_3(T) - x_3(0)$.

If dx_1^i & $dx_3^i < \xi$, Stop the program, the orbit is found, otherwise go to the following steps.

Step 5: Introduce a perturbation δ to $x_1(0)$ and $x_3(0)$.

Step 6: Find the corresponding $\omega_2^i(0)$, $\omega_4^i(0)$ for the perturbed values of $x_1(0)$ and $x_3(0)$.

Step 7: Find the differences dx_1^i and dx_3^i.

Step 8: Compute the matrix of partial derivatives P.

Step 9: Apply corrections using the relation 2.13 and obtain the corrected values $x_1^{i+1}(0)$, $x_3^{i+1}(0)$.

Step 10: Repeat the whole process for $i = i + 1$

4.6 Chapter summary

In this chapter, we described the six-body system with non-aligned triangles. We first explained the initial configuration of the system of six bodies placed at the vertices of two non-aligned triangles and moving under their mutual gravitational interaction. We then calculated the regular equations of motion of the system by using the Levi-Civita regularisation along with a time transformation. The motion of the system is described in rotating coordinates in order to simplify the description of the periodic orbits. Then we discussed the numerical procedure that is used to find the solutions of the six-body system with non-aligned triangles. The periodic solutions of this system are presented in the next chapter.

Chapter 5

Family of periodic orbits of the planar six-body problem

In this chapter, we provide a detailed description of the family of periodic orbits generated from the Schubart orbit using the algorithm and numerical methods described in the previous chapter. Section 5.1 explains the procedure and technique to find the first member of the planar family, which is represented in Figure 5.4. The family presented in Section 5.2 is an equal mass planar family of periodic orbits.

Figures 5.5−5.8 show selected members of the family of periodic orbits in real and rotating coordinates. We labeled each orbit with an individual number. In order to see the behaviour of the bodies with time and to make the periodicity clearer the orbits are also represented in different rotating frames, as shown in Figures 5.6−5.8. Note that the representation of orbits in rotating coordinates is not unique because θ is defined only modulo 2π. Table 1 lists the quantities of interest for the selected orbits as shown in Figure 5.5, which includes the period T, the initial positions x_1, x_3, the initial velocities $\dot{x}_2$, $\dot{x}_4$, the angular momentum A, the angle of rotation θ and the distance d_{12} between bodies b_1 and b_2.

5.1 A planar orbit close to the equal-mass Schubart orbit

The planar six-body problem with non-aligned triangles is symmetric about the centre of mass as described in the previous chapter. If we strictly restrict the motion of the planar six-body problem with non-aligned triangles in a radial direction, then this planar six-body problem becomes the symmetric six-body problem with aligned triangles (described in Chapter 2).

A significant orbit of the symmetric six-body problem with aligned triangles is the Schubart periodic orbit found in Section 2.2 and shown in Figures 5.1 and 5.2. As described earlier in Chapter 3, there are alternating interactions of two different types in the Schubart orbit, first between the inner bodies and then a simultaneous double interaction of inner bodies with outer bodies. Starting from positions near the simultaneous double collision of the Schubart orbit we found another member of the family of periodic orbits for the planar six-body problem.

The first planar orbit of the family to be found, which is relatively close to the equal mass Schubart orbit, is illustrated in Figures 5.4a and 5.4b. The search for this planar orbit started when the initial positions $x_1(0)$ and $x_3(0)$ of the bodies b_1 and b_2 are close to the simultaneous double collision of the Schubart orbit as can be seen from Figures 5.3a and 5.3b. Initially, we provide a small value of angular momentum as $A = 0.886$. The corresponding velocities perpendicular to the line of bodies are found using the relations 4.2 and 4.3 with $A = 0.886$ and $E = -1$. The differential correction technique, which is explained in Chapter 4 is used to find this planar orbit with an accuracy of 10^{-13}. The approximate

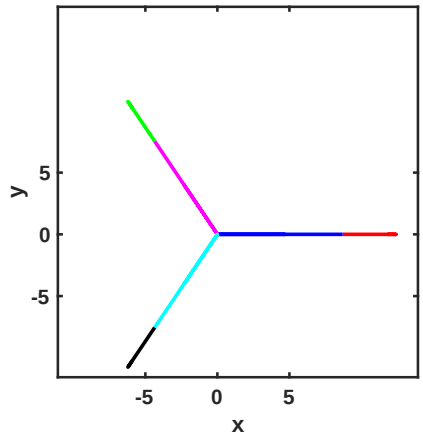

Figure 5.1 The Schubart six-body orbit in x-y coordinates.

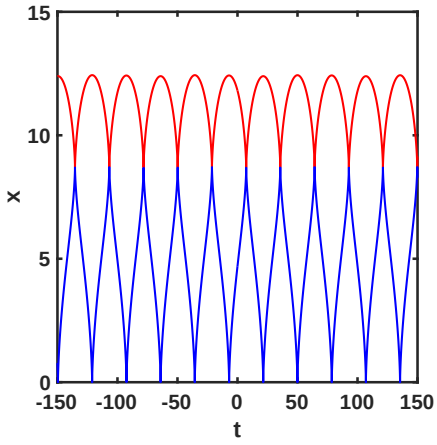

Figure 5.2 The Schubart six-body orbit with x coordinate against time t.

initial conditions for this orbit are given as follows

$$\begin{aligned} x_1 &= 8.654349884844795, \\ x_3 &= 8.607844254308425, \\ \omega_2 &= 4.634644411589807, \\ \omega_4 &= -4.625375191671544. \end{aligned}$$

The value of the angle of rotation θ is approximately -3.189 degrees. In Figure 5.4, the outer bodies are illustrated by blue, pink, and cyan paths. The inner bodies are represented by red, green, and black paths. The planar orbit has interplay-type motion, where the close encounter of the six bodies alternate between the central and outer parts of the system. The inner bodies closely interact with each other and the corresponding outer body, each outer body interacts primarily with the closest inner body. The Schubart orbit found for the six-body problem with aligned

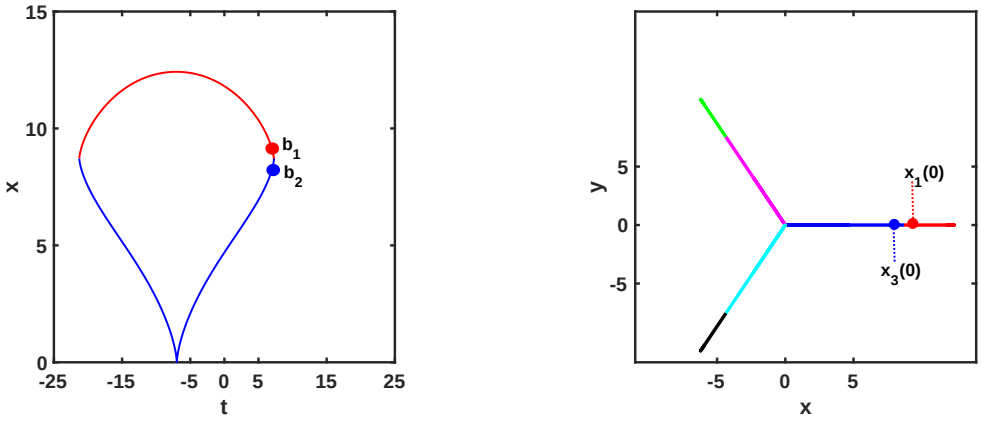

(a) (b)

Figure 5.3 Initial positions of the bodies b_1, b_2 of the planar orbit near the double collision of the Schubart orbit.

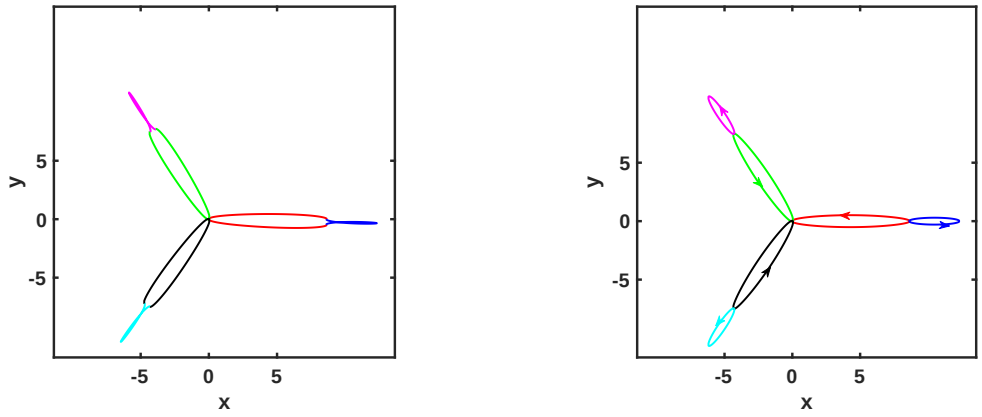

(a) (b)

Figure 5.4 The first planar orbit of the family that was found plotted in physical coordinates (left), and rotating coordinates (right). Arrows indicate the direction of motion.

triangles exhibits the same type of motion. However, the periodic motion of the Schubart orbit is strictly radial with zero angle of rotation, θ, and zero angular momentum, A.

It can be noted from Figures 5.3 and 5.4 that the three pairs of bodies b_1 and b_2, b_3 and b_4, and b_5 and b_6, are swapped for the planar orbits.

This is due to the fact that the Schubart orbit motion starts from the binary collision of the bodies b_1 and b_2, b_3 and b_4 and b_5 and b_6. This means that at the start of the motion, the bodies b_1 and b_2 (similarly the other two pairs of the bodies) are at the same point, So, it makes no difference if we label the bodies as $b_1, b_2, b_3, b_4, b_5, b_6$ or $b_2, b_1, b_4, b_3, b_6, b_5$.

5.2 Family of periodic orbits with equal masses

The search for the family of periodic orbits is performed using the numerical methods and techniques described in Chapter 4. We started our search with the planar orbit presented in Figures 5.4a and 5.4b. We found some neighbouring orbits by changing the angular momentum and initial coordinates of this planar orbit with $\Delta x = 0.04$. This search procedure is utilized for the next few orbits. After finding a range of initial orbits we used them for extrapolation, in order to find the best possible location to search for the new orbits of the family. We initially performed the extrapolation by manipulating the polynomial of degree 2. But when we become stuck in finding the new orbits in the region $-7.25 \leq A \leq 9.13$ then we made an extrapolation using a higher order polynomial.

To start a search for the new orbits we initially decrease the angular momentum from that of the orbit in Figure 5.4a. The initial coordinates x_1 and x_3 are moved close together in order to find the orbits close to collinear and collisional motion. When the value of angular momentum decreases from $A = 0.886$, which is the angular momentum of the first planar orbit, towards $A = 0$ and the initial coordinates become closer together, our planar orbits tend towards the Schubart orbit. This relates the first planar orbit represented in Figures 5.4a and 5.4b with the Schubart orbit and it also checks that our family of periodic orbits

starts with the Schubart orbit found in the aligned case. The search is then resumed from the first planar orbit, by first increasing and then decreasing angular momentum and increasing the distance between x_1 and x_3, until more members of the family are obtained.

During the search process, it was observed that the parameter d_{12}, that is the initial distance between the bodies b_1 and b_2, has a prominent role in the family of periodic orbits. It increases monotonically from zero to its final value which is the value of d_{12} for orbit 21. However, the other parameters are non-monotonic as they change their behaviour with the passage of time through the family of orbits. This constant increment in the value of d_{12} makes it an appropriate parameter in the family. Later in this chapter we also plot the other parameters of the family against d_{12} in Figures 5.14−5.18, to analyze their behaviour.

The magnitude of perturbation that is used in the differential correction technique is managed by the distance d_{12}. If a perturbation greater than d_{12} is applied, it can change the order of bodies, especially when the search is closer to the near-collision orbits. In our search, the size of perturbation changes from 10^{-9} to 10^{-12}. For most of the orbits, it was 10^{-9} but a variable size is used for the near-collision orbits.

As we mentioned before the initial point of the family of periodic orbits is the Schubart orbit and the interplay periodic motion of this orbit is linear with no rotation $\theta = 0, A = 0$ as can be seen in Figure 5.1. So, the collinear components ω_1, ω_3 of momentum corresponding to colliding bodies are zero and the transverse components ω_2, ω_4 of momentum are infinite at the moment of collision. However, right after and before collision ω_1, ω_3 are infinite in magnitude and ω_2, ω_4 are zero.

Initially, at time $t = 0$ the motion of bodies b_1 and b_2 is collinear along the

x-axis with purely transverse velocities so we have $x_2 = x_4 = \omega_1 = \omega_3 = 0$. The remaining coordinates of position and momenta, x_1, x_3, ω_2, and ω_4, contribute to the initial conditions at time $t = 0$. However, for a specified value of energy, $E = -1$, and angular momentum, our system is parameterized by just two coordinates x_1 and x_3.

As we proceed along the family starting from the Schubart orbit, we notice that b_1 and b_2 begin to expand in the y-direction. A peculiar change in the shapes of orbits is noticed in the family. In rotating coordinates the shape of orbits is more elliptical at the beginning (Figure 5.6), then it becomes circular until orbit 11 and after this, it changes to an oval-like shape. However, if we move a little after orbit 15, the oval-shaped paths of bodies b_1, b_3 and b_5 (red, green, and black) change into a heart-like shape (see orbits 16−21 in Figure 5.6).

For the negative values of the angle of rotation, θ, the orbits rotate in a clockwise direction, and with positive values of θ the rotation becomes anticlockwise. The initial rotation of orbits is clockwise with a negative angle of rotation as shown by grey lines in Figure 5.5. The values of θ continue to decrease from orbit 1 with $\theta = 0$ to orbit 11 with $\theta = -180°$. Then the motion changes from a clockwise to an anticlockwise direction with a positive angle of rotation for the orbits 12 to 19. Afterward, it again reverts to a clockwise direction (orbits 20 and 21).

The angular momentum of our system increases rapidly from zero (the Schubart orbit) to its maximum possible value $A = 1.36$ (orbit 6). Then the value of angular momentum A starts to decrease (orbit 7) and move towards negative values. The value of A keeps on decreasing, with negative values, until orbit 21 with $A = -13.1$.

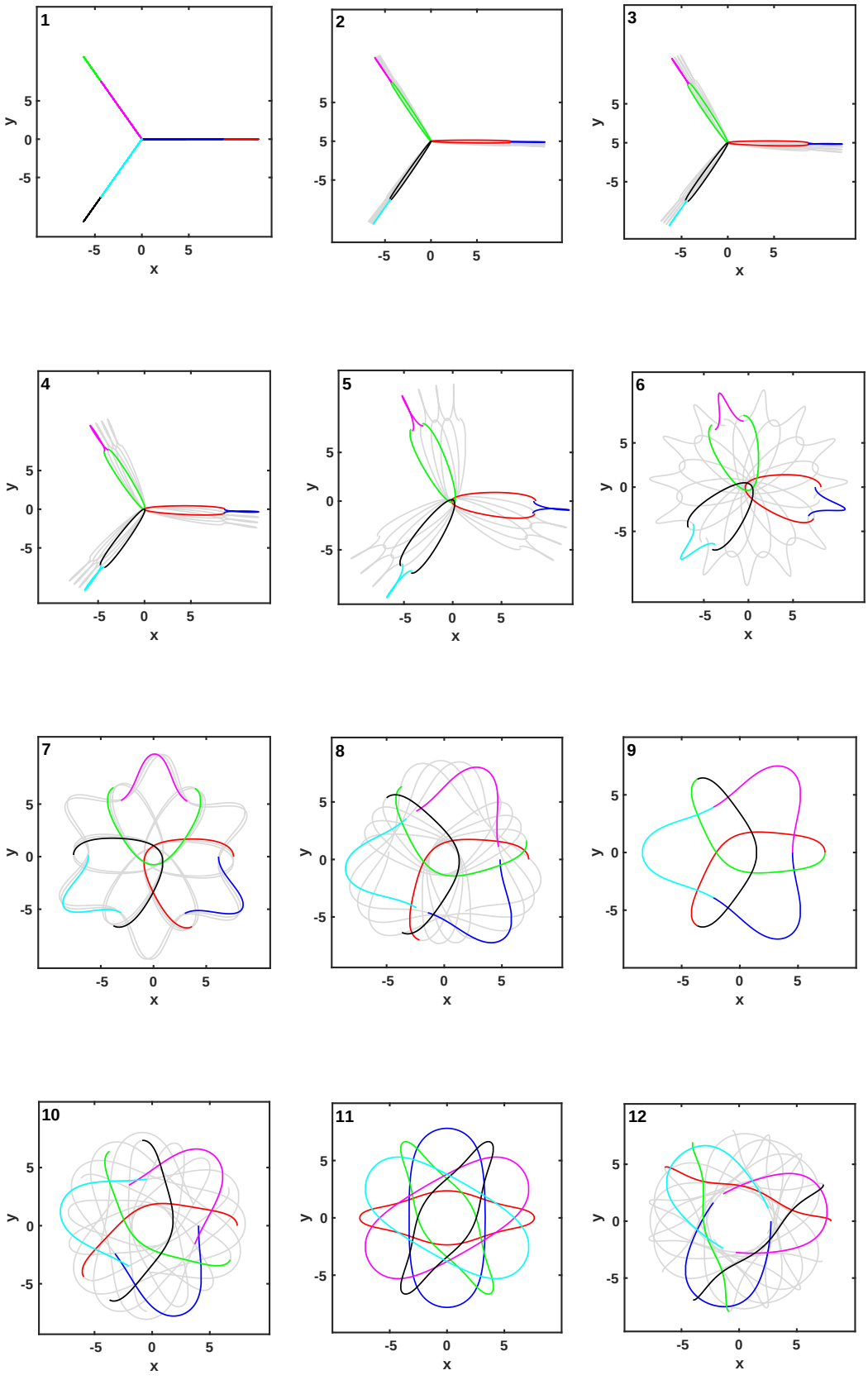
1
2
3
4
5
6
7
8
9
10
11
12
x
y
-5
0
5

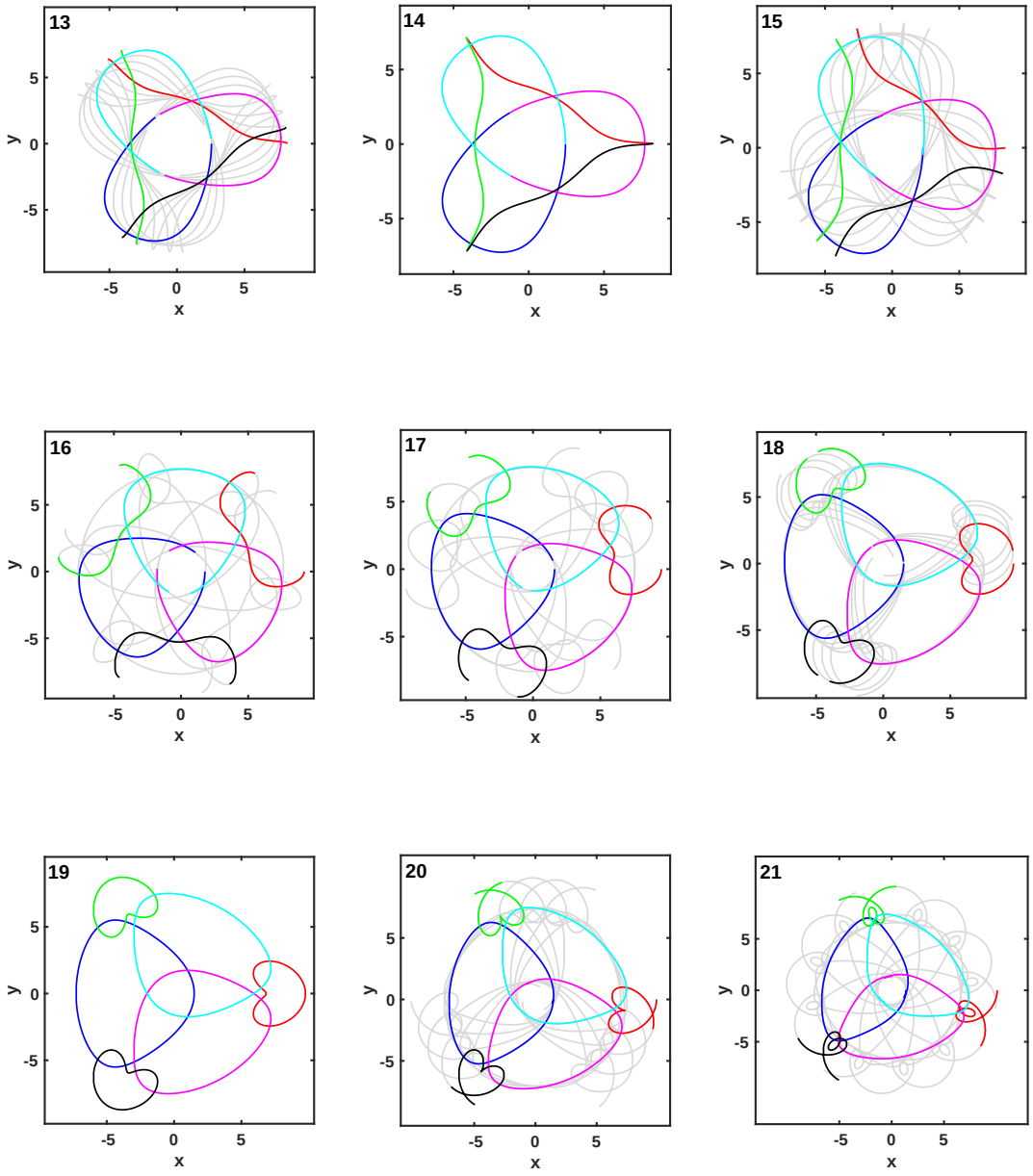

Figure 5.5 Selected members of the family of periodic orbits: The motion starts when the bodies b_1 and b_2 are positioned on the x-axis. The bodies b_1 and b_2 follow blue and red paths. The green, magenta, black, and cyan are paths of bodies b_3, b_4, b_5 and b_6 respectively. Coloured paths show one period. Grey lines represent a further four periods.

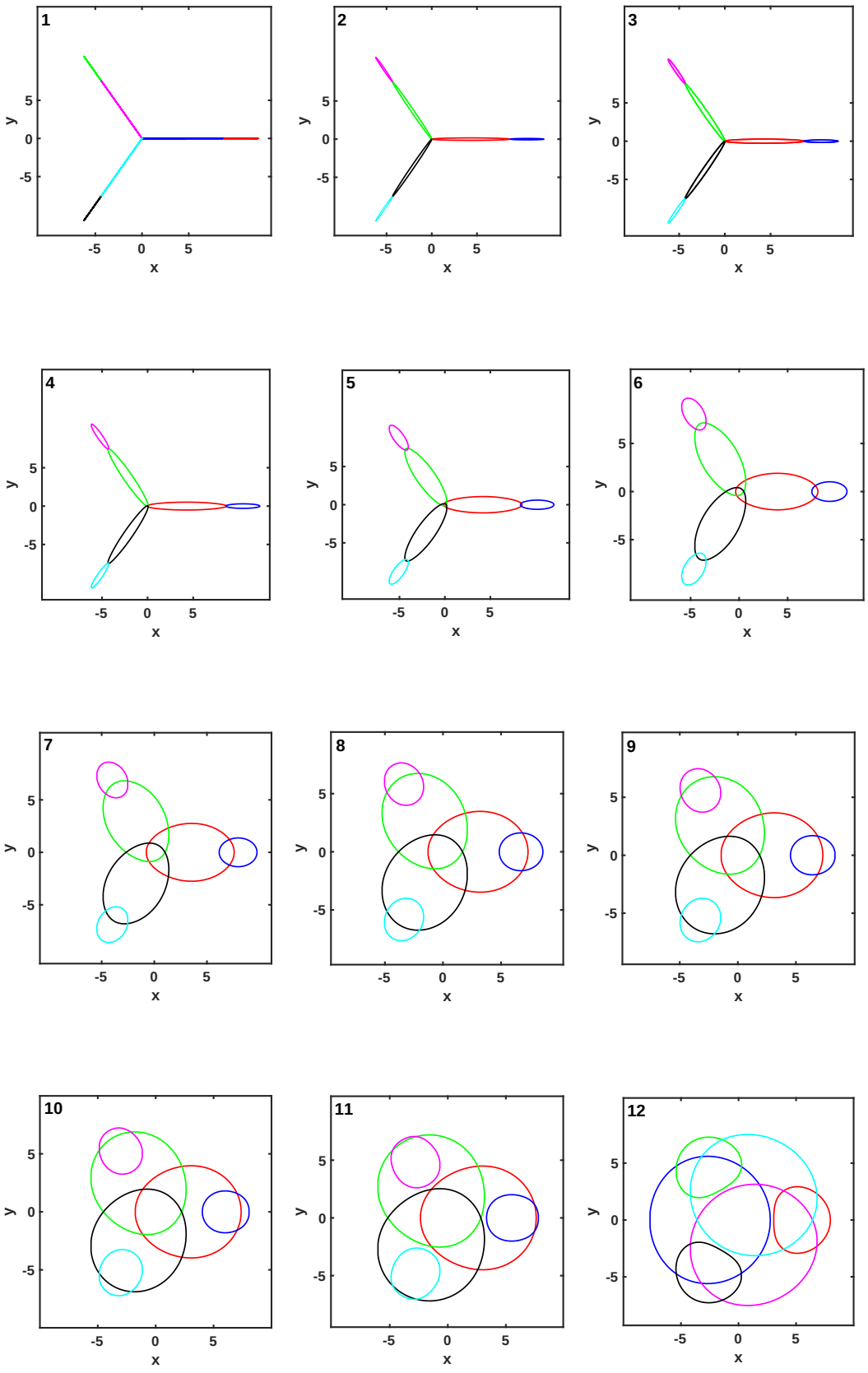
1
2
3
4
5
6
7
8
9
10
11
12
x
y
-5
0
5

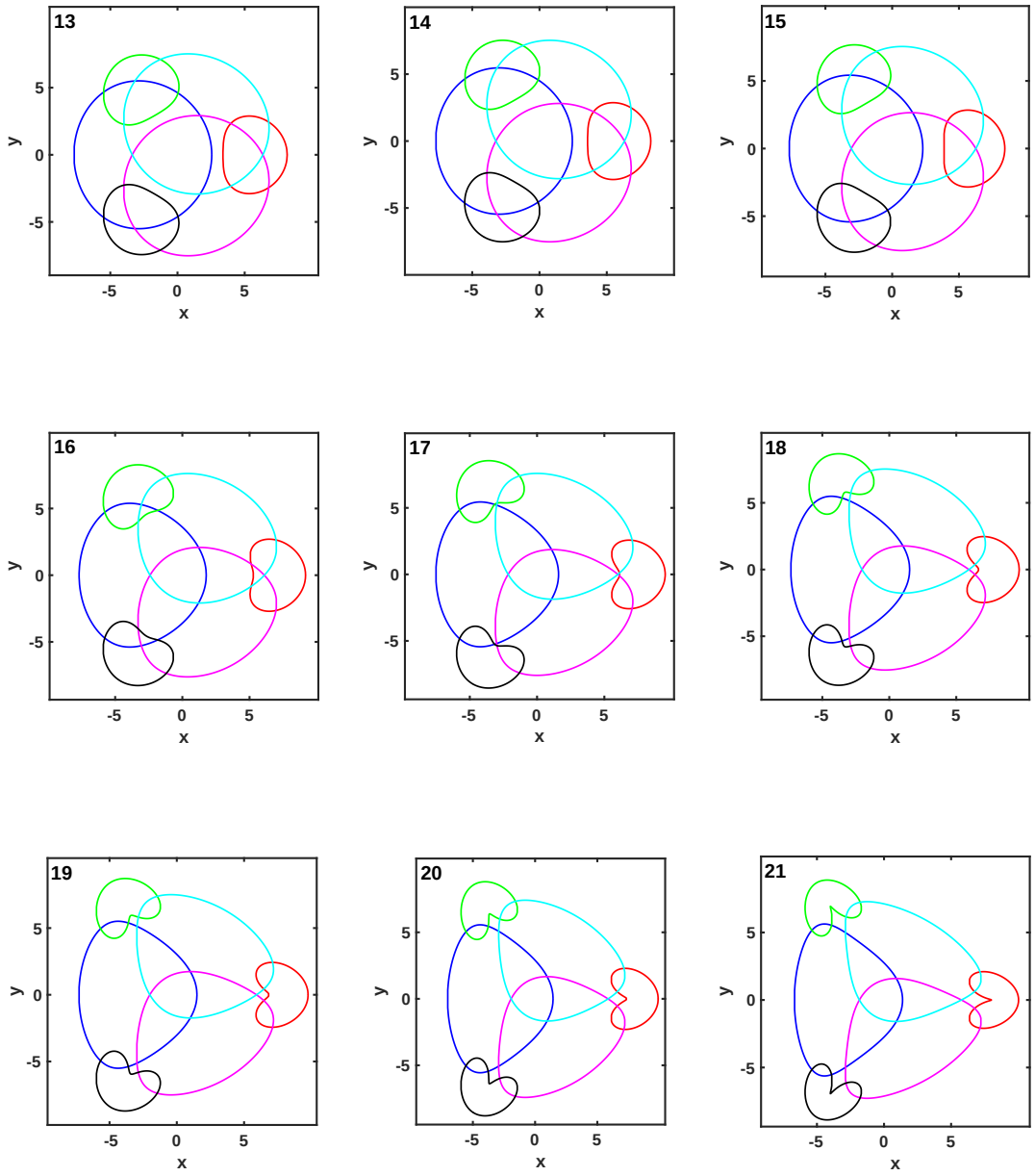

Figure 5.6 Orbits of the family in Figure 5.5 plotted in a rotating coordinate system, where the angle of rotation θ is measured between $-\pi$ and π. The same colour code is used for the family as in Figure 5.5. All the curves are closed in these figures which confirms the periodicity of the orbits.

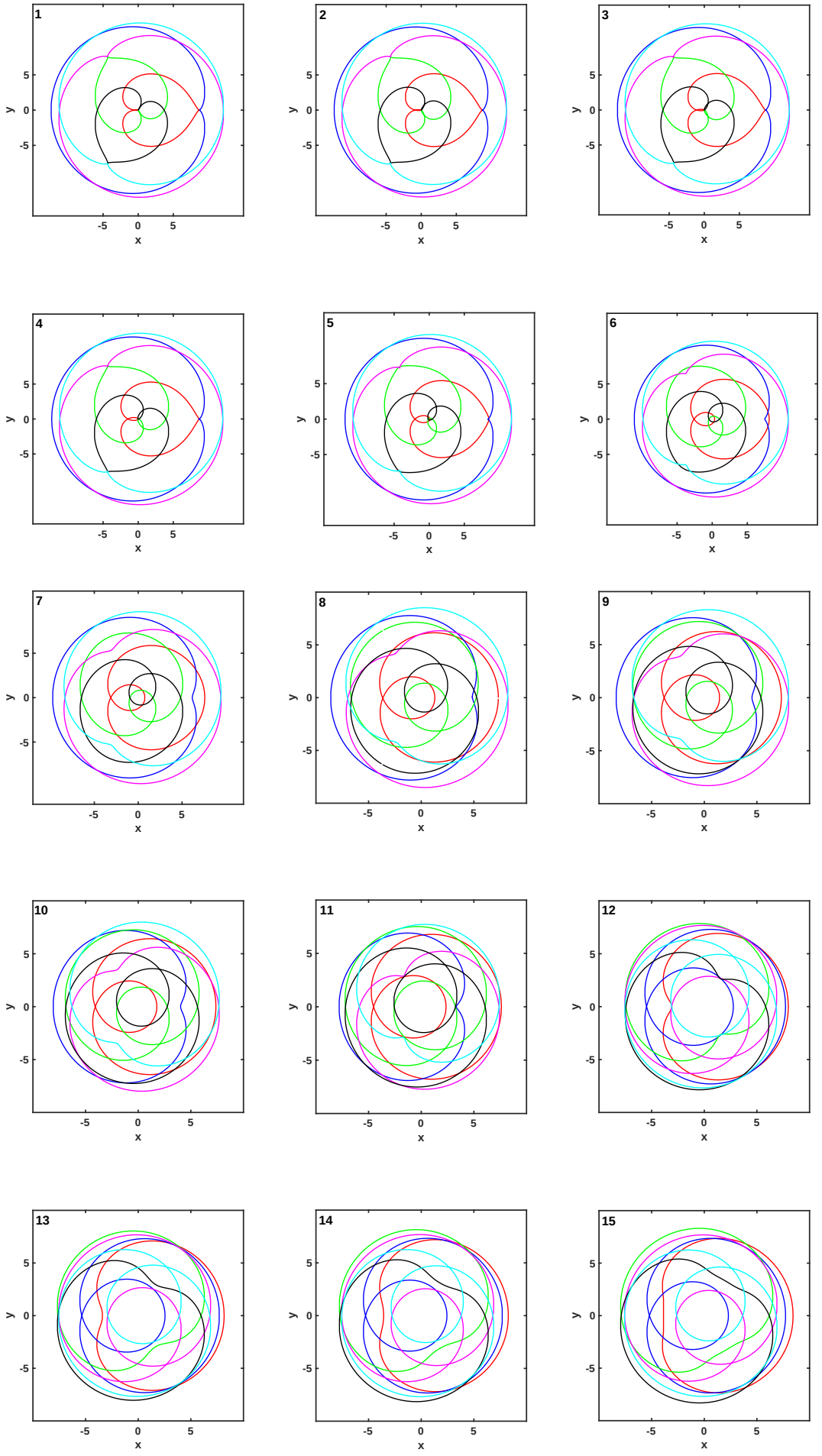
1
2
3
4
5
6
7
8
9
10
11
12
13
14
15
x
y
-5
0
5

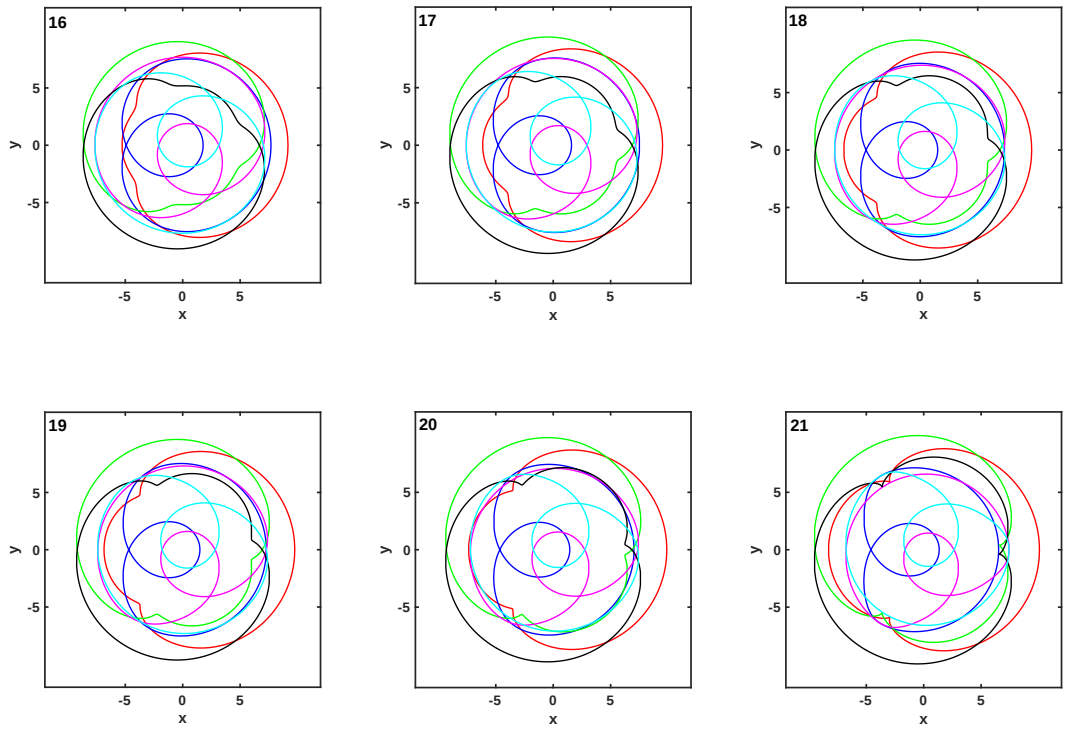

Figure 5.7 The orbits in Figure 5.5 represented in another rotating coordinate system, where θ is measured in the region $[0, 2\pi]$.

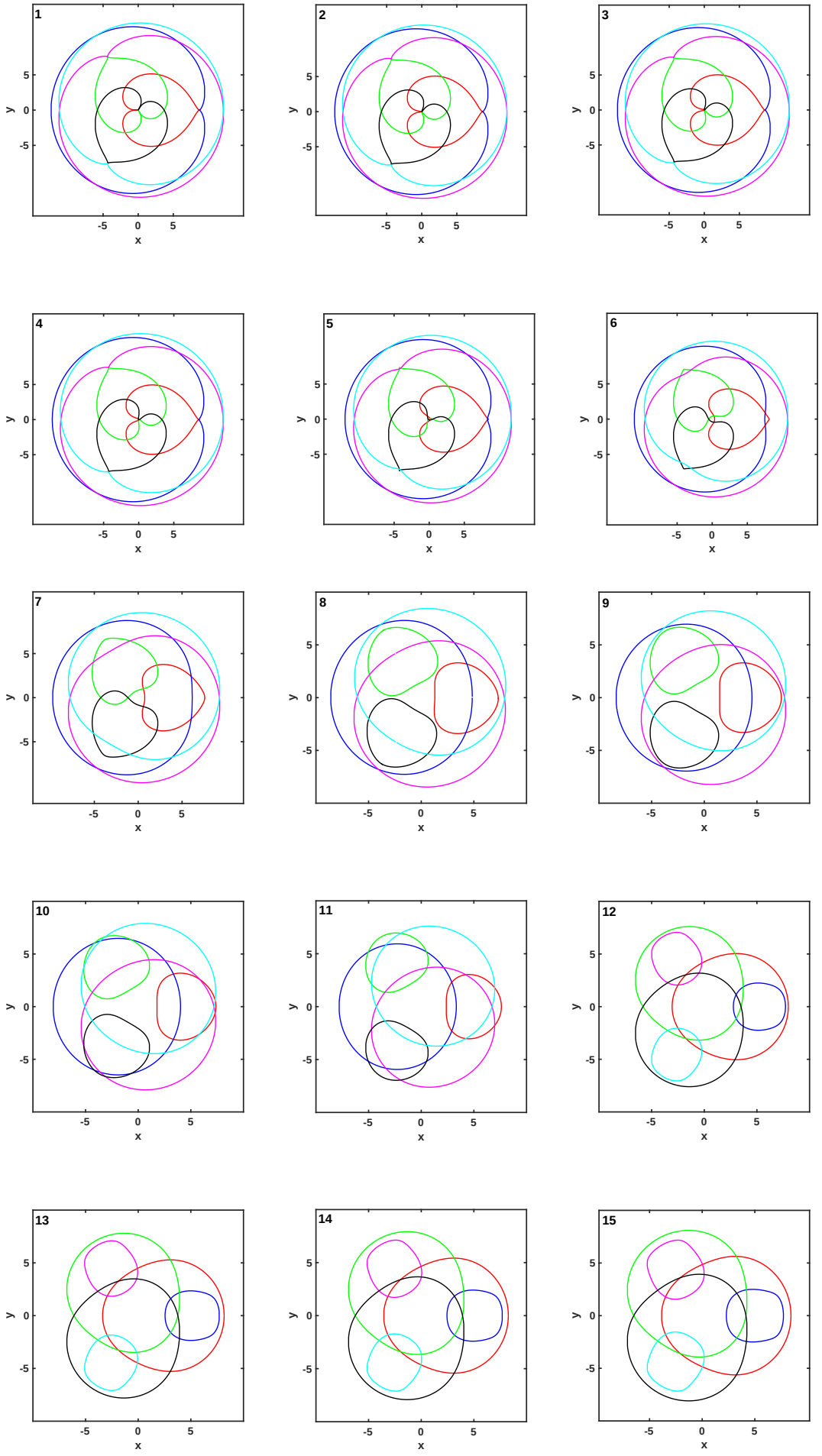
1
2
3
4
5
6
7
8
9
10
11
12
13
14
15
x
y
-5
0
5

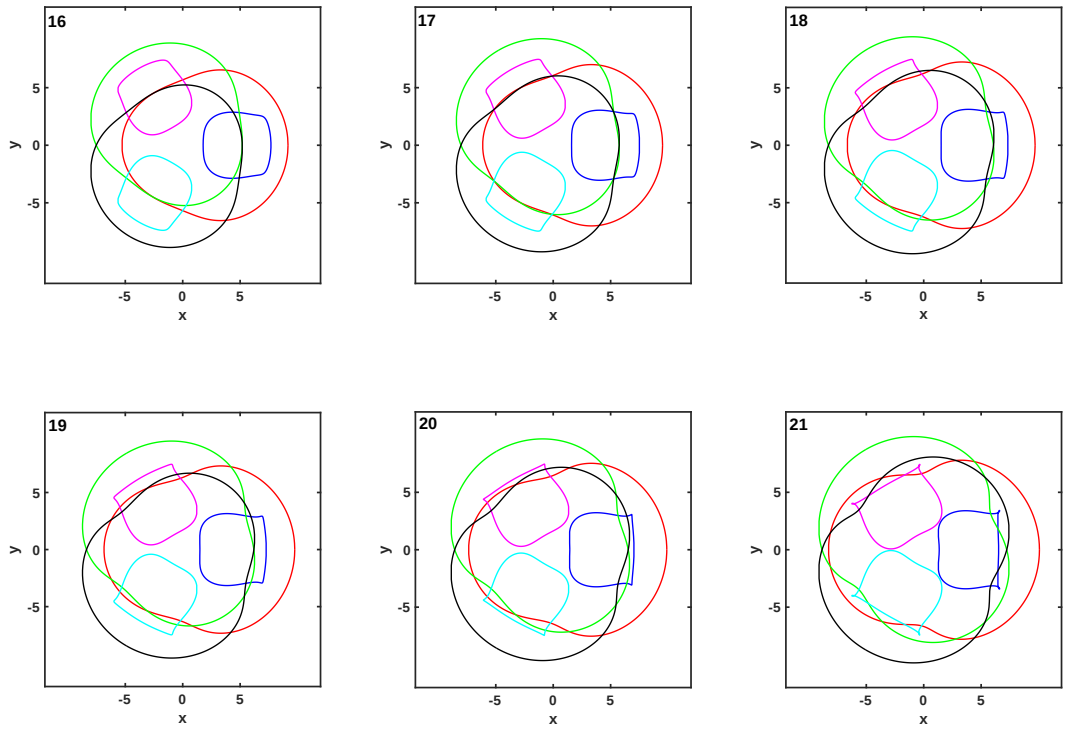

Figure 5.8 The orbits in the Figure 5.5 represented in another rotating coordinate system, where θ is measured in the region $[-2\pi, 0]$

Table 5.1 Details of the Schubart family.

Orbit	A	θ	d_{12}	T	x_1	x_3	$\dot{x}_2$	$\dot{x}_4$
1	0	0	0	28.47855914	8.69371305	8.68907413	∞	$-\infty$
...	...	...	...	...	...	...	...	...
2	0.3	-0.92677213	0.004	28.47855914	8.69371305	8.68907413	14.68176499	-14.67809455
3	0.5	-1.59385487	0.013	28.47620647	8.68559982	8.67235191	8.68723685	-8.68128933
4	0.886	-3.20902152	0.047	28.46614521	8.65387603	8.60686477	4.60961344	-4.6003228
5	1.36	-8.71100984	0.202	28.40772330	8.50972315	8.30760139	2.21145460	-2.21069021
6	0.4	-25.95640202	0.639	28.25809877	8.12131102	7.48262811	1.19361888	-1.27768168
7	-1.9	-61.21682363	1.428	28.51967249	7.59004429	6.16190812	0.69662672	-0.96086485
8	-3.3	-107.01622894	2.481	29.60346236	7.32562895	4.84460027	0.41786015	-0.85891263
9	-3.51	-120	2.792	29.98871354	7.32305137	4.53069462	0.36371674	-0.84612111
10	-3.8	-143.31933340	3.359	30.73249250	7.38249963	4.02319727	0.28174671	-0.83184129
11	-4.2373	180	4.283	32.01797356	7.616001154	3.33286035	0.17518398	-0.82410735
12	-4.9	143.83885410	5.222	33.44746129	7.98151713	2.75929959	0.08185895	-0.82872188
13	-5.3	128.76323139	5.614	34.11818231	8.16391367	2.55037384	0.04394174	-0.83336929
14	-5.56	120	5.828	34.51338572	8.27045816	2.44244013	0.02293806	-0.83647559
15	-6.0	108.04590320	6.141	35.13845675	8.43398924	2.29256374	-0.00836021	-0.84162984
16	-8.7	53.24664197	7.391	38.60972820	9.16968563	1.77887777	-0.14824638	-0.86606697
17	-10.5	23.01645463	7.926	41.14171409	9.52361896	1.59752471	-0.22078769	-0.87466703
18	-11.5	5.70303919	8.180	42.80470359	9.70058413	1.52031185	-0.25769837	-0.87712831
19	-11.81	0	8.258	43.38471578	9.75591244	1.49784622	-0.26875126	-0.87776227
20	-12.5	-14.05057946	8.446	44.87856706	9.89036114	1.444749540	-0.29270776	-0.88020878
21	-13.1	-32.48115375	8.724	46.94266748	10.07766360	1.35285114	-0.31304832	-0.89579032

Orbit 9 with the angle of rotation $-120°$ and angular momentum $A = -3.51$ is a double choreography orbit. This special type of periodic orbit consists of two different types of closed curves, where the six bodies split into two groups. Within each group, the member bodies chase each other around a fixed closed curve without collision. Figure 5.9 illustrates the position of the bodies from the two groups at different times. The bodies from Group 1 (blue, magenta, and cyan) travel on the closed curve C_1 while the bodies of Group 2 (red, green, and black) travel on the curve C_2 in the opposite direction.

Orbit 9 has an absolute period $\tilde{T} = 3T$. Broucke [8] named the kind of orbit which looks the same in both fixed and rotating coordinate systems an "absolute periodic orbit". That is all six bodies return to their initial positions after time $\tilde{T}$ in this orbit (see 5.9a−5.9f). If we consider the period $\tilde{T}$ for orbit 9 then the orbit looks the same in both the real and rotating coordinate systems, where each group of bodies b_1, b_3, b_5 and b_2, b_4, b_6 share the same curve, respectively.

We found an absolute periodic orbit (orbit 11 in Figure 5.5) with angular momentum $A \approx 4.2373$ and angle of rotation $-180°$ or $180°$. An important characteristic of this orbit is that the bodies move on six separate fixed closed curves. All the curves intersect with each other at different points. The bodies of Group 2 (red, green, and black) travel on three identical closed curves, which intersect in such a way that they make a starfish-like shape. Similarly, the paths of bodies from Group 1 (blue, magenta, and cyan) are also identical. The absolute period for this orbit is $2T$, as the bodies complete one cycle along their paths in time $2T$. The motion of the bodies at different times is shown in Figure 5.10.

After the absolute periodic orbit 11, the angle of rotation θ switches its direction from clockwise to anticlockwise with positive values. The angle

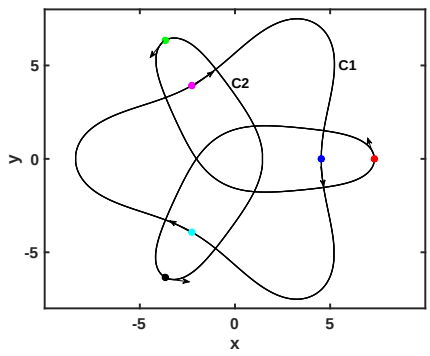

(a) $t = 0$

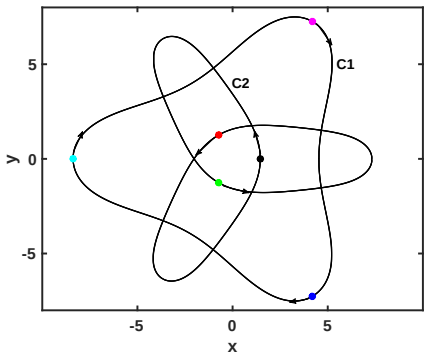

(b) $t = T/2$

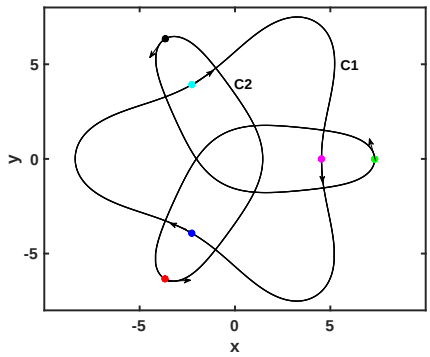

(c) $t = T$

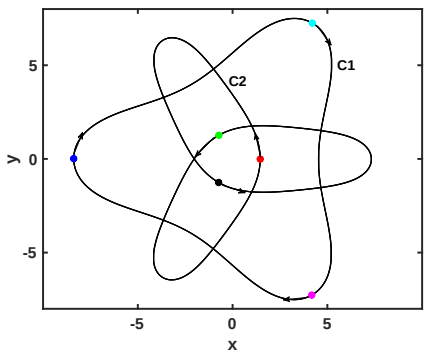

(d) $t = 3T/2$

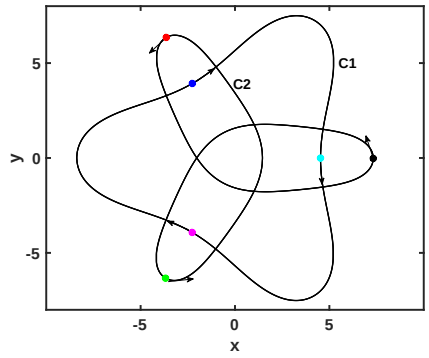

(e) $t = 2T$

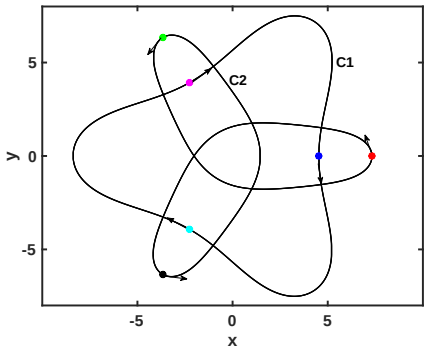

(f) $t = 3T$

Figure 5.9 Double Choreography orbit with $\theta = -120°$: Each body is represented with a different colour, and arrows show the direction of motion.

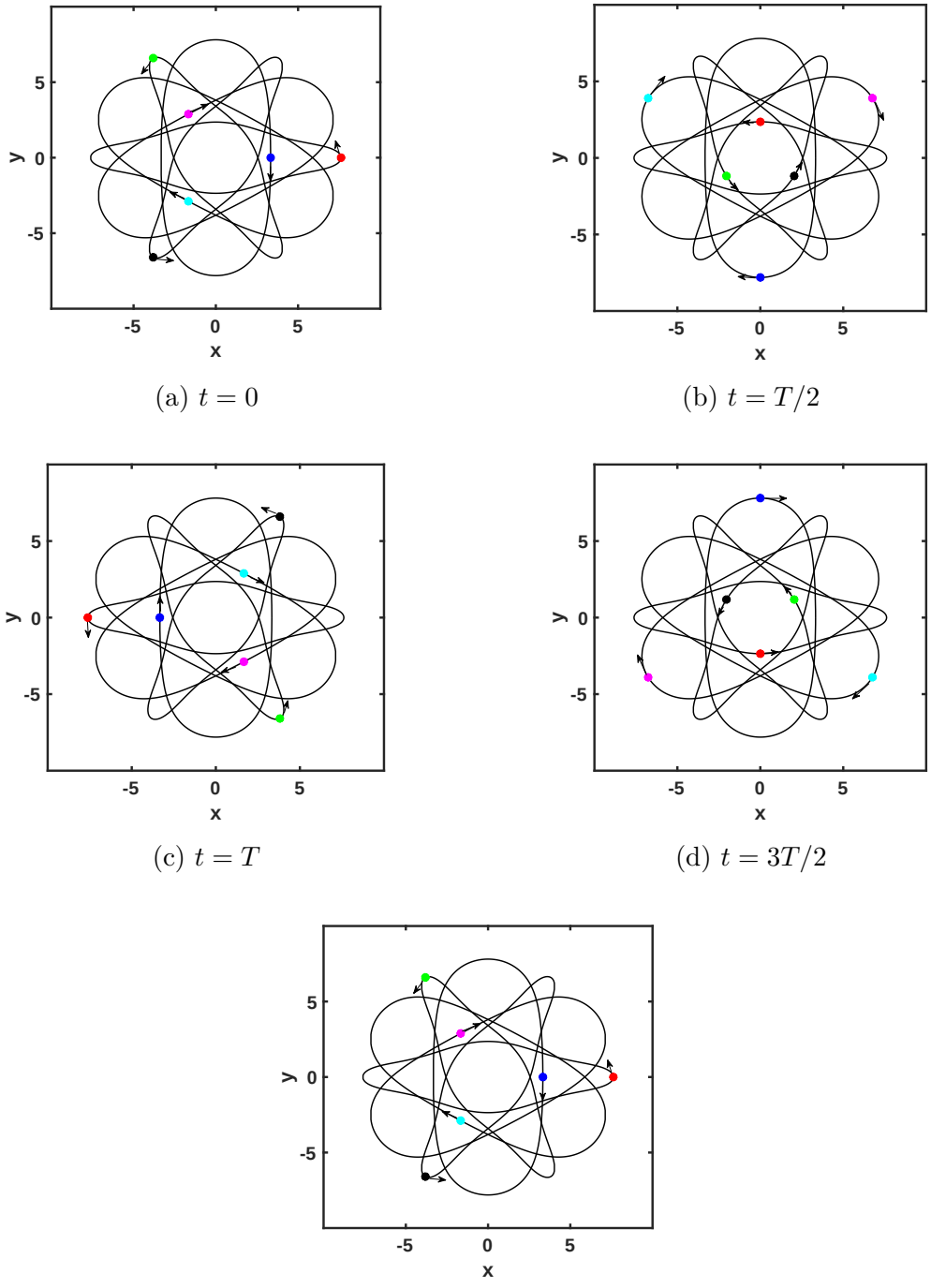

(a) $t = 0$

(b) $t = T/2$

(c) $t = T$

(d) $t = 3T/2$

(e) $t = 2T$

Figure 5.10 An absolute periodic orbit with $\theta = 180°$: Each body is represented with a different colour. The arrows show the direction of motion.

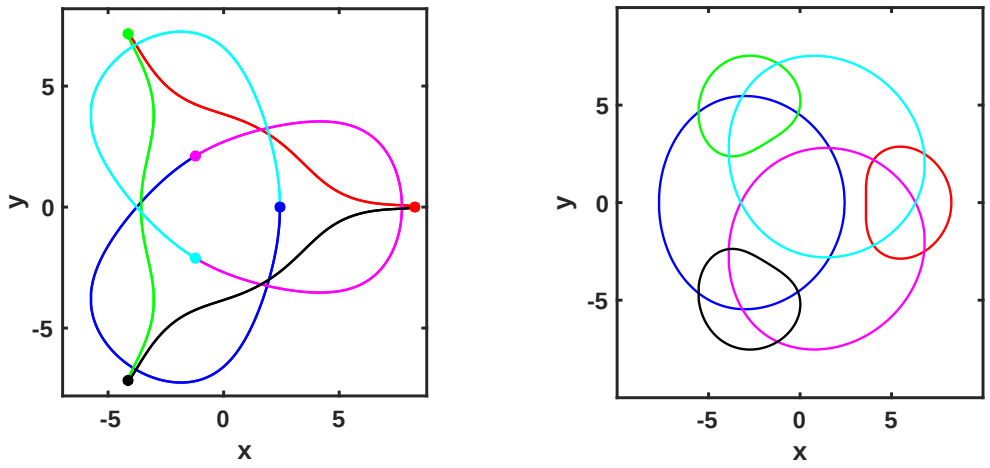

(a) Fixed coordinates. (b) Rotating coordinates.

Figure 5.11 The double choreography orbit with $\theta = 120°$: Coloured filled circles represent the initial positions of the bodies.

of rotation continues to decrease from 180° and we encounter another double choreography orbit 14 with $\theta = 120°$ and $A \approx -5.56$. This orbit has a similar characteristic to that of orbit 9, where each group of bodies performs a simple choreography on two different closed curves (as shown in Figure 5.11).

We noticed a twist in red, green, and black trajectories (orbits $12 - 19$ in Figure 5.5) at time $t = T/2$, which transformed into a loop for orbit 21. It is also observed that the periodic solutions discovered after orbit 11 follow a similar property, that is, the distance between initial coordinates and coordinates after one period is reduced for all the bodies (see orbits 19 to 21). Orbit 19 is another absolute periodic orbit, which consists of six closed curves, with zero angle of rotation and it looks the same in the fixed and as well as in the rotating coordinate systems (see Figure 5.12).

The trajectories of orbit 21 with $\theta = -32$ and $A = -13.1$ are divided

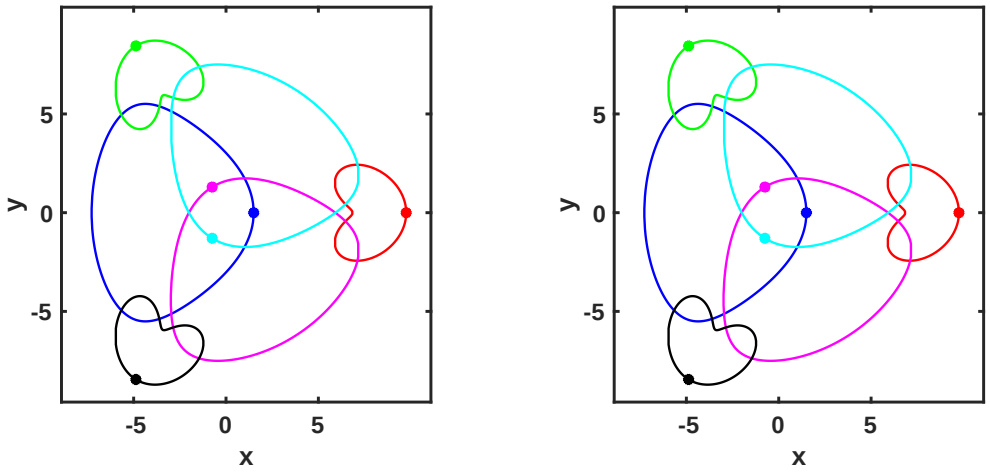

(a) Fixed coordinates. (b) Rotating coordinates.

Figure 5.12 Absolute periodic orbit with $\theta = 0$: The initial position of each body is shown with a filled circle.

into two different categories. Each category has three identical curves. Each outer trajectory (red, green, and black) intersects with two different inner trajectories at six different points. However, each inner trajectory intersects with two outer trajectories and they intersect with one another at the vertices of an equilateral triangle. The outer curves make a loop at time $t = T/2$. Figure 5.13 shows the motion of the bodies along their paths at six different times from $t = 0$ to $t = T$. It can be seen from Figures 5.13a and 5.13b that the inner bodies (magenta, blue and cyan) come very close to the corresponding outer bodies (red, black, and green) at time $t = T/4$, So, the outer bodies move quickly towards the loop and avoid the collision. Similarly, at $t = 7T/10$ the cyan, magenta, and blue bodies pass very close to the red, black, and green bodies respectively but the bodies run toward the final point without any collision. We also observe that when the bodies in Figure 5.13 complete one cycle, their curves cross themselves.

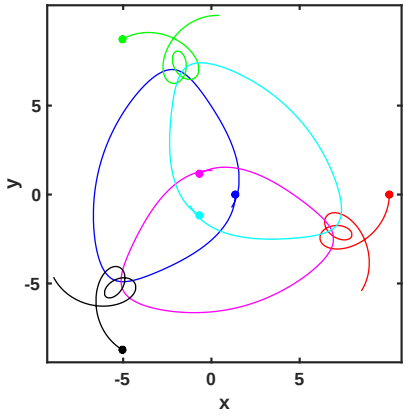

(a) $t = 0$

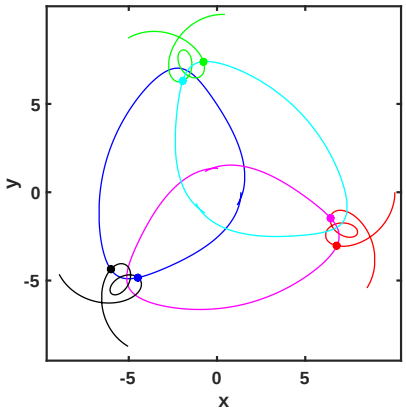

(b) $t = \frac{T}{4}$

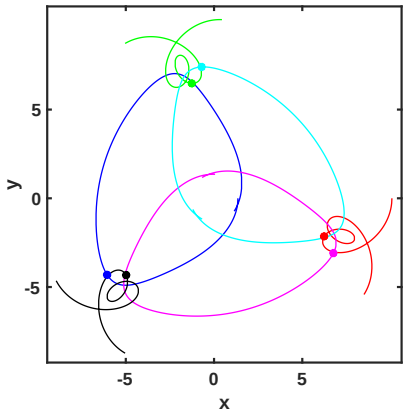

(c) $t = \frac{T}{3}$

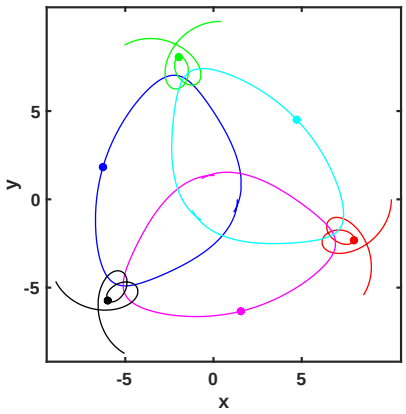

(d) $t = \frac{T}{2}$

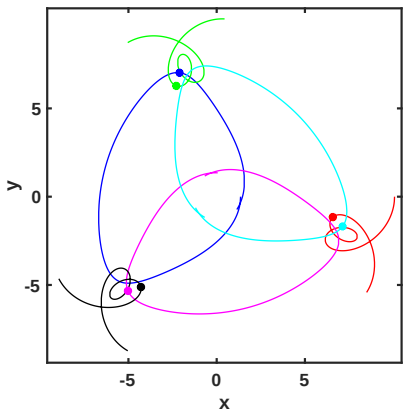

(e) $t = \frac{7T}{10}$

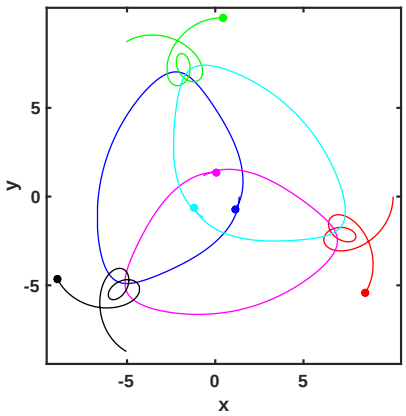

(f) $t = T$

Figure 5.13 Orbit 21 with $\theta = 32°$. Each body is represented with a different colour, and arrows show the direction of motion.

Thus we summarize the Schubart family of the six-body problem as follows: the equal mass family of periodic orbits presented in this chapter can be considered as being generated from the Schubert six-body orbit with $\theta = 0°$, continuing towards the first double choreography orbit at $\theta = -120°$, then moving towards the absolute periodic orbit at $\theta = 180°$ or $-180°$ (orbit 11).

After moving back from 180° to 0°, we encounter another choreography orbit at 120°, then the family progresses towards the absolute periodic orbit 19. If we proceed along the family after the orbit 19 we observe the trajectories of orbits become more complicated by making multiple loops, as can be seen from orbit 21 in Figure 5.13.

5.2.1 Graphs of physical properties against parameter d_{12}

The graph of angular momentum A against the parameter d_{12} is shown in Figure 5.14. The values of selected orbits presented in Table 1 are marked. Initially, its value increases from zero for the Schubart orbit to its maximum value $A \approx 1.36$ for orbit 5, after which it starts decreasing and becomes negative. Most of the orbits of this family are found with negative angular momentum, as can be seen from Figure 5.14.

The behaviour of the angle of rotation along the planar family is presented in Figure 5.15. The angle of rotation starts from zero (the Schubart orbit) and moves towards negative values until orbit 11, which is the same orbit for $\theta = -180°$ or $\theta = 180°$. After orbit 11, it travels back from 180° to zero with positive values. However, when the angle of rotation again reaches zero, the family does not stop here, and the value of θ once again starts to move towards negative values (orbit 19 to 21).

The initial positions x_1 and x_3 of the bodies b_1 and b_2, respectively are the same for the Schubart orbit because the bodies are at collision.

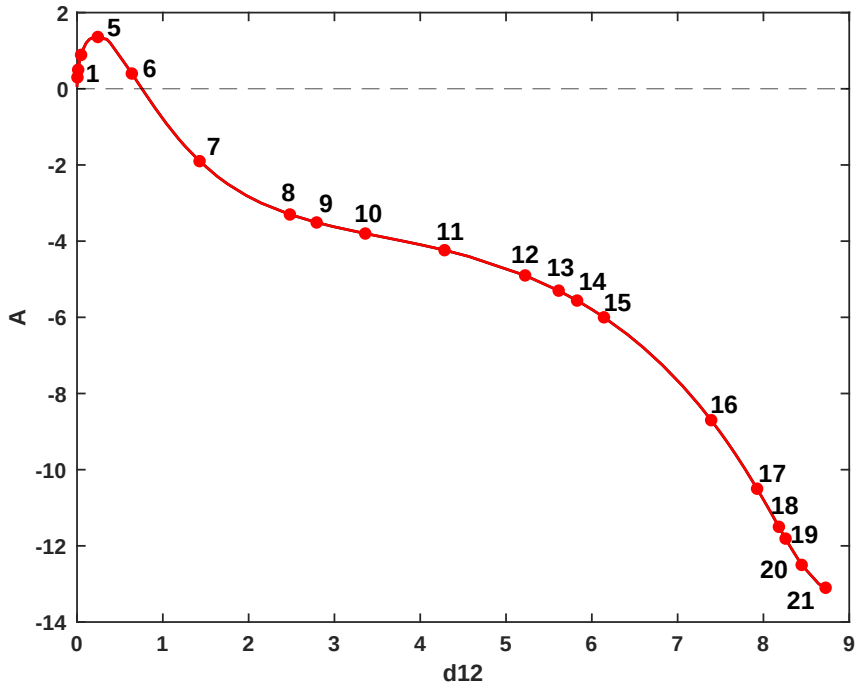

Figure 5.14 The angular momentum A against the distance d_{12} along the family.

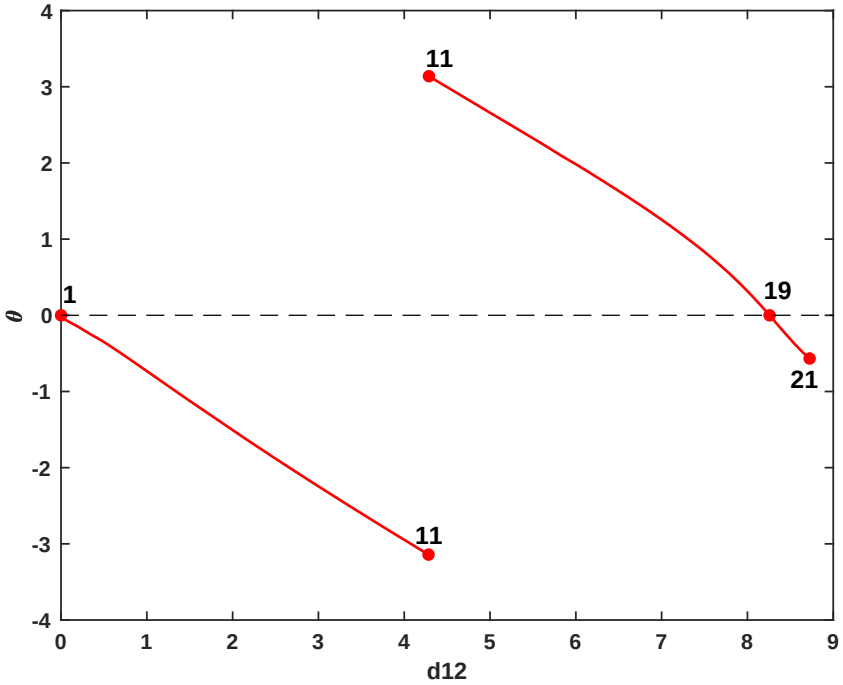

Figure 5.15 The angle of rotation θ (in radians) against the distance d_{12} along the family of periodic orbits.

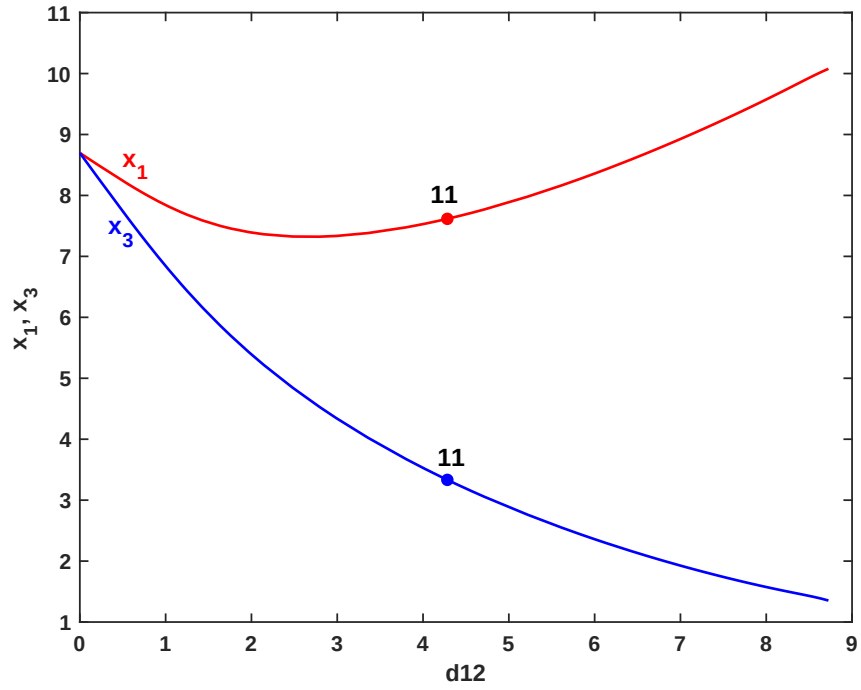

Figure 5.16 The initial position coordinates x_1 and x_3 of the bodies along the family of periodic orbits.

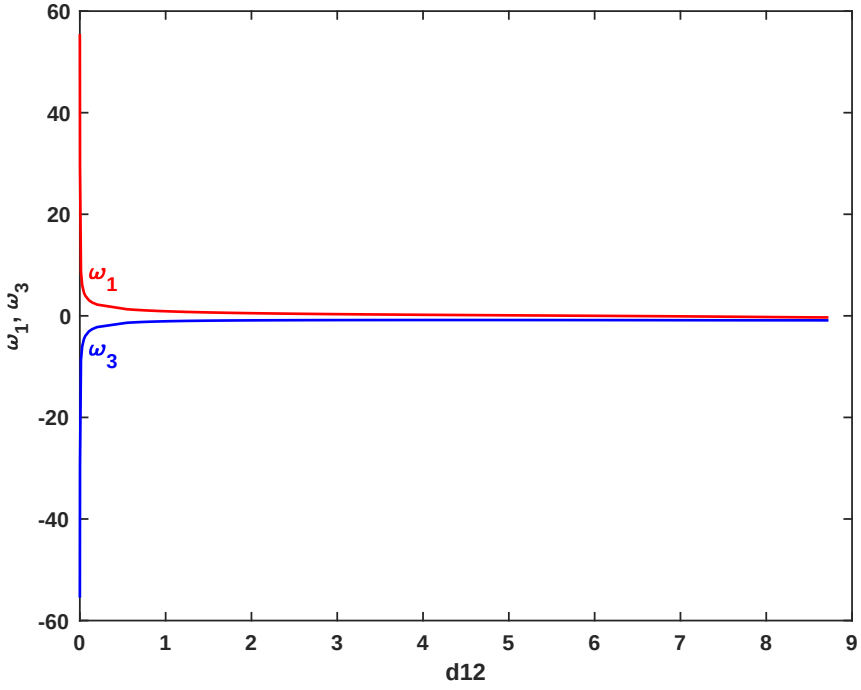

Figure 5.17 The transverse momenta v-coordinates against d_{12} (along the family).

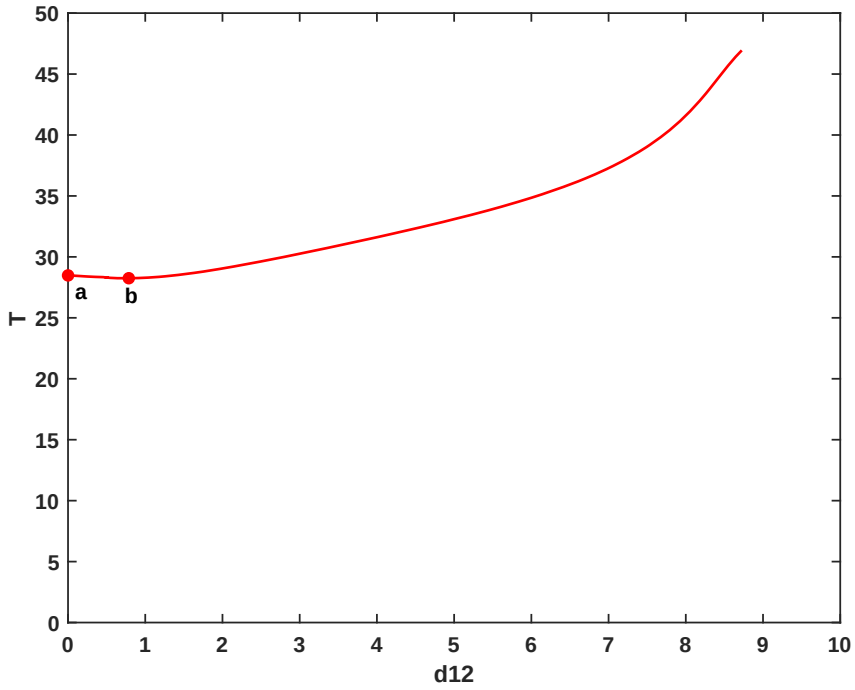

Figure 5.18 The period T of the orbits against the distance d_{12} along the family. A slight decrease in T is noticed between a and b.

We proceed along the family, and the initial positions of both of the bodies decrease: more rapidly for the body b_2 than the body b_1 (Figure 5.16). At some stage (orbit 11), the position x_1 reaches a threshold and again starts increasing. But position x_3 continues to decrease along the family. Figure 5.17 illustrates the initial transverse momenta against the parameter d_{12}.

Figure 5.18 represents the period T of the orbits along the continuous family. Its value varies between 28.294 and 46.943. But initially, a slight decrease in the period of the family is noticed that is represented by a small region between points a and b in Figure 5.18, and then it increases constantly along the family.

5.3 Discussion of the planar family

An equal mass family of periodic orbits of the six-body system is generated and presented in this Chapter. A description of selected members of the family is provided here. The physical properties of the system, such as the initial coordinates of the bodies, their period, angular momentum, and angle of rotation are also discussed in detail. (see Figures 5.16−5.18).

We observe a behaviour of the planar family of the six-body system compared to the equal mass families of the three-body [26] and the four-body systems [15]. It is noted that the planar family of the three-body problems starts with a Schubart orbit (found by Schubart in 1956) and ends in a hierarchy of two binaries revolving in opposite directions. The planar family of the four-body system starts from the Schubart orbit, continues towards the double choreography orbit with $\theta = 180^\circ$ or -180° and then returns to the Schubart four-body orbit. In this family, the orbits before and after the double choreography orbit are essentially the same with similar properties. However, for the family of the six-body problem, the orbits that appear after the absolute periodic orbit 11 do not have similar behaviour to those that come before it. The present family does not seem to travel back toward the Schubart orbit. The angle of rotation grows from zero (Schubart orbit) to -180° or 180° (orbit 11) and then returns to zero (orbit 19), but this family does not end at this point. By extending the family after the orbit 19, we found looped orbits for our system in the fixed coordinates. These types of orbits are observed in the restricted three-body problem, where trajectories make the loops in rotating coordinates. Szebehely [68] presented multiple loop orbits in his book "Theory of orbits" for the restricted three-body problem, some of which are similar to those presented in Figure 5.7.

5.4 The non-linear stability test

The non-linear stability of the equal mass family of the periodic orbits is checked by an approach already performed for the Schubart orbit in Chapter 2. A similar approach was used by Mikkola and Hietarinta [40] for the one-dimensional Newtonian three-body problem and Sweatman [63, 64] for the one-dimensional Newtonian four-body problem. Every orbit of the family is integrated from its initial conditions over a long duration in a simulation that is constrained to be symmetrical and in the plane.

In the present study, we performed the non-linear stability check by simulating the symmetrical planar code for 2000 periods. During the integration of an orbit over a long period, numerical errors introduce symmetric perturbations to the orbit. If an unstable mode is present the orbit deviates from its original pattern.

We visually inspect the stability or instability of every orbit of the family. If the orbit deviates from the regular pattern of collisions between bodies then it is considered to have broken apart. It is observed under the non-linear stability check that most of the members of the family of periodic orbits are unstable except for a small region of orbits as shown by the green line in Figure 5.19.

The stable and unstable orbits of the family are distinguished by two regions $R_1 : 0 \leq A \leq 1.36$ or $0 \leq d_{12} \leq 0.202$ and $R_2 : 0.202 < d_{12} \leq 8.725$. The orbits within the region R_1 are found to be stable under the symmetric perturbation. An example of a stable orbit from $R_1 : 0 \leq A \leq 1.36$ is presented in Figure 5.20. It can be seen from Figure 5.20b that after integrating the orbit over the 2000 periods it does not deviate from the regular pattern.

The region $R_2 : 0.202 < d_{12} \leq 8.725$ is an unstable region. Instability appears in the orbits of the region R_2 even if we integrate these orbits over a small number of periods, which can be seen in Figure 5.21. It is also observed that the orbits found after the absolute periodic orbit 11 are highly unstable as they show deviation from their regular path after the fourth period as shown in Figure 5.22.

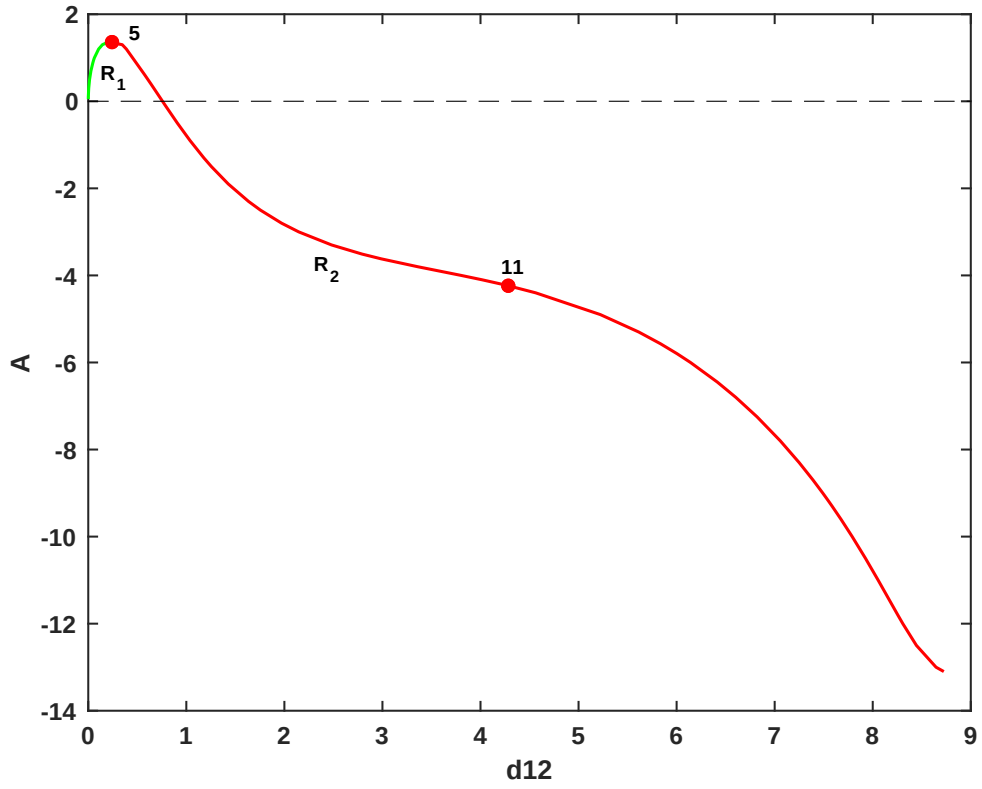

Figure 5.19 The regions R_1 and R_2 of non-linear stability for different values of angular momentum along the family. The green region R_1 indicates the stable solutions and the red unstable solutions.

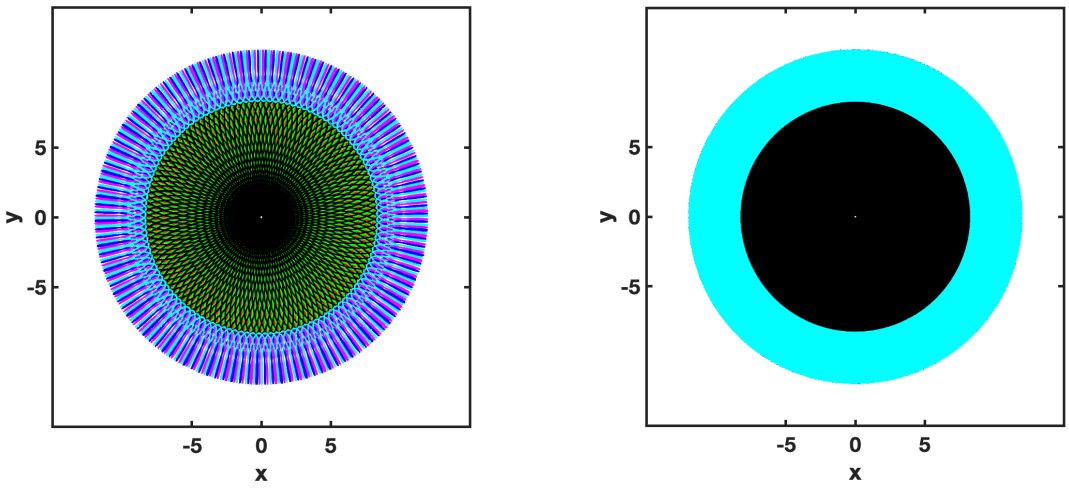

(a) The behaviour of orbit 5 over 150 periods (b) The behaviour of orbit 5 over 2000 periods

Figure 5.20 A stable orbit from the region R_1 in the x-y plane.

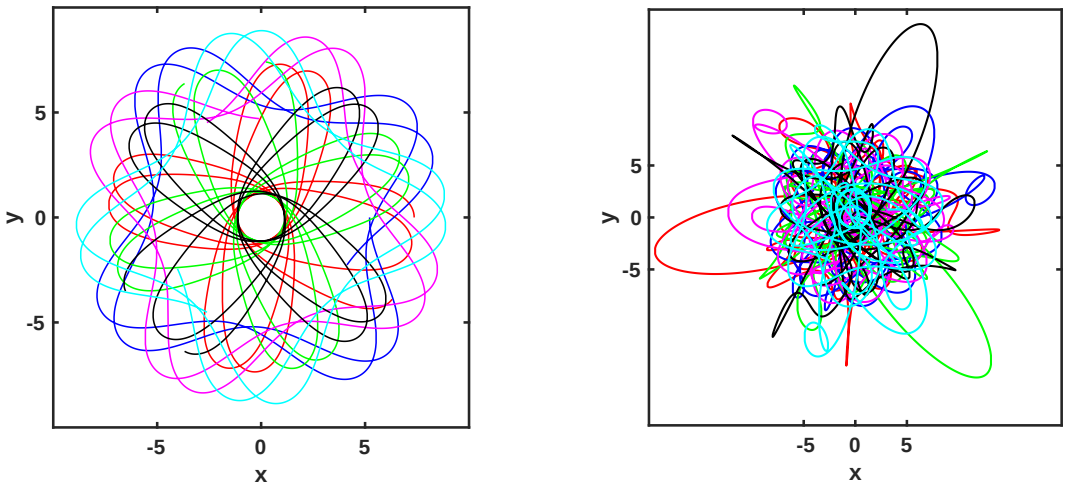

(a) The behaviour of orbit 8 over 10 periods (b) The behaviour of orbit 8 over 30 periods

Figure 5.21 An unstable orbit from the region R_2 in the x-y plane.

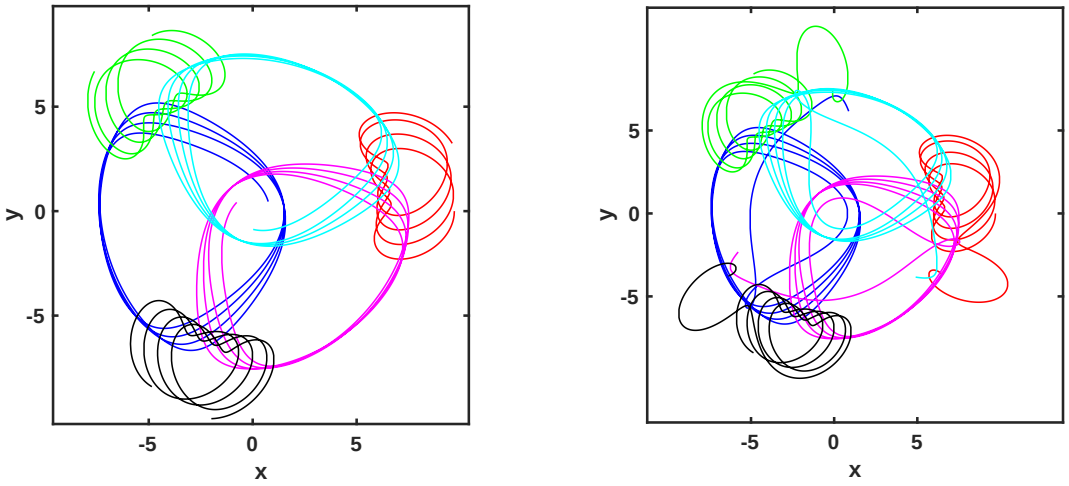

(a) The behaviour of orbit 18 over 4 periods. (b) The behaviour of orbit 18 over 6 periods.

Figure 5.22 An unstable orbit from the region R_2 in the x-y plane.

5.5 Chapter summary

In this Chapter, we presented periodic solutions to the six-body problem with non-aligned triangles, implementing the numerical procedure described in Chapter 4. An equal-mass family of periodic orbits starting from the Schubart orbit has been generated by varying the angular momentum, A, of the system. Selected members of the family are presented.

We performed the search procedure for the periodic orbits by introducing the differential corrections to an initial dataset of orbits. After every successful iteration, the dataset is updated with the newly discovered orbit. The orbit 5.4a is taken as the initial orbit for the search procedure. We provided a detailed description of the family in order to distinguish the properties and peculiarities of the periodic orbits.

A non-linear stability analysis of the family of periodic orbits is conducted, which is done by integrating the orbits from their initial conditions using the planar symmetric code. The non-linear stability analysis is performed

in a similar fashion to Mikkola and Hietarinta [40] and Sweatman [63].

The stability of periodic orbits without a singularity could have alternatively been investigated by using an ODE bifurcation package, such as AUTO, or by determining the Floquet Multipliers of the periodic orbits [50].

Chapter 6

Summary and Discussion

In this research, we have investigated equal mass families of periodic orbits in the framework of the planar symmetric six-body problem. In our setting, the six bodies are arranged on the vertices of two equilateral triangles. We examined two different versions of the problem, the systems of six bodies with aligned triangles and with non-aligned triangles. A planar family of periodic orbits with equal mass is generated from the Schubart orbit that is found in the aligned case in Chapter 2. Another equal mass family is presented in Appendix B and is generated by a hexagonal orbit. A few more examples of periodic orbits are presented in Appendix C.

It is observed during the period of integration that bodies in the system follow two different types of interactions. One of which is a simultaneous close approach by three pairs of bodies (b_1, b_2),(b_3, b_4), and (b_5, b_6) on three sides of the system's centre of mass. Another is the encounter of three bodies near the centre of mass.

All six bodies gravitationally interact with each other. Three bodies, which are placed at the vertices of the outer triangle in the aligned case are moving about their common centre of mass but they never approach close to each other. Each outer body interacts with a nearby inner body.

The three inner bodies attract each other and undergo a close encounter near the centre of mass.

The planar six-body problem that we used is a simplified problem that explores the six-body system with special symmetries: symmetry in time and about the centre of mass. The time symmetry defines the initial configuration of the system, while the central symmetry fixes the centre of mass at the origin. These two types of symmetries enabled us to significantly lessen the initial number of variables.

In Chapter 1 we have provided the literature review dedicated to few-body systems, especially, that which is closely related to the study of the Schubart orbit and the family of periodic orbits for three- and four-body systems. The analytical and numerical study of the problem has been discussed. We have also provided a survey of the regularization techniques and the history of their development. An overview of the Poincaré map is given at the end of Chapter 1.

In Chapter 2 we have presented a mathematical model of the six-body problem in the aligned case. The Levi-Civita coordinate transformation is used to remove the two- and three-body collisions. The initial conditions of the system are defined in a two-dimensional grid of parameters R and θ as defined by Hietrinta and Mikkola [27] for the three-body system and Sweatman [63] for the four-body system.

The significant result of the aligned case is the Schubart orbit that is found using the Poincaré map. Some general orbits of six bodies are presented in Chapter 2 which are helpful to understand the possible motions of bodies in our six-body system.

Chapter 3 is dedicated to proving analytically the existence of a Schubart orbit for arbitrary masses in the regularised Hamiltonian system. We

followed the approach of Ouyang and Yan [47] for the symmetric collinear four-body system and Yan [73] for the collinear three-body system. We first establish a connection between the nature of the orbit and the initial condition. Then we showed if we restrict the initial condition in a proper interval, there exists no extra collision between the triple collision and a simultaneous binary collision which is a feature of the six-body Schubart orbit. A turning point technique is used to estimate this interval. This technique has an important role in the present work and it confirms that the shape of the orbit is the same as the Schubart orbit. The existence of the Schubart orbit follows by the intermediate value theorem.

In Chapter 4 we have provided the equations of motion for the six-body system in a non-aligned case and the methods that are utilized for solving it. To deal with singularity all the inter-body distances are regularised by the Levi-Civita regularisation scheme. Following the approach of Heggie [23], we introduced a rescaled time τ with an exponent power of 7/2 to best suit the planar six-body problem with symmetrical inter-body distances. We defined the rotating frame of our system and the periodicity criterion that is used for specifying the time at which the bodies complete one period within both real and rotating coordinate frames.

A detailed description of the program that is developed to search and analyze the orbits of our system is provided in Chapter 4. This program is based on an algorithm that is suitable for the solution of the planar six-body system when given the initial guess of the configuration of the bodies and the existence of the solution.

We have presented the algorithm of the overall program and differential correction that is used to search for a single orbit. The equal mass family of periodic orbits is generated by varying the initial positions x_1, x_3,

and the angular momentum A. The search process for the orbits of our system is conducted by applying the linear differential correction to the data set of the orbits, which is modified with the data set of new orbits after every successful iteration of the algorithm. The initial data set of the planar family is provided by the six-body Schubart orbit found in Chapter 2. We have used polynomial extrapolation in each round of differential correction to predict the initial configuration for the new orbit that corresponds to the chosen value of angular momentum A or distance d_{12}.

One of the major results of the study of a six-body problem with non-aligned triangles is the planar family of periodic orbits presented in Chapter 5. These orbits are periodic relative to a rotating frame where the bodies return back to their initial configuration. In the real physical space, the configuration is rotated by an angle θ, which is related to the angular velocity ω of the system about the centre of mass. These kinds of orbits are sometimes known as relative periodic orbits [8, 9].

We have also examined the changes that take place in the physical variables of the system along the planar family, for example, angle of rotation, period, angular momentum, and the initial positions and the velocity coordinates of the system.

A nonlinear stability analysis is conducted for the planar family of periodic orbits. It is observed that only a small set of orbits is stable that is close to the Schubart orbit. However, the majority of the orbits in the equal-mass family are unstable, especially, the ones found after the absolute periodic orbit 11 are highly unstable.

The search for the equal-mass planar family starts by using the results of Chapter 2. The equal-mass planar family starts from the Schubart

orbit but does not return to it. This is unlike the equal mass family of the four-body system that starts and finishes with the Schubart orbit [15]. The search for the orbits of the family after the absolute periodic orbit 11 was not very simple. We made some changes in our search for orbits after the angular momentum $A = -7.25$, such as using smaller perturbations, making the extrapolation with a polynomial of degree up to 6, and changing the distance formulae that are used as a criterion to find the period of the orbit. It was found that the relation derived in Equation (4.16) works well for finding these orbits.

One of the reasons for finding difficulty in the search of orbits after $A = -7.25$ is that these are highly unstable orbits and follow their regular pattern for a very short time. It is noted the orbits of the planar six-body problem easily change their hierarchy and lead to a different solution that does not belong to the family. This problem was controlled by making the perturbation small.

6.1 Future directions

The study of the planar symmetric six-body problem presented in this thesis could be beneficial for further research as we suggest below

It would be interesting to investigate the family with an added central mass m_0, the planar symmetric seven-body problem. This has been done for a four-body problem [16]. The seven-body problem can be explored using six equal masses studied in this thesis with added central mass. It is probably more practical to explore a system moving about the centre of mass which keeps its own mass. Especially, in the case when the central body has more mass as compared to six orbiting bodies.

Another important aspect of the problem is to extend our study to the

case of unequal masses m_1 and m_2 using the same mechanism as for the equal mass case. This family would be parameterized by varying the masses m_1, m_2, and angular momentum A.

In the future, we intend to look at more general stability for the periodic orbits of the planar six-body problem. A planar linear stability analysis can be applied to the whole range of orbits, which will provide more accurate boundaries for the stable and unstable regions.

Bibliography

[1] Aarseth, S. J. (2003). *Gravitational N-body simulations*. Cambridge Monographs on Mathematical Physics. Cambridge: Cambridge University Press.

[2] Aarseth, S. J. and Zare, K. (1974). A regularization of the three-body problem. *Celestial mechanics*, 10(2):185–205.

[3] Alexander, M. E. (1986). Simulation of binary-single star and binary-binary scattering. *Journal of Computational Physics*, 64(1):195–219.

[4] Alsaedi, A., Yousef, F., Boshnaq, S., and Momani, S. (2019). New styles of periodic solutions of the classical six-body problem. *Mathematics and Computers in Simulation*, 159:183–196.

[5] Andreev, V. S., Goryaino, S. V., and Krasilnikov, A. V. (2016). Six-body problem solution using symplectic integrators. *IEEE NW Russia Young Researchers in Electrical and Electronic Engineering Conference (EIConRusNW) (Conference Paper)*.

[6] Bettis, D. G. and Szebehely, V. (1974). Treatment of close approaches in the numerical integration of the gravitational problem of n bodies. *Astrophysics and Space Science*, 14:133–150.

[7] Broucke, R. (1971). Periodic collision orbits in the elliptic restricted three-body problem. *Celestial Mechanics*, 3:461–477.

[8] Broucke, R. (1975). On relative periodic solutions of the planar general three-body problem. *Celestial Mechanics*, 12(4):439–462.

[9] Broucke, R. and Boggs, D. (1975). Periodic orbits in the planar general three-body problem. *Celestial Mechanics*, 11(1):13–38.

[10] Celletti, A. (2003). Basics of regularization theory. *Chaotic Worlds: from Order to Disorder in Gravitational N-Body Dynamical Systems (Conference Proceedings)*, 227:203–230.

[11] Celletti, A. (2010). Regularization theory. In: Stability and chaos in celestial mechanics. *Berlin, Heidelberg: Springer Berlin Heidelberg*, pages 207–226.

[12] Chen, K. (2001). Action-minimizing orbits in the parallelogram four-body problem with equal masses. *Archive for Rational Mechanics and Analysis*, 158(4):293–318.

[13] Chenciner, A. and Montgomery, R. (2000a). Minima de L'intégrale d'action du probléme Newtonien de 4 Corps de Masses Égales Dans ℝ3: Orbites 'hip-hop'. *Celestial Mechanics Dynamical Astronomy*, 77(2):139–151.

[14] Chenciner, A. and Montgomery, R. (2000b). A remarkable periodic solution of the three-body problem in the case of equal masses. *Annals of Mathematics*, 152:881–901.

[15] Chopovda, V. and Sweatman, W. L. (2018). The family of planar periodic orbits generated by the equal-mass four-body Schubart interplay orbit. *Celestial Mechanics and Dynamical Astronomy*, 103(5):1–15.

[16] Chopovda, V. and Sweatman, W. L. (2022). Four- and five-body periodic Caledonian orbits. *Multi-Scale (time and mass) Dynamics of Space Objects*, 15(364):140–145.

[17] Cline, D. (2018). *Variational Principles in Classical Mechanics*. University of Rochester River Campus Libraries.

[18] Cronin, J., Richards, P. B., and Russell, L. H. (1964). Some periodic solutions of a four-body problem. *Icarus*, 3:423.

[19] Goldstein, H., Poole, C., and Safko, J. (2011). *Classical Mechanics*. Pearson Education.

[20] Hadjedemetriou, J. D. and Christides, T. (1974). Families of periodic orbits in the planar three-body problem. *Celestial Mechanics*, 12(2):175–187.

[21] Hadjedemetriou, J. D. and Christides, T. (1975). The stability of periodic orbits in the three-body problem. *Celestial Mechanics*, 12(3):255–276.

[22] Heggie, D. and Hut, P. (2003). *The Gravitational Million-Body Problem. A Multidisciplinary Approach to Star Cluster Dynamics*. Cambridge: Cambridge University Press.

[23] Heggie, D. C. (1974). A global regularisation of the gravitational N-body problem. *Celestial Mechanics*, 27(2):217–241.

[24] Heggie, D. C. (2005). The classical gravitational N-body problem. *arXiv:astro-ph/0503600v2*.

[25] Hénon, M. (1974). Families of periodic orbits in the three-body problem. *Celestial Mechanics*, 10(3):375–388.

[26] Hénon, M. (1976). A family of periodic solutions of the planar three-body problem, and their stability. *Celestial Mechanics*, 13(3):267–285.

[27] Hietarinta, J. and Mikkola, S. (1993). Chaos in the one-dimensional gravitational three-body problem. *Chaos*, 3(2):183–203.

[28] Idrisi, M. J. and Ullah, M. S. (2020). Central-body square configuration of restricted six-body problem. *New Astronomy*, 79(4):101381.

[29] Kenyon, S. J. and Bromley, B. C. (2019). A Pluto–Charon Sonata: The Dynamical Architecture of the Circumbinary Satellite System. *The Astronomical Journal*, 157(2).

[30] Martínez, R. (2012). On the existence of doubly symmetric "Schubart-like" periodic orbits. *Discrete and Continuous Dynamical Systems*, 17(3):943–975.

[31] Martínez, R. (2013). Families of doubly symmetric "Schubart-like" periodic orbits. *Celestial Mechanics and Dynamical Astronomy*, 117(3):217–243.

[32] McGehee, R. (1974). Triple collision in the collinear three-body problem. *Inventiones mathematicae*, 27(3):191–227.

[33] Mikkola, S. (1983). Encounters of binaries. I - Equal energies. *Monthly Notices of the Royal Astronomical Society*, 203(4):1107–1121.

[34] Mikkola, S. (1985). A practical and regular formulation of the N-body equations. *Monthly Notices of the Royal Astronomical Society*, 215(2):171–177.

[35] Mikkola, S. (2007). A brief history of regularisation. *Dynamical Evolution of Dense Stellar Systems, Proceedings of the International Astronomical Union, IAU Symposium*, 246:218–227.

[36] Mikkola, S. and Aarseth, S. J. (1989). A chain regularization method for the few-body problem. *Celestial Mechanics and Dynamical Astronomy*, 47(4):375–390.

[37] Mikkola, S. and Aarseth, S. J. (1993). An implementation of N-body chain regularisation. *Celestial Mechanics and Dynamical Astronomy*, 57(3):171–177.

[38] Mikkola, S. and Hietarinta, J. (1989a). A numerical investigation of the one-dimensional Newtonian three-body problem. *Celestial Mechanics and Dynamical Astronomy*, 46(1):1–18.

[39] Mikkola, S. and Hietarinta, J. (1989b). A numerical investigation of the one-dimensional Newtonian three-body problem II. positive energies. *Celestial Mechanics and Dynamical Astronomy*, 47(4):321–331.

[40] Mikkola, S. and Hietarinta, J. (1991). A numerical investigation of the one-dimensional Newtonian three-body problem. III. Mass dependence in the stability of motion. *Celestial Mechanics and Dynamical Astronomy*, 51(4):379–394.

[41] Moeckel, R. (2008). A topological existence proof for the Schubart orbits in the collinear three-body problem. *Discrete and Continuous Dynamical Systems*, 10(2-3):609–620.

[42] Moore, C. (1993). Braids in classical dynamics. *Physical Review Letters*, 70(24):3675–3679.

[43] Nauenberg, M. (2001). Periodic orbits for three particles with finite angular momentum. *Physics Letters A*, 292(1-2):93–99.

[44] Nauenberg, M. (2006). New periodic orbits for the N-body problem. *Computational and Nonlinear Dynamics*, 1(4):307–311.

[45] Oswaldo, R. B. (2013/2014). The implicit and inverse function theorem: easy proofs. *Real Analysis Exchange*, 39(1):207–218.

[46] Ouyang, T. and Xie (2018). A continuum of periodic solutions to the planar four-body problem with two pairs of equal masses. *Journal of Differential Equations*, 264(7):4425–4455.

[47] Ouyang, T. and Yan, D. (2011). Periodic solutions with alternating singularities in the collinear four-body problem. *Celestial Mechanics and Dynamical Astronomy*, 109:229–239.

[48] Poincaré, H. (1892). *Les methodes nouvelles de la mechanique celeste*, volume 1. Gauthier-Villars, Paris.

[49] Powel, B. P. (2021). Tic 168789840: A sextuply-eclipsing sextuple star system. *The Astronomical Journal*, 161(4).

[50] Roberts, G. (2007). Linear stability analysis of the figure-eight orbit in the three-body problem. *Ergodic Theory and Dynamical Systems*, 27:1947–1953.

[51] Roy, A. E. (2005). *Orbital motion (4th ed.)*. Bristol, UK: IOP Publishing.

[52] Schubart, J. (1956). Numerische Aufsuchung periodischer Lösungen im Dreikörperproblem. *Astronomische Nachrichten*, 283(1):17–22.

[53] Sekiguchi, M. and Tanikawa, K. (2003). On the symmetric collinear four-body problem. *Publications of the Astronomical Society of Japan*, 56(1):235–251.

[54] Siddique, M., Kashif, A., Shoaib, M., and Hussain, S. (2021). Stability analysis of the rhomboidal restricted six-body problem. *Advances in Astronomy*, 2021:15–21.

[55] Siddique, M. A. R. and Kashif, A. R. (2022). The restricted six-body problem with stable equilibrium points and a rhomboidal configuration. *Advances in Astronomy*, 2022:15–21.

[56] Sivasankaran, A., Steves, B. A., and Sweatman, W. L. (2010). A global regularisation for integrating the Caledonian symmetric four-body problem. *Celestial Mechanics and Dynamical Astronomy*, 7(1):157–168.

[57] Standish, E. M. (1970). Periodic Orbits, Stability and Resonances. *D. Reidel Publ.Co., Dordrechet, Holland*, page 375.

[58] Steves, B. A. and Roy, A. E. (1998a). Some special restricted four-body problems - I. modeling the Caledonian problem. *Planetary and Space Science*, 46(1112):1465–1474.

[59] Steves, B. A. and Roy, A. E. (1998b). Some special restricted four-body problems - II. from Caledonia to Copenhagen. *Planetary and Space Science*, 46(1112):1475–1486.

[60] Stiefel, E. L. and Scheifele, G. (1971). *Linear and Regular Celestial Mechanics*. Berlin, Germany: Springer-Verlag Berlin Heidelberg.

[61] Strogatz, H. S. (2015). *Nonlinear Dynamics and Chaos: With Applications to Physics, Biology, Chemistry, and Engineering*. (2nd ed.): CRC Press.

[62] Sundman, K. F. (1913). Mémoire sur le probléme des trois corps. *Acta Math*, 36(1):105–179.

[63] Sweatman, W. L. (2002). The symmetrical one-dimensional Newtonian four-body problem: A numerical investigation. *Celestial Mechanics and Dynamical Astronomy*, 82(2):179–201. doi:10.1023/a:1014599918133.

[64] Sweatman, W. L. (2006). A family of symmetrical Schubart-like interplay orbits and their stability in the one-dimensional four-body problem. *Celestial Mechanics and Dynamical Astronomy*, 94(1):37–65.

[65] Sweatman, W. L. (2014). Symmetric four-mass Schubart-like systems. *Proceedings of the International Astronomical Union, Complex Planetary Systems*, 9:106–107.

[66] Sweatman, W. L. (2015). Symmetric four-body problems. *In G. M. Cojocaru, S. I. Kotsireas, N. R. Makarov, N. R. V. Melnik, H. Shodiev (Eds.), Interdisciplinary Topics in Applied Mathematics, Modeling, and Computational Science*, pages 439–444.

[67] Szebehely, V. and Peters, C. (1967). A new periodic solution of the problem of three bodies. *Astronomical Journal*, 72:1187.

[68] Szebehely, V. G. (1967). *Theory of orbits, the restricted problem of three bodies*. New York, NY: Academic Press.

[69] Tanikawa, K. and Mikkola, S. (2000a). One-dimensional three-body problem via symbolic dynamics. *Chaos*, 10(3):649–657.

[70] Tanikawa, K. and Mikkola, S. (2000b). Triple collisions in the one-dimensional three-body problem. *Celestial Mechanics and Dynamical Astronomy*, 76(1):23–24.

[71] Waldvogel, J. (1972). A new regularization of the planar problem of three bodies. *Celestial Mechanics*, 6(2):221–231.

[72] Whittaker, E. T. (1917). *A Treatise on the Analytical Dynamics of Particles and Rigid Bodies*. (2nd ed.) Cambridge: Cambridge University Press.

[73] Yan, D. (2012). A simple existence proof of Schubart periodic orbit with arbitrary masses. *Celestial Mechanics and Dynamical Astronomy*, 7(1):145–160.

Appendix A

Generating function

We consider Hamilton's principle for the original coordinates of our six-body system [19]

$$\int w_i \dot{x}_i - H(x, w, t) = 0.$$

If p and q are canonical coordinates, then the Hamilton principle in terms of p and q can be written as

$$\int p_i \dot{q}_i - K(q, p, t) = 0.$$

Since the general form of the Hamilton principle has zero variation at the end points, both of the above equations are satisfied if the integrands are connected by the following expression

$$\lambda(w_i \dot{x}_i - H) = p_i \dot{q}_i - K + \frac{dF}{dt}, \tag{A.1}$$

where F is any function of the phase space coordinates and λ is a constant independent of canonical coordinates.

The last term in (A.1) is related to the variation of action at the end points. Therefore, it vanishes if we choose F as a mixture of old and

new coordinates because these have zero variation at end points. We choose the generating function F_2 for our six-body system as

$$F = F_2(x, p, t) - p_i q_i.$$

Substituting the F into (A.1), we have

$$w_i \dot{x}_i - H = p_i \dot{q}_i - K + \frac{\partial F}{\partial t} + \frac{\partial F}{\partial x_i}\dot{x}_i + \frac{\partial F}{\partial p_i}\dot{p}_i - p_i \dot{q}_i - q_i \dot{p}_i.$$

Collecting the coefficients of $\dot{x_1}$ and $\dot{p_1}$, we get the following relations

$$w_i = \frac{\partial F}{\partial x_i}, \quad q_i = \frac{\partial F}{\partial p_i}.$$

Appendix B

Hexagonal family of periodic orbits

We present here another family of periodic orbits for the planar six-body problem with equal masses, that is generated from the hexagonal orbit. The hexagonal orbit is found analytically and is shown in Figure B.1. To find this orbit, we place the six bodies at the vertices of a regular hexagon and take x_1 as the distance of each body from the centre of mass. The position coordinates of the body, b_1 are $(x_1, 0)$ as it lays on the x-axis. The body b_2 has position coordinates $(x_1 \cos 60°, x_1 \sin 60°) = (\frac{x_1}{2}, \frac{\sqrt{3}x_1}{2})$. The corresponding velocity coordinates for bodies b_1 and b_2 are $(\dot{x}_1, 0)$ and $(-\frac{\dot{x}_1}{2}, -\frac{\sqrt{3}\dot{x}_1}{2})$, respectively. The numerical values of x_1 and $\dot{x}_1$ are found using the Hamiltonian of the six-body system with non-aligned triangles.

The search for the hexagonal family started when one group of bodies, as shown by blue, magenta and cyan paths in Figure B.2, was close to the centre of mass. The other group, as represented by the red, green and black paths in Figure B.1, was at maximum distance from the centre of mass. We adopted the same algorithm and procedure, presented in Chapter 4, for the search of this family as we used for the equal mass family of the Schubart orbit.

Selected members of the family are presented in Figure B.3. While

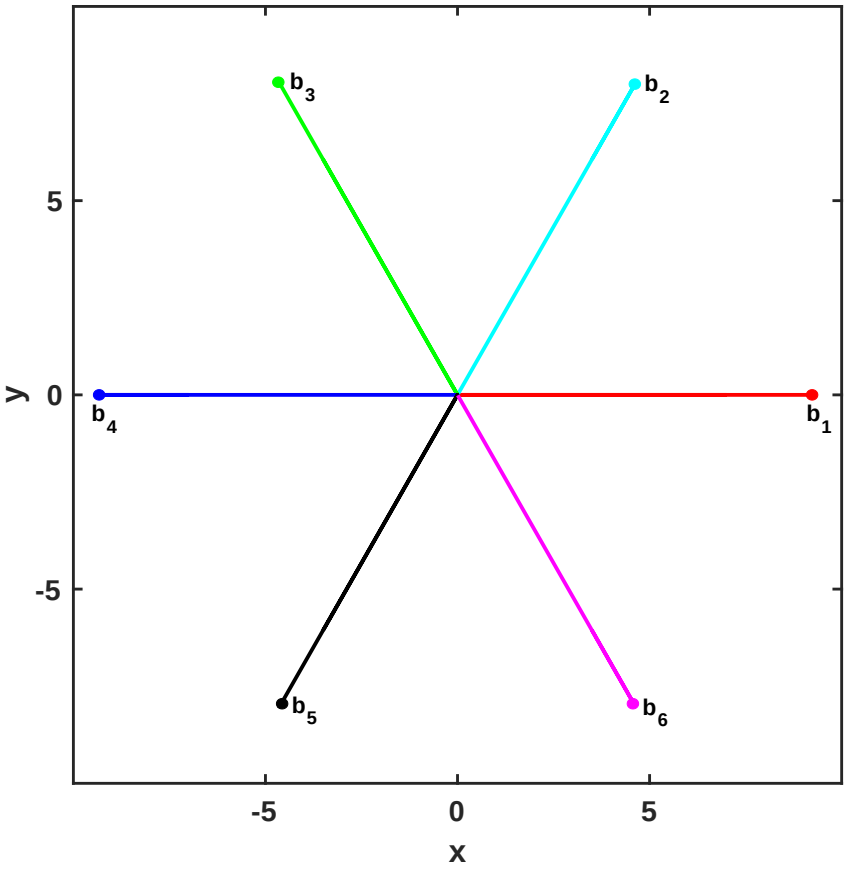

Figure B.1 Hexagonal orbit: coloured circles represent six bodies b_i for $i = 1, 2, ..., 6$, which are placed on the vertices of a regular hexagon.

Figure B.4 shows the same hexagonal family in rotating coordinates. This hexagonal family shows the same behaviour as the Schubart family of periodic orbits. The family starts from the hexagonal orbit and it does not seem to have an end, just like the Schubart family of periodic orbits.

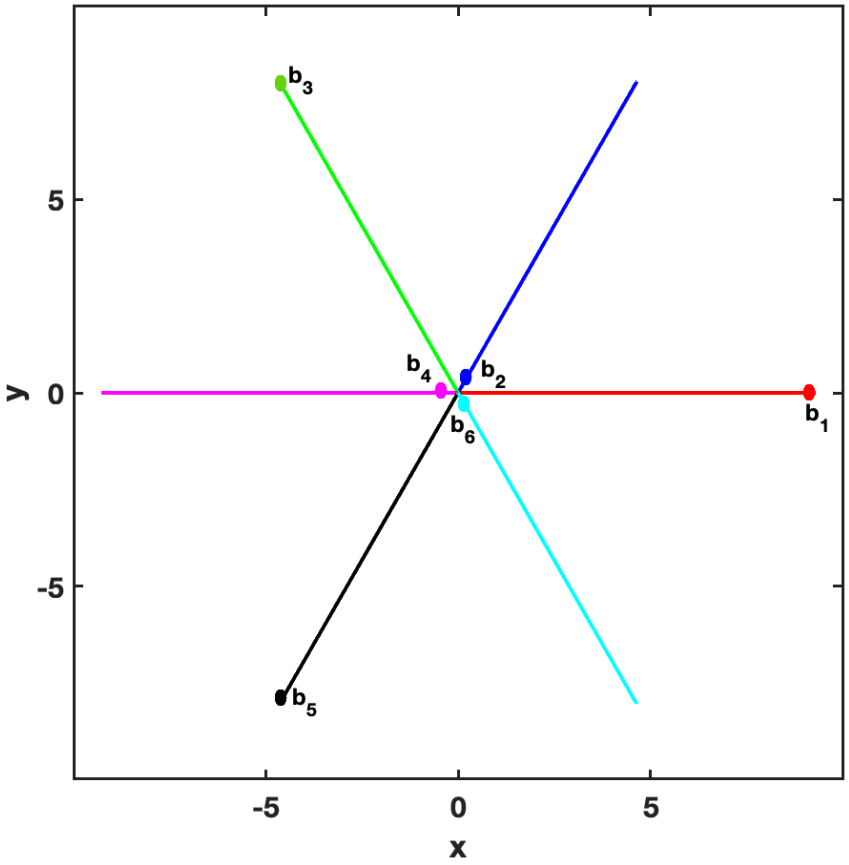

Figure B.2 Hexagonal orbit: The initial positions of bodies b_i are shown when the search started for the hexagonal family. One group of bodies b_2, b_4 and b_6 is positioned close to the centre of mass, however, the other group of bodies b_1, b_3 and b_5 is at a maximum distance from the centre of mass.

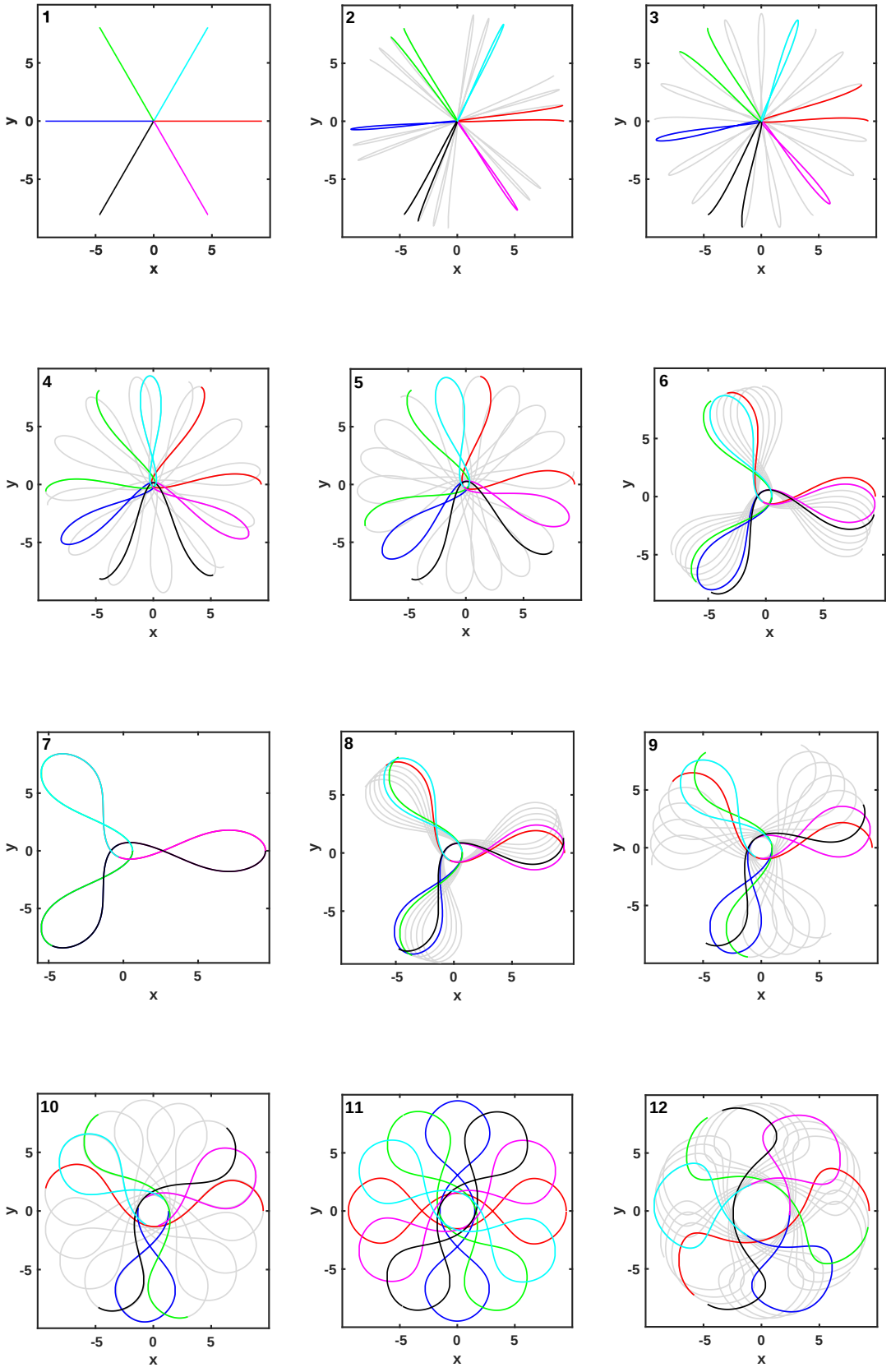
1
2
3
4
5
6
7
8
9
10
11
12
x
y
-5
0
5

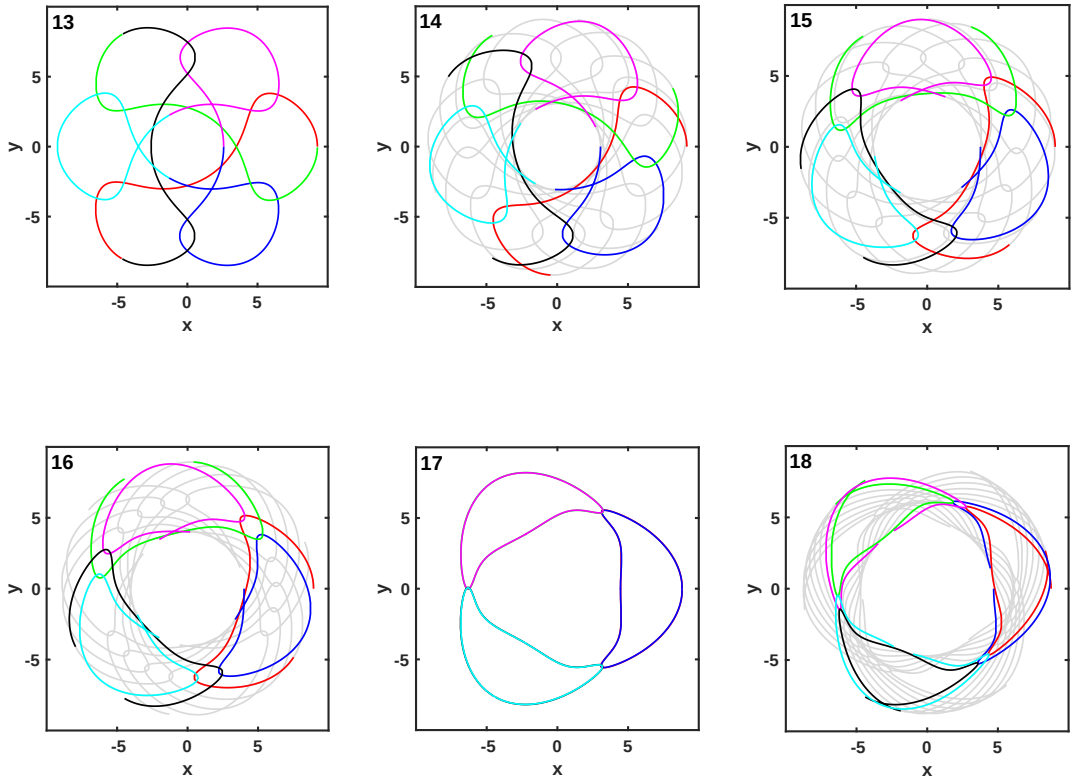

Figure B.3 Selected members of the hexagonal family of periodic orbits: The motion starts when the body b_1 is at maximum distance from the centre of mass and b_2 is positioned close to the centre of mass. The bodies b_1 and b_2 follow blue and red paths, However, the green, magenta, black, and cyan are paths of bodies b_3, b_4, b_5 and b_6 respectively. Coloured paths show one period.

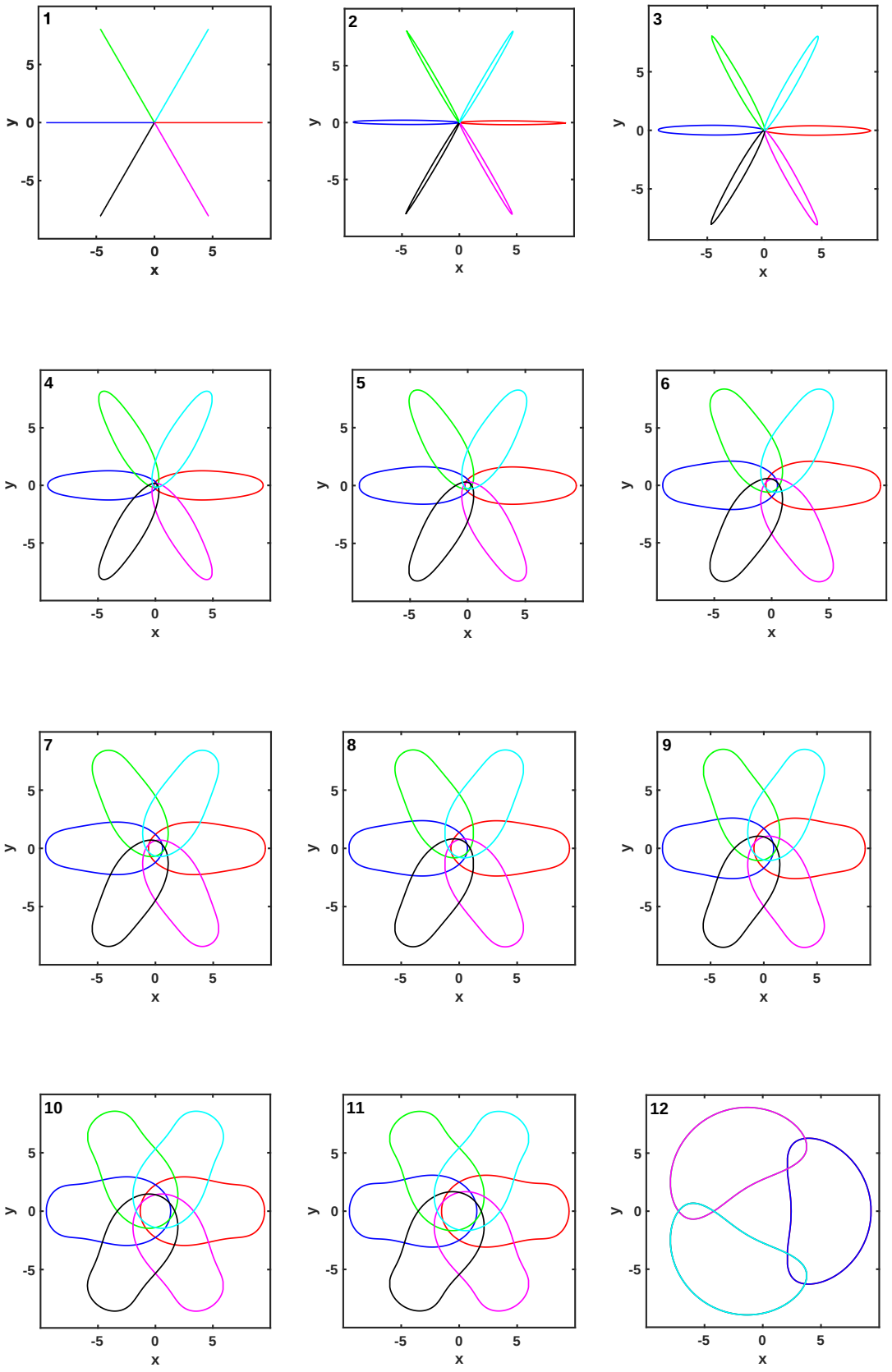
1
2
3
4
5
6
7
8
9
10
11
12
x
y
-5
0
5

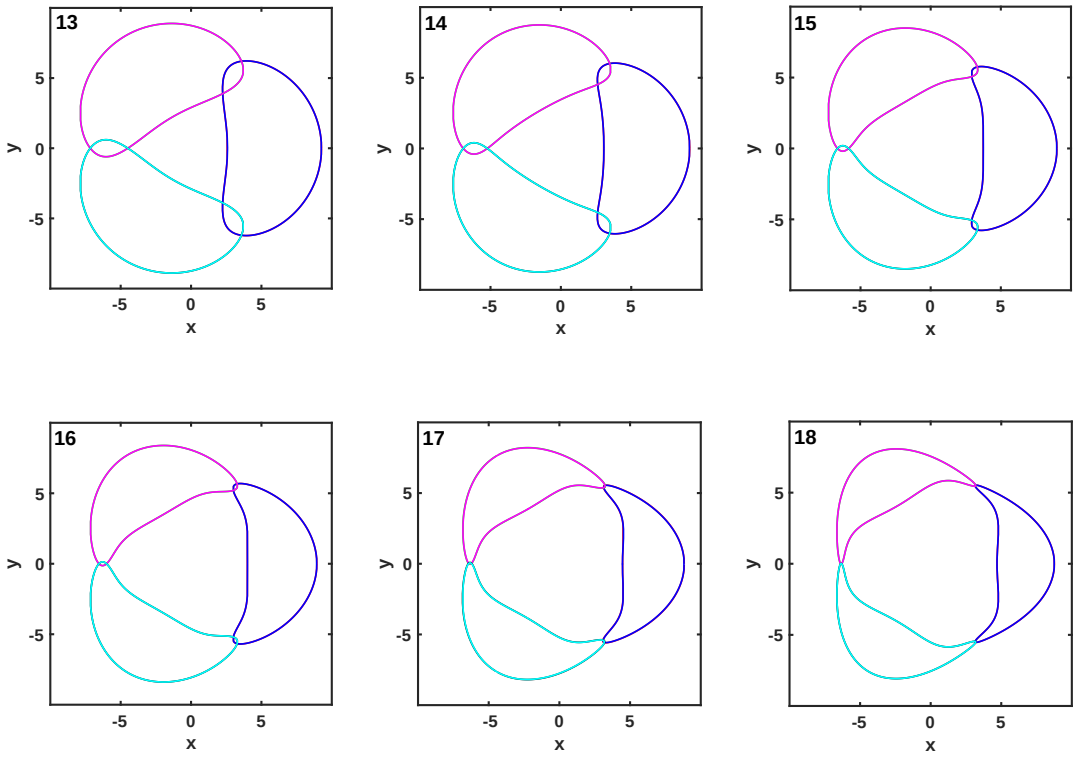

Figure B.4 Same orbits as represented in Figure B.2 are shown in rotating coordinates.

Table 1 Details of the Hexagon family.

Orbit	A	θ	d_{12}	T	x_1	x_3	$\dot{x}_2$	$\dot{x}_4$
1	0	0	9.386	30.67096245	9.38674376	0	0	$-\infty$
...	...	...	...	...	...	...	...	...
2	0.3	9.04698184	9.274	40.97213984	9.27647376	0.00247972	0.01654899	-21.58147186
3	0.7	20.34798976	9.272	41.02180985	9.28545356	0.01361663	0.03864119	-9.21428651
4	1.8	52.11691234	9.247	41.36892932	9.34309171	0.09585777	0.09995890	-3.48354843
5	2.2	63.68733231	9.225	41.57726352	9.37393823	0.14902562	0.12271645	-2.79819690
6	3.6	110.82891343	8.982	42.77912792	9.49550931	0.51337518	0.20824806	-1.51433381
7	3.826	120	8.892	43.08174430	9.51131127	0.61889084	0.22382455	-1.37913117
8	4.0	127.91845654	8.805	43.34719888	9.52062922	0.71606121	0.23643964	-1.28162345
9	4.3	143.16399222	8.600	43.89846079	9.52709887	0.92707934	0.25985893	-1.12435725
10	4.7	168.31018299	8.176	44.89013706	9.50221521	1.32655320	0.29536434	-0.93471477
11	4.856	180	7.953	45.37216829	9.477222780	1.52456943	0.31057686	-0.86892695
12	5.5	-128.62778632	6.859	47.70352970	9.30144981	2.44253058	0.37413766	-0.67417347
13	5.61	-120	6.679	48.10055717	9.26827375	2.58944746	0.38414934	-0.65280384
14	6.0	-92.93609061	6.099	49.48662712	9.15909368	3.06004180	0.41711661	-0.59489713
15	6.7	-50.00101158	5.249	51.86173014	8.99907335	3.75035600	0.46966195	-0.53146662
16	7.0	-32.71106736	4.930	52.89658658	8.93960912	4.00948749	0.49115345	-0.51312956
17	7.549	0	4.359	54.98203073	8.82879759	4.469583503	0.53248389	-0.48886565
18	7.8	1 7.67433796	4.065	56.15990161	8.76438599	4.69947552	0.55520664	-0.48219111

Appendix C

Orbits of the Planar Symmetric Six-body Problem

We present here a few examples of the orbits found in the planar symmetric six-body problem that do not belong to either of the two equal-mass families of periodic orbits. Orbit A, as shown in Figure C.1 is a double choreography orbit where the six bodies chase each other along the two equilateral triangles about their common centre of mass. In orbits $B-D$, illustrated in Figures C.2−C.4, respectively, the bodies split into three separate binaries and start to move away from the centre of mass.

All the orbits, represented in Figures C.1−C.4 are the members of the same family. These orbits are integrated over different periods of time, which helps to understand that the bodies rotate in a circle around the centre of mass as three separate binaries.

Figure C.5 shows another interesting orbit I, where the bodies are chasing each other on two non-intersecting closed curves. It is noted that during their motion the bodies remain on the vertices of two equilateral triangles for all time in orbit I.

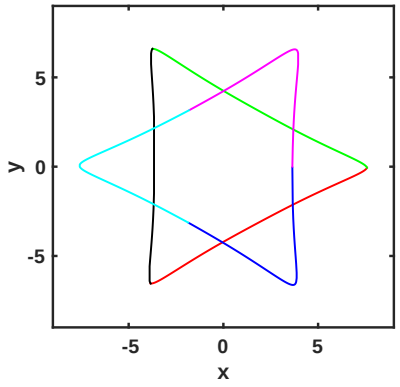

(a) Physical coordinates

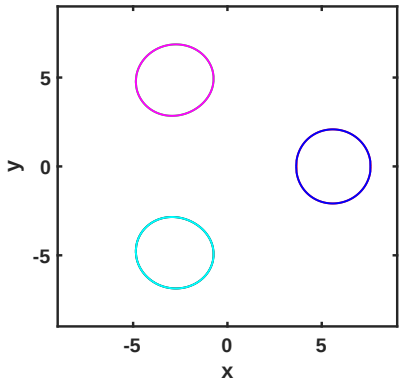

(b) Rotating coordinates

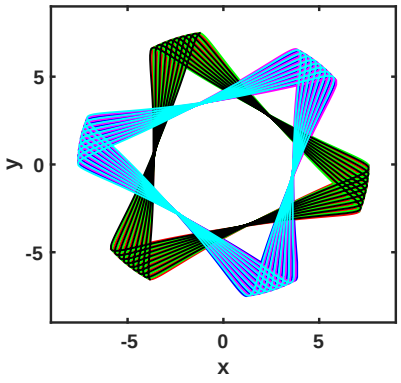

(c) $t = 25T$

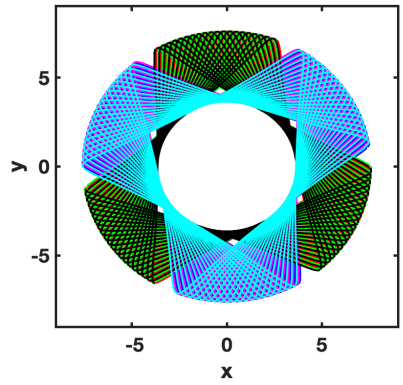

(d) $t = 60T$

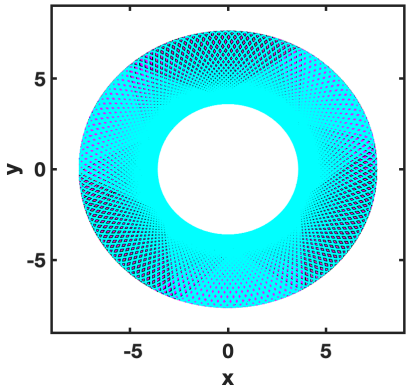

(e) $t = 200T$

Figure C.1 Double choreography orbit with $\theta = -120°$: The same orbit is integrated over different periods of time. Six different colours represent the paths of six bodies

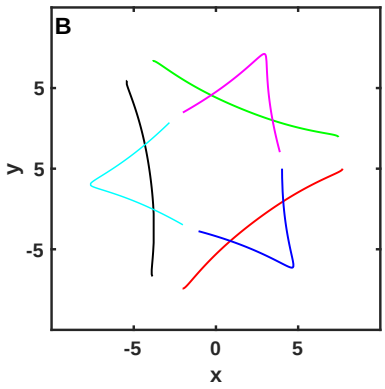

(a) Physical coordinates

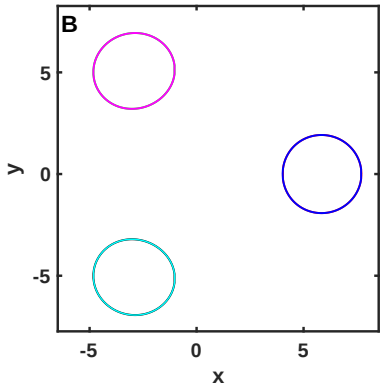

(b) Rotating coordinates

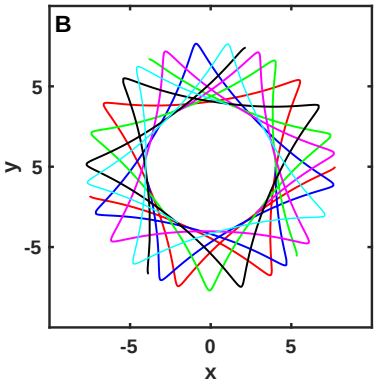

(c) $t = 5T$

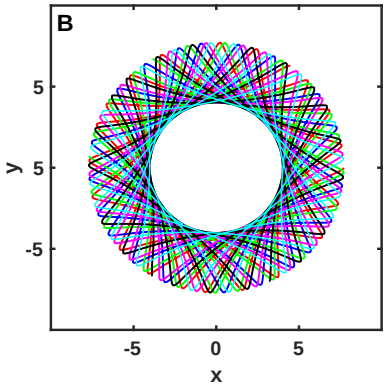

(d) $t = 20T$

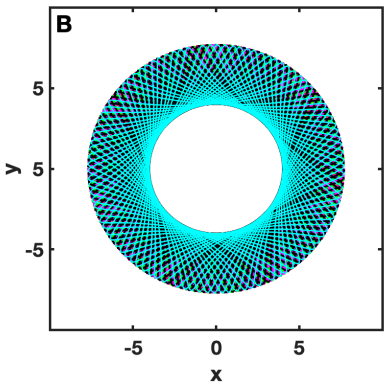

(e) $t = 100T$

Figure C.2 Orbit B: Six bodies start to separate as three binaries.

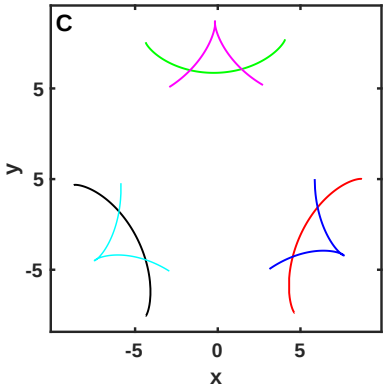

(a) Physical coordinates

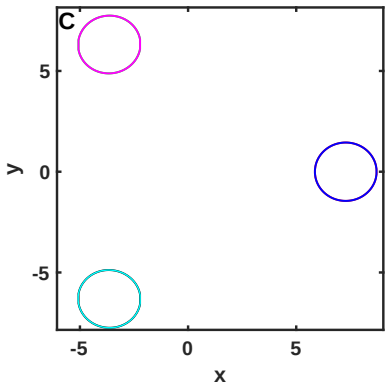

(b) Rotating coordinates

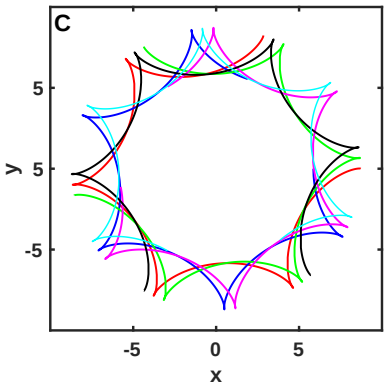

(c) $t = 5T$

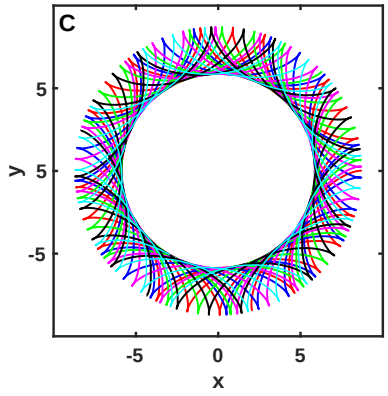

(d) $t = 20T$

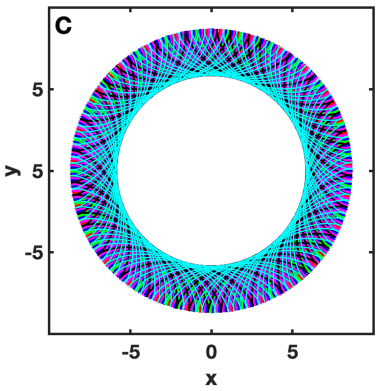

(e) $t = 100T$

Figure C.3 Orbit C: Each body is represented with a different colour, and the same orbit is integrated over different periods.

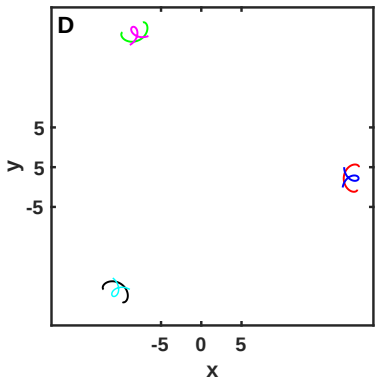

(a) Physical coordinates

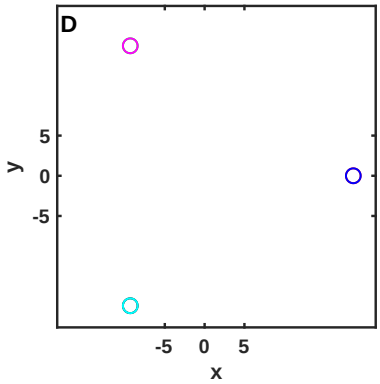

(b) Rotating coordinates

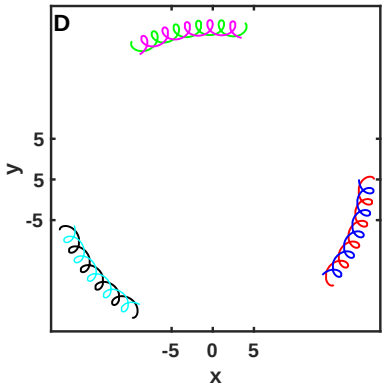

(c) $t = 5T$

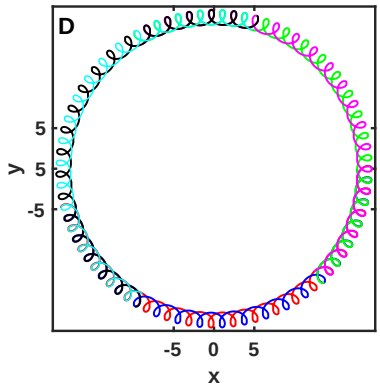

(d) $t = 20T$

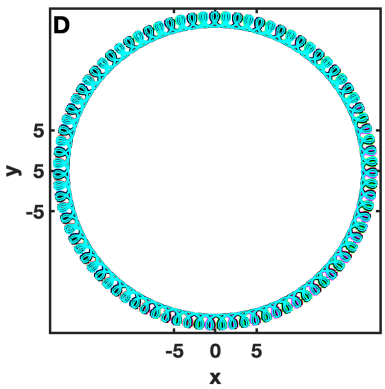

(e) $t = 200T$

Figure C.4 Orbit D: Bodies are separated as binaries and rotating in a circle about the centre of mass.

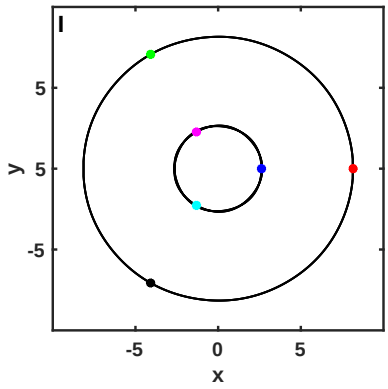

(a) $t = 0$

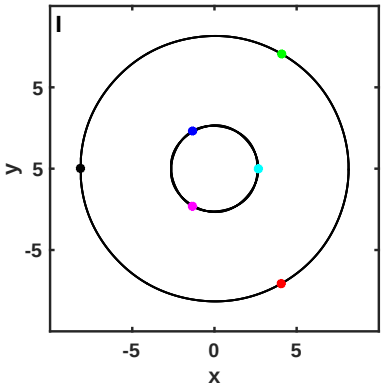

(b) $t = T/2$

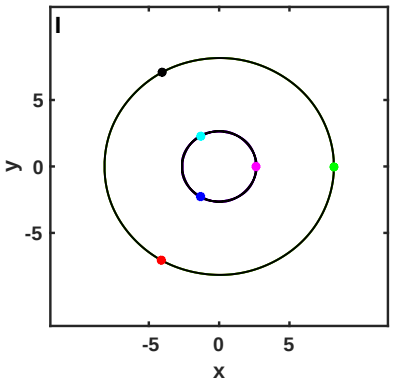

(c) $t = T$

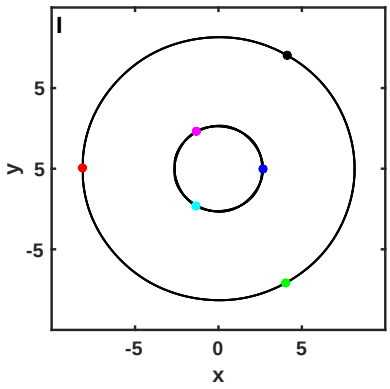

(d) $t = 3T/2$

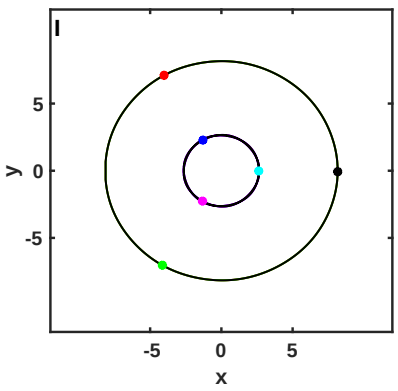

(e) $t = 2T$

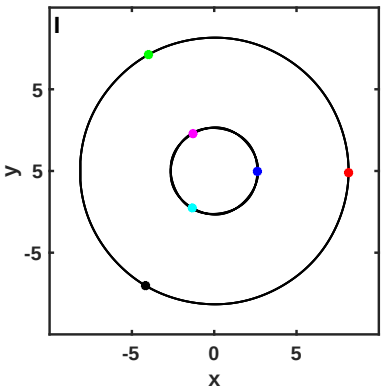

(f) $t = 3T$

Figure C.5 Choreography orbit with $\theta = 120°$: Each body is represented with a different colour, and the positions of the bodies over different times are shown.

Appendix D

Intermediate Value and Implicit Function Theorems

The existence of the Schubart orbit is proved by using the intermediate value and implicit function theorems defined below [45]

A.1 Intermediate value theorem

"If f is a continuous function on a closed interval $[a, b]$ and if y_0 is any value between $f(a)$ and $f(b)$, then $y_0 = f(c)$ for some c in $[a, b]$."

A.2 Implicit function theorem

"Suppose a continuously differentiable function $f(x_0, y_0)$, such that $f(x_0, y_0) = c$. If $f_y(x_0, y_0) \neq 0$, then there is a neighbourhood of (x_0, y_0) so that whenever x is sufficiently close to x_0, then there is a unique y so that $f(x, y) = c$ and y is a continuous function."